OUT-OF-PLANE BEHAVIOUR OF CONCRETE BLOCK WALLS

WITH UNBONDED REINFORCEMENT

A Thesis Submitted to the College of

Graduate and Postdoctoral Studies

In Partial Fulfillment of the Requirements

For the Degree of Master of Science

In the Department of Civil, Geological, and Environmental Engineering

University of Saskatchewan

Saskatoon

By

HENRY PAUL MIRANDA ORELLANA

Permission to Use and Disclaimer Statement

In presenting this thesis in partial fulfillment of the requirements for a Postgraduate degree from the University of Saskatchewan, I agree that the Libraries of this University may make it freely available for inspection. I further agree that permission for copying of this thesis in any manner, in whole or in part, for scholarly purposes may be granted by the professor or professors who supervised my thesis work or, in their absence, by the Head of the Department or the Dean of the College in which my thesis work was done. It is understood that any copying or publication or use of this thesis or parts thereof for financial gain shall not be allowed without my written permission. It is also understood that due recognition shall be given to me and to the University of Saskatchewan in any scholarly use which may be made of any material in my thesis.

Requests for permission to copy or to make other uses of materials in this thesis/dissertation in whole or part should be addressed to:

> Head of the Department of Civil, Geological, and Environmental Engineering
> 57 Campus Drive
> University of Saskatchewan
> Saskatoon, Saskatchewan S7N 5A9
> Canada

Or

> Dean
> College of Graduate and Postdoctoral Studies
> University of Saskatchewan
> 116 Thorvaldson Building, 110 Science Place
> Saskatoon, Saskatchewan S7N 5C9
> Canada

Abstract

The use of grout in conventional reinforced masonry construction increases the cost and time of construction but, when used in combination with reinforcing steel, allows walls subject to out-of-plane loads an enhanced ability to span between lateral support levels. Reinforced concrete block walls constructed in this manner can typically span at least two stories in constrast to the limited single storey capacity of unreinforced walls. However, the use of grout as needed for the construction of these walls increases their self-weight, and requires an additional trade on-site. A novel, potentially cost-efficient, approach to achieve reasonable load-carrying capacity in masonry walls was therefore investigated that involves the use of minimally stressed reinforcement anchored at the top and bottom of the wall. This allows for a grout-free structural system that relies upon arching to resist the flexural effects resulting from out-of-plane loads and so make more effective use of the compressive capacity of the masonry assembly.

An experimental program was therefore conducted at the University of Saskatchewan to investigate the performance of concrete masonry block walls reinforced with non-prestressed, unbonded reinforcement. This study included a total of 21 walls that were built to identify potential alternatives to unreinforced and conventionally grouted and reinforced walls. The strength and serviceability of these walls was evaluated. All walls in this program were two and a half blocks wide and 14 courses tall and were built in running bond using standard 200 mm concrete blocks. Six replicates of both unreinforced and partially grouted, conventionally reinforced walls served as control specimens.

An analysis of the data obtained during testing revealed that the walls with unbonded reinforcement were inherently stable with maximum loads approaching those of partially grouted, conventionally reinforced walls. Furthermore, an analytical approach is presented herein that is based on the assumption that the walls with unbonded reinforcement could be modeled using a three hinged mechanism. The analytical model was found to match with the experimentally obtained load versus mid-height deflection data reasonably well throughout the post-cracking range.

Co-Authorship

All of the experimental work presented in this thesis was conducted by Henry Paul Miranda Orellana and reviewed by Dr. L.R Feldman and Dr. B.F. Sparling. The results of a select number of wall specimens presented in the experimental program were published in the proceedings of the 2016 CSCE Annual General Conference in London, Canada. A manuscript summarizing the findings of this research program related to walls with unbonded reinforcement was published in the Journal of Civil Engineering in November 2018.

The Chapter 3 is presented as manuscript #1: Feasibility of using unbonded reinforcement in concrete block walls. The contributions of the current MSc. candidate were 1) designing the concrete grade beams and wall specimens; 2) designing the test frame and instrumentation; 3) building the concrete grade beams; 4) assembling the test frame; 5) leading the construction of the wall specimens; 6) preparing companions and masonry prisms; 6) leading the testing of the wall specimens; 7) testing the companion and masonry prisms; 8) analyzing the data and plotting the figures; and 9) writing drafts and revising the final manuscript.

Aditionally, the Chapter 4 is presented as manuscript #2: Proof of Concept Investigation of Unbonded Reinforcement in Concrete Block Masonry. The contributions of the current MSc. candidate were 1) installing the camera system 1 and camera system 2 of the DIC for testing wall specimens; 2) determining of the speckle size for measuring strain contours on large specimens; 3) preparing wall surfaces for acquiring images; 4) leading the testing of UB and PGR wall specimens; 5) testing the associated companion and masonry prisms; 6) calibrating the analytical model through different assumptions; 7) analyzing the data and plotting the figures; and 9) writing drafts and revising the final manuscript.

Acknowledgements

Dedication

I would like to express deep gratitude to my parents, Marianita Orellana de Miranda and Daniel Miranda, my brothers, Boris Miranda Orellana and Christian Miranda Orellana, and their families for all their blessings, support, and love that I have received during this academic journey at the University of Saskatchewan. I am grateful to them for all the efforts that they have always provided for taking care of my problems and encouraging me to keep going to reach my dreams.

I would also like to thank my wife, Alexandra Bastidas de Miranda, who is the love of my life for being tolerant and supportive not only during this experience in this country, Canada, but for most of my life. Thanks to my daughter, Evelyn Miranda Bastidas, and my son, Henry A. Miranda Bastidas, for all the efforts and sacrifices that you make day by day for overcoming obstacles with courage and determination. Your attitude and unconditional love encouraged me to go ahead and overcome all the challenges during this journey.

Thanks all of you for being the happiness in my life…

Table of Contents

List of Tables

List of Figures

List of Abbreviations

ASTM   American Society for Testing and Materials

COV   Coefficient of Variation

CSA   Canadian Standards Association

DICS   Digital Image Correlation System

LVDT   Linear Variable Differential Transducers

LED   Light-emitting Diode

PGR   Partially grouted and conventionally reinforced walls

UR   Ungrouted and unreinforced walls

UB-G   Ungrouted walls with unbonded reinforcement with the first course grouted

UB-U   Ungrouted walls with unbonded reinforcement with the first course ungrouted

List of Symbols

a Distance at the edge of a masonry segment measured between its centerline and a contact point with the support

A_{Bx} Horizontal reaction force at Point A at the bottom of the wall

A_{By} Vertical reaction force at Point A at the bottom of the wall

b Portion or width of the masonry wall in contact with the support, as a result of the wall rotation

C_b Compression force in the concrete reinforced beam

C_f Compression force per unit length resulting of the arching action on the masonry wall

d Half depth of the masonry section as defined by McDowell et al. 1996

e_c Strain associated with the crushing strength of the masonry

f_b Maximum masonry compressive stress

f_c Stress over the compression zone in the wall

F_{Bx} Horizontal reaction force at point B at mid-height of the wall

F_{By} Vertical reaction force at point B at mid-height of the wall

F_{six} Horizontal force component of the reinforcement at alignment plate location

F_{siy}	Vertical force component of the reinforcement at alignment plate location
F_s	Spring force
L	Masonry wall and beam span
i	Number of alignment plates from bottom to top of the wall
jd	Flexural lever arm
N_i	Number of unreinforced wall samples in specimen type i
M	Bending moment
$M(u)$	Moment due to arching forces
R	Dimensionless variable resulting of the relationship among the e_c, L and d.
$r(u)$	Moment arm as defined by McDowell et al. 1996
P	Applied load
P_{cr}	Cracking load
$(P_{max})_{model}$	Maximum applied load obtained using the analytical model
$(P_{max})_{test}$	Maximum applied load obtained during the test
$P(u)$	Arching force per unit width
R_{rod}	Axial force in the rod
Sc	Specified compressive strength of the masonry material
t	Wall thickness
T	Internal thrust force
T_r	Tension force
$(T_{max})_{model}$	Maximum tension in the reinforcement obtained from the analytical model
$(T_{max})_{test}$	Average maximum tension in the reinforcement obtained from the strain gauges
V	Shear force
w	Deflecion at midspan of a masonry wall, as a result of the masonry rotation and defined by McDowell et al. 1996
w_u	Applied uniform pressure
w_f	Factored uniform load resistance
W_{D_bot}	Self-weight of the lower segment of the wall
W_{D_top}	Self-weight of the upper segment of the wall
W_{pl}	Self-weight of the top steel plate
X_i	Average out-of-plane resistance in specimen type i

α	Angle between segments B^*C^* and B^*D
β	Angle between segments B^*D and the horizontal projection of B^*
γ	Angle between the thrust force and the vertical axis
Γ	Portion of thickness of the masonry wall at midspan no longer in contact
δ	Wall lateral displacement at mid-height
Δ_c	Axial deformation associated with crushing of a masonry wall segment as defined by McDowell et al. 1996
Δ_h	Assumed horizontal displacement
Δ_{mid}	Displacement at the mid-height of the wall
Δ_v	Wall vertical displacement
Δ_{vdi}	Axial deformation of the wall
θ	Angle of rotation of half masonry beam considered as a rigid body
θ_{base}	Angle of rotation at the bottom edge of the lower wall segment, θ_{AB}
θ_{mid}	Angle of rotation at mid-height of the upper wall segment, θ_{BC}
θ_{rod}	Angle of rotation of the rod as a result of the wall movement
θ_v	Angle of rotation of the wall with respect to the vertical
σ_i	Standard deviation in specimen type i
ϕ_m	Resistance factor for masonry wall

Chapter 1: Introduction

The motivation for this research is briefly discussed in this chapter with an emphasis on the importance of enhancing the out-of-plane resistance of ungrouted (UR) masonry walls through engaging the arching effect by using unbonded reinforcement. Advantages in using this mechanism in comparison to those associated with unreinforced and ungrouted walls, and grouted and conventionally reinforced walls (PGR) are described. Previous studies investigating various aspects of arching effect in walls are also reviewed. The knowledge gap and the objectives and scope of this research project are then presented.

1.1 Background

Masonry is one of the oldest and most durable building materials. It is commonly used for low rise structures, including educational, commercial, and recreational buildings. Advantages of masonry include its low maintenance costs, enhanced fire resistance, thermal insulation, sound control, and high compressive strength. However, the tensile resistance of masonry, when unreinforced, is weak due to the poor bond that exists between the mortar and the concrete blocks. In fact, the compressive strength of the concrete blocks cannot be fully developed since the cracks formed do not allow the wall assemblage to work as a fully functional composite (Page 1979). Fully or partially grouted and conventionally reinforced concrete block walls can effectively resist out-of-plane loads; however, the techniques required for their construction result in additional time, increased total project costs, and additional self-weight of the walls due to the grout used to fill the block cores. Workplace injuries may also result due to the need for masonry workers to thread blocks up and over reinforcement that has already been grouted in place.

The grouting process for fully or partially grouted and conventionally reinforced concrete block walls can be more time consuming and expensive. In part, this is due to the requirement for additional tasks, skilled workers on the jobsite, and the need for additional materials required for the mixture process. The time required for placing grout and the two – four hour wait time between lifts, regardless of the type of lift used, slows down the project schedule (CSA 2014c).

Arching action generated through the use of unbonded reinforcement could be an alternative for providing a sufficiently robust wall system to withstand out-of-plane loading. Unbonded reinforcement will enhance wall capacity through a better usage of the masonry materials' properties. McDowell et al. (1956) described how the resistance of a masonry wall utilizing arching to resist lateral loads could be attributed to compressive forces developed in the plane of the wall which takes advantage of the inherent wall compression capacity. Researchers have long been aware of this physical mechanism in beams, walls, and thick slabs; most have noted a resulting increase in the out-of-plane resistance of the structural element in comparison to those without constraints at their supports, a condition that is necessary in order for arching to occur (McDowell et al. 1956, Abrams et al. 1996, Liebenberg 1966, Rankin & Long 1997). Construction time may also be reduced compared to that required for conventionally grouted and reinforced walls since the need for grouting is eliminated.

The existing literature does not adequately address arching action due to unbonded, non-prestressed internal reinforcement as a means of increasing the out-of-plane resistance of masonry walls. Rather, studies dealing with arching in masonry walls have focused on confined panels in which the rigidity of their supports has enabled the generation of compressive forces set up in the plane of the walls (Gabrielsen & Wilton 1974, Abrams et al. 1996, Drysdale & Hamid 2005). Walls of this type typically experience failure by crushing of the masonry at mid-height and at the boundaries. It is hypothesized that arching action resulting from masonry members that include unbonded reinforcement may increase the performance of concrete block walls as compared to unreinforced walls while also addressing some of the disadvantages identified for conventionally reinforced walls. Specifically, this novel system can potentially reduce self-weight, cost, and construction time.

1.2 Problem Statement

An experimental study was therefore conducted to evaluate whether the performance of ungrouted concrete block walls could be improved by incorporating unbonded steel reinforcement to increase the out-of-plane resistance, and to contrast the behaviour of such walls with those that are grouted and conventional reinforced. Masonry walls were constructed using realistic support conditions, and were subjected to out-of-plane loading. Comparisons to control specimens including partially

grouted and conventionally reinforced walls, and unreinforced and ungrouted walls were conducted.

1.3 Objectives

The main objective of this study was to investigate the potential for using unbonded reinforcement to improve the out-of-plane resistance of ungrouted block walls. Sub-objectives were:

- To compare the cracking load, load resistance, and mid-height deflection at the ultimate load level for concrete block walls with unbonded reinforcement to that of unreinforced and ungrouted, and conventionally grouted and reinforced masonry walls;
- To compare the strain field on the surface of concrete block walls with unbonded reinforcement to those of unreinforced and ungrouted, and conventionally grouted and reinforced masonry walls; and
- To compare experimental applied load versus mid-height deflection curves from tests of ungrouted block walls with unbonded reinforcement to those predicted by analytical models, and to determine the influence of material behaviour and crack location on predicted behaviour.

1.4 Scope and Methodology

This experimental investigation focused on determining the difference in load resisting behaviour between unreinforced and ungrouted, partially-grouted and conventionally reinforced, and unbonded reinforced masonry walls. All walls featured realistic supports at their bases created by placing the first masonry block course on a concrete grade beam using a standard mortar joint. An ideal "roller" connection was included at the top of the walls, which provided lateral support without any rotational restraint. The top supports were also designed in a manner that did not induce any axial force in the wall.

Four point out-of-plane loading was applied to simulate lateral load, such as that resulting from wind or earthquake. This applied load was monotonically increased under deflection control until failure.

3

All specimens had the same overall geometry and were fourteen courses tall and two and a half blocks wide. All walls were constructed with 200 mm concrete blocks. Deformed Grade 515 steel wires (6.4 mm diameter) were used to reinforce the conventionally reinforced and unbonded reinforced masonry walls.

A digital imaging camera system (DICS) was used to measure the strain contours on the unloaded face and one side face of the wall specimens. Both systems were comprised of two cameras with similar resolution and two focal lenses with different focal lengths. Results were compared between the strain contours from the unloaded wall specimens prior to testing (i.e. reference image) and the strain contours as the applied load reached the cracking load. A second comparison was made using the reference images and the resulting images of the walls as the maximum load was approached.

Three analytical models of the walls with ubonded reinforcement were established in accordance with several assumptions regarding: crack location, reinforcement behavior, and rigid body motion of the wall segments. The applied load versus mid-height deflection curves were compared with the experimental results obtained during the test.

1.5 Thesis Overview

This manuscript includes five chapters, plus references and appendices. Chapter One presents the background, objectives, scope, and methodology of this work.

Chapter Two presents a literature review related to the performance of masonry walls subject to out-of-plane loading. This chapter also provides a review of the effect of unbonded reinforcement and arching action in concrete and masonry members. A series of analytical models are presented that were developed to predict the maximum out-of-plane load resistance of masonry specimens considering the arching mechanism. Studies of prestressed masonry walls specimens are also included.

Chapter Three presents the experimental design, construction, and testing of the concrete masonry block walls. Also, it provides an initial comparison between experimental results from walls with unbonded reinforcement with those obtained for unreinforced and ungrouted walls.

Chapter Four includes the detailed results and analysis of all specimens included in the experimental investigation. A description of the proposed numerical model is also provided, along with a comparison of the calculated and experimental results.

Versions of Chapter 3 and 4 have been published previously as individual papers in the 2016 CSCE Annual Conference and in the Canadian Journal of Civil Engineering, respectively. Modifications have been made herein to improve the cohesiveness of this Thesis.

Chapter Five includes a summary and conclusions resulting from this research and recommendations for future work.

Chapter 2: Literature Review

This chapter addresses the effects of arching action and pre-compression on unreinforced walls when they are subjected to out-of-plane loading. Unreinforced masonry walls have considerable resistance to axial loads, but when subjected to out-of-plane loads, their performance is relatively poor. Investigations related to out-of-plane loading of unreinforced masonry walls have been conducted by a number of researchers, and have included investigations of variables such as: span length, support conditions, and loading methods. Studies revealed that the out-of-plane behaviour of walls could be improved taking advantage of the inherent compressive capacity of the masonry. Enhancement in strength capacity has been attained through the use of various pre-compression methods. Additionally, this chapter includes a discussion of the general principles of arching action, and analytical models for masonry elements subjected to arching. Finally, this chapter describes some studies that were conducted to evaluate the addition of external unstressed unbonded reinforcement as a means to enhance the mechanical and physical properties of concrete beams.

2.1 The Effects of the Mechanical Interlocking Between Mortar and Concrete Blocks in the Performance of Unreinforced Masonry Walls

Unreinforced walls fail as a result of their flexural tensile strength because the interface region between the mortar and concrete blocks is weak (Anderson 1984; Tabbakhha & Deodatis 2017). Unreinforced masonry is commonly used as partition or load-bearing walls to support lightweight roof structures. During severe windstorms, external block walls are subject to high out-of-plane pressures, thus producing high flexural stresses mainly at midspan of the wall (i.e. in the high moment region) that may be sufficient to cause the block walls to fail. The tensile bond strength between the block and the mortar in the bed joint is therefore a major factor in determining the flexural strength of block walls.

Many researchers have been concerned with establishing reliable values for the flexural tensile strength of masonry walls (Al-Menyawi 2001; Hamid et al. 1998). Grouted and ungrouted concrete masonry walls have been built using different mortar types and subjected to two-way bending to determine the performance of the mortar placed in the head and bed joints. Tensile strength values

obtained by researchers therefore exhibit high variability and cannot be identified precisely at this time.

2.2 The Effects of Support Conditions on Unreinforced Walls Subjected to Out-of-Plane Loading

Previous work conducted by Udey (2014) at the University of Saskatchewan included the use of twenty replicate specimens to evaluate statistical differences between two types of support conditions for unreinforced and ungrouted concrete block walls. The first was an ideal pinned condition created by using a steel plate with knife edge at the bottom and a top support that was free to rotate and move vertically (Figures 2.1(a) and (b)), while the second was a realistic simple support condition which included a mortar joint between the bottom edges of the concrete block wall and the supporting concrete grade beam at the bottom as well as full-width angles adjacent to both sides of the wall at the top that were connected to a steel beam above, which effectively produced some rotational resistance (Figures 2.1(c) and (d)). The masonry walls were loaded laterally with monotonically increasing quasi-static four point loading representative of the effects of uniform load.

Udey (2014) concluded that the realistically supported walls withstood an average moment that was 63% larger than the average moment required to cause midspan cracking in the walls with ideal pinned support conditions. Furthermore, it was stated that the ductility of the ideally pinned walls was considerably smaller than the realistically supported walls. In fact, the ductility of the realistically supported walls was 70% higher. A beneficial behaviour of these walls was observed in which binding of the wall at the top angle supports was found to generate a compression force once the walls displaced laterally and attempted to rotate at the top end as a result of the lateral load. This resisting mechanism appeared to enhance wall capacity in a manner similar to arching action within a wall with sufficiently rigid supports. It seems that the effect of arching compressed the masonry walls and generated a strut force along the wall segments. However, as the crack width at mid-height increased, the unreinforced walls became unstable, increasing the risk of a sudden collapse.

2.3 Arching Action Studies

Researchers have studied the effect of arching action in masonry. They defined arching action as the counteractive force generated in the plane of the masonry wall after the initiation of some localized cracking (Figure 2.2(a)) (McDowell et al. 1956; Gabrielsen & Wilton 1974). Regardless of the type of lateral loading used in the experimental tests, one of the main requirements to generate arching was the support conditions. Studies have revealed that the masonry element must be built within rigid supports that allow the masonry segments to rotate once the masonry develop cracks at the supports and near mid-span (McDowell et al. 1956; Gabrielsen & Wilton 1974; Abrams et al. 1996). It was suggested that masonry could resist out-of-plane loads due to the presence of thrust forces (i.e. a force having a lateral component of similar magnitude but contrary to the applied force) that could be generated on the contact areas once cracks formed (Figure 2.2(b)) (McDowell et al. 1956; Drysdale & Hamid 2005; Abou-Zeid et al. 2010). The contact area is defined as the portion of a cross sectional surface located at the edges of a masonry segment which is in contact with the masonry wall support or between masonry segments. These contact areas between the masonry segments and the supports must develop a significant magnitude of compressive stresses that depends on the level of fixidity at the supports, and increases as the width of the generated cracks increases (Abrams et al. 1996).

Arching action has been studied in masonry beams under lateral quasi-static load (McDowell et al. 1956; Abrams et al. 1996; Drysdale & Hamid 2005; Varela et al. 2012). A study revealed that arching effect can increase the flexural capacity in masonry beams by three to six times (McDowell et al. 1956). Masonry walls subjected to out-of-plane blast loading have demonstrated four to five times the flexural resistance in rigidly supported walls as compared to those that were not rigidity supported (Gabrielsen & Wilton 1974). A research investigation involving cracked infill masonry panels subjected to monotonically increasing lateral pressure showed that the strength of these walls was significant despite the fact that the cracks had previously formed (Abrams et al. 1996). Other studies have demonstrated that arching action can enhance the cracking load of masonry walls by a factor of 2.5 (Drysdale & Hamid 2005).

Tests conducted using masonry walls showed that the supports should be able to resist the resulting thrust force without substantial movement; otherwise, the potential magnitude of the arching action

would be compromised (McDowell et al. 1956, Abou-Zeid et al. 2010). Furthermore, the failure mode is controlled either by the crushing strength of masonry at the contact points between segments and supports or by a large lateral displacement at mid-span (McDowell et al. 1956).

Analytical models have been developed to quantify the magnitude of the flexural resistance that adds to the arching effect in masonry members. The idealized models consider some main assumptions such as: 1) masonry fixity between rigid supports, 2) a uniform masonry cross section, 3) cracks that develop at bottom, at top, and mid-heigth of the wall, and 4) rigid body motion of the masonry segments, and 5) the capacity of masonry to withstand in-plane compressive forces. Based on the research programs mentioned above, Section 2.4 describes the analytical approaches used to calculate the actual flexural resistance of masonry walls.

2.4 Analytical Models for Arching Action

McDowell et al. (1956) idealized a masonry brick beam restrained between rigid supports, as shown Figure 2.3. The idealized beam featured a uniform cross section and a span length, L, divided in two equal segments, $L/2$. It was observed that a beam subjected to out-of-plane loading deformed at midspan and developed cracks on the tension face at the ends and at midspan. Subsequent to cracking, it was assumed that each portion of the beam rotated about one end and at the center. A relationship was established to describe the beam deflection at midspan as a function of beam depth, u. Opposition to this motion was provided by a couple that was caused by opposing forces of equal magnitude, $P(u)$, separated by a lever arm , $r(u)$. The rotation, θ, continues to increase until either the load is removed or the beam collapsed.

The main assumption of this model is that the contact area (i.e. $2d$ x unit width) decreases when the midspan deflection increases. As shown in the Figure 2.3, a is measured vertically from the longitudinal axis to the nearest point of contact with the support, as given by equation [2.1]:

$$a = \frac{L}{4}\left(\frac{1-\cos\theta}{\sin\theta}\right) \qquad [2.1]$$

where θ is the angle of rotation of rigid body rotation of the beam half segment, and L is the total span length.

The deflection at midspan, w, is given in terms of the rotation by equation [2.2]:

$$w = L \left(\frac{1 - \cos \theta}{\sin \theta} \right) \qquad [2.2]$$

McDowell et al. (1956) introduced the dimensionless notation $u = \frac{w}{2d}$, and $n = \frac{2d}{L}$ to determine the variable R as shown in equation [2.3], which relates the masonry strain, the length of the masonry beam and its depth. This variable evaluates the state of stress (i.e. elastic and inelastic ranges) of the cross section at the supports and midspan and is used to compute, using Table 2.1, the forces and resisting moment due to arching effect:

$$R = \frac{e_c}{4n^2} = \frac{e_c L^2}{16 d^2} \qquad [2.3]$$

where e_c is the strain associated with crushing strength, and d is half of the wall depth.

The arching force per unit width of the beam $P(u)$ was determined as a function of the dimensionless parameter u and $\frac{4P(u)}{s_c d}$. In addition, the moment resistance of the beam, $M(u)$, was defined as the moment due to the arching force (i.e. forces generated in the contact areas) times the lever arm $r(u)$, and was computed for several values of R. The analytical expressions for $P(u)$ based on the state of stress in the contact area are given in terms of the dimensionless parameters, u and $\frac{4M(u)}{s_c d^2}$, as shown in Table 2.1.

Gabrielsen and Wilton (1974) noted that, when the arching action occurs, the wall acts as a restrained-end plate or slab until cracking takes place. After cracking has occurred, the wall still resists out-of-plane motion and forces. This post-fracture resistance results from the geometric fixity provided by the rigid edge frames. For instance, if a wall is fixed at the ends, cracks will occur at the top, bottom, and midspan of the structure and so will form two wall segments. The authors considered that both wall segments had a similar out-of-plane behaviour. Furthermore, the authors used computer software to represent one half of the wall as a strut model. Figure 2.4 illustrates such a model representing a brick wall segment subjected to static load. The effective vertical supports at the top and bottom ends were assumed to be located 25 mm inside the each face, which appeared to be the approximate location of the center of the resultant thrust force

10

resulting from crushing. This strut model demonstrated the influence of the compressive forces resulting from three-hinge arching action to enhance the flexural resistance of the full wall subjected to out-of-plane blast loading.

Abrams et al. (1996) conducted a series of experiments to study the effect of damage due to in-plane loads on the out-of-plane strength of eight unreinforced masonry infill panels. This study focused on the out-of-plane strength and behaviour of cracked infill panels subjected to transverse pressures, as shown in Figure 2.5(a). The authors suggested that cracked, unreinforced masonry panels might generate flexural strength as a consequence of axial compressive stress from internal struts which formed when the two portions of the panel tended to rotate by an angle θ_v with respect to the vertical. In this model, the panels of height L and thickness t were assumed to develop cracks at midspan. After cracking, an internal thrust force, T, was generated in the surface area affected by compressive stresses, b x unit length, to resist the applied pressure.

Based on the results of an experimental study, and using an analytical model, Abrams et al. (1996) suggested that the out-of-plane strength of a masonry wall will be governed by arching action. Figure 2.5(b) presents the upper wall segment used to clarify some of the terms used to determine the magnitude of the out-of-plane uniform pressure on the masonry wall. Equation [2.4] shows the magnitude of the out-of-plane uniform pressure, w_u, as a function of L/t ratio, b/t ratio, the maximum masonry compressive stress, f_b, and the angle γ between the thrust force and the vertical axis:

$$w_u = 2f_b \frac{b/t}{L/t} \sin \gamma \tag{2.4}$$

where b is the width of the compressed zone, t is the panel thickness and L the panel height.

Based on McDowell's theory, Drysdale and Hamid (2005) proposed a three-hinged model, as shown in Figure 2.6(a), which involves a bottom and a top segment of the masonry wall. It was noted that a compression zone is formed at midspan as both segments rotate. The compression zone was formed by the interaction of a portion of both segments as a result of their common contact area along wall thickness direction. During the rotation of both segments, the contact area is reduced by a portion of the thickness that is no longer in contatct, Γ. A value of $(1-\Gamma)t$ was

assumed as the depth of the compression zone, which depended of the wall geometry and size of the contact area between the two segments. However, the British Masonry Standard (BS 2005) simply recommends a depth of 10% of the wall thickness based on experimental results. A second assumption considered a constant stress, f_c, over the compression zone (i.e. f_c is defined as a force applied in a specific contact area that causes a continuous deformation in the masonry). These assumptions were made in an attempt to replicate a rectangular stress block for ultimate limit states design that included the strength and stability of the wall under the maximum design load (Figure 2.6(b)). The compression force per unit length resulting from the arching action, C_f, is given by [2.5]:

$$C_f = \phi_m f_c (1 - \Gamma) t \qquad [2.5]$$

where ϕ_m is the resistance factor for masonry that was taken to be equal to 0.60, t is the thickness of the wall and Γ is the portion of thickness of the masonry wall at midspan that is no longer in contact.

The relationship between the deflection δ resulting of the out-of-plane loading, and the factored resisting moment is the shown using equation [2.6]:

$$M_r = C_f (\Gamma t - \delta) \qquad [2.6]$$

Then, taking moments about point a located on the contact zone at the top of the upper wall segment, as show in the Figure 2.6(c), the factored lateral load resistance of the masonry wall is given in equation [2.7]:

$$w_f = \frac{8 C_f}{L^2} (\Gamma t - \delta) \qquad [2.7]$$

Recently, studies conducted by Varela et al. (2012) presented two analytical methods for computing the maximum out-of-plane pressure, w_u, that a masonry wall might resist such as: using 1) the compressive strut method (Figure 2.7), and 2) the spring-strut method (Figure 2.8). In the first method, the flexural strength was calculated from the equilibrium of horizontal forces between the acting pressure and the horizontal components of the compressive struts, C_1 and C_3, at points

B and C which are localized at the compressive face of a block course at midspan of the wall, and are computed using the equation [2.8] and [2.9].

$$C_1 = w_u \left(\frac{L_1}{2} + \frac{L_2}{2} \right) \qquad [2.8]$$

$$C_3 = w_u \left(\frac{L_2}{2} + \frac{L_3}{2} \right) \qquad [2.9]$$

where L_i is the vertical dimension of each wall segment

For the second method, Varela et al. (2012) tested six full-scale confined masonry walls subjected to uniform pressure using two airbags. The results were then compared with an analytical spring-strut model (Figure 2.8). This method used an iterative procedure for calculating the out-of-plane strength based on the assumption that the contact width between two consecutive wall segments was constant. The stiffness of the confining elements was included by using a linear spring placed on the top of the wall.

The analytical spring-strut method is initiated by assuming a horizontal displacement at midspan, Δ_h. The vertical displacement at the top of the wall, Δ_v, the angle of rotation of a wall segment, α, and spring force F_s are then computed. Assuming a linear relationship between axial deformation and stress up to the crushing strength of the wall, the axial deformation Δ_{vdi} of each wall segment is determined by using the equation [2.10]:

$$\Delta_{vdi} = \sqrt{\frac{2F_s \cos\left(\frac{\Delta_h}{\Delta_i}\right) \Delta_h \Delta_{ci}}{f_b L_i}} \qquad [2.10]$$

where Δ_{ci} is the axial deformation associated with crushing of a wall segment, f_b is the axial compressive strength of the masonry, and L_i is the vertical dimension of each wall segment.

Based on the relationship between the spring force F_s and the angle between the compressive strut and the vertical axis, γ_i, the compressive strut force C_i is obtained by the equation [2.11]:

$$C_i = \frac{F_s}{\cos(\gamma_i)} \qquad\qquad [2.11]$$

In the spring-strut method, the maximum out-of-plane pressure, w_u, is calculated by using the equation [2.12]:

$$w_u = \frac{C_1 \sin(\gamma_1) + C_3 \sin(\gamma_3)}{\left(\frac{L_1}{2} + L_2 + \frac{L_3}{2}\right)} \qquad\qquad [2.12]$$

The process has to be repeated for increasing horizontal displacements until the maximum value of w_u is obtained.

2.5 The Effects of Pre-Compression on Unreinforced Masonry Walls

Researchers have identified that the performance of a wall assemblage can be enhanced taking advantage of the inherent compression capacity using pre-compression procedures. Walls specimens were pre-compressed in a number of studies using mechanical devices positioned on the wall specimens or though prestressing methods.

Griffith and Vaculik (2005) built a series of 2.5 m high unreinforced wall specimens with a horizontal span lengths of either 2.5 m or 4 m, with loads applied using an air bag system, as shown in Figure 2.9. The walls were fixed on both sides and compressed before the test using two levels of vertical pressure (i.e. 0.05 MPa and 0.10 MPa) distributed along their top surface and compared with a non-compressed control specimen. The maximum displacement measured from the specimens with the highest pre-compression was 19% higher than the specimen without pre-compression. In this research, the wall featuring the highest precompression load was able to resist an out-of-plane loading that was 50% higher than the control specimen. Masonry walls did not show a sudden drop in resistance after reaching the ultimate strength and so had reasonably high ductility.

Studies involving prestressing procedures and rehabilitation techniques using different levels of an induced pre-compression force have shown that masonry walls can absorb a large amount of energy, as well as exhibit improved cracking resistance and ultimate load capacities (Dawe & Aridru 1993; Rodriguez et al. 1998). A study conducted on post-tensioned walls showed that this

14

method increased the cracking moment of masonry walls by a factor between eight to nine, with an average displacement ductility ratio of 52 (i.e. the ratio between the deflection at cracking to the deflection at the ultimate load level) when they were subjected to out-of-plane loading. Tendons in these walls were tensioned to an average of 28% of their ultimate tensile strength, while the walls were prestressed by an average magnitude of 0.89 MPa (Rodriguez et al. 1998). An average higher initial stiffness of approximately 155% at lower levels of applied pressure and an average of 99% higher cracking load resistance as compared to conventionally reinforced walls was observed in research conducted by Dawe and Aridru (1993), where a series of masonry concrete walls were prestressed to an average force of 7.5 kN.

A study investigating the behaviour of slender post-tensioned walls (aspect ratio: 38 and 40.5) with low magnitudes of prestress ranging from 0.24 MPa to 1.03 MPa concluded that the observed difference of the maximum moment resistance at the post-cracking stage is not substantially affected by the wide range in the magnitudes of prestress (Bean Popehn et al. 2007). Similar pre-compression procedures were considered in the rehabilitation of unreinforced walls by using carbon fibre rope reinforcement to enhance flexural capacity. Walls were subjected to out-of-plane pressure using an air bag. It was observed that by using this technique, the ultimate capacity of masonry walls increased by a maximum of 160%, in comparison with the control specimens (Korany & Drysdale 2006). Figure 2.10 shows a typical prestressed masonry wall and the normal stress distributions across the cross section. The stress in the masonry due to self-weight, W, and the induced stress due to the tensioned tendon, P_e, counteract the flexural tensile stress generated by the applied lateral load.

The researchers above described how pre-compression mechanisms can be used to enhance the out-of-plane resistance of the masonry. However, this construction method is more expensive than conventional methods since it requires highly skilled labor and specialized construction equipment. Alternative methods for increasing the capacity of structural elements made using brittle materials such as concrete have been studied to overcome the disadvantages of using prestressing techniques. However, to date, no studies have been identified that address this technique in walls with unbonded reinforcement.

2.6 Arch Action and Beam Action

The influence of the bond between concrete and reinforcement, as well as its contribution to the shear capacity of a reinforced concrete beam, was analyzed to determine how the shear forces are transferred once cracking has initiated. Figure 2.11 shows a portion of a concrete beam between two cracks, where V is the shear force, T_r is the tension force, C_b is the compression force, M is the bending moment, jd is the flexural lever arm (Wight & MacGregor 2009). Equation [2.13] is derived from Figure 2.11, as well as through force and moment equilibrium of the element:

$$\Delta T_r = \frac{V \Delta x}{jd} \qquad [2.13]$$

The relationship between shear, V, and the tension bar force, T_r, can be presented as Equation [2.14]:

$$V = \frac{d}{dx}\left(T_r jd\right) \qquad [2.14]$$

If the Equation [2.15] is expanded, two terms can be identified. The first term represents the beam action, while the second term represents the effect of arching action:

$$\frac{d}{dx}\left(T_r jd\right) = \frac{d(T_r)}{dx} jd + \frac{d(jd)}{dx} T_r \qquad [2.15]$$

When the flexural lever arm is constant along the beam span, $\frac{d(T_r)}{dx} jd$ is the shear flow transmitted across any horizontal plane in contact between the reinforcement and the surrounding concrete. However, when the reinforcement is unbonded, the shear flow is equal to zero, and the shear will be transferring by arching action, $\frac{d(jd)}{dx} T_r$ which requires a variation in the lever arm jd ; for instance, $\frac{d(jd)}{dx} \neq 0$.

2.7 Unbonded Reinforcement in Non-prestressed Concrete Beams

Concrete structures strengthened by unbonded reinforcement have shown promising behaviour that is relevant to the study of walls with unbonded reinforcement. Testing performed by Cairns and Rafeeqi (2002), and Kothandaraman and Vasudevan (2010) of simply supported concrete

beams with non-stressed unbonded reinforcement demonstrated appreciable increases in the ultimate flexural strength, crack control capability and structural efficiency.

Cairns and Rafeeqi (2002) tested nine tests of reinforced concrete beams. All beams featured cross sections of 230 mm with depths varying from 230 mm to 400 mm, and a span length of 3500 mm. Different reinforcing bar diameters and yield strengths that ranged from 497 MPa to 534 MPa were used in lightly and heavily reinforced specimens, respectively. Bars of 16 mm, 20 mm and 25 mm diameter with an ultimate tensile strength of 600 MPa were used as unbonded reinforcement. It was determined that external unbonded reinforcement can significantly increase the ultimate flexural strength of reinforced concrete beams. It was also observed that there was a variation in strain in the bonded reinforcement along the span length while the strain in the external non-prestressed unbonded reinforcement was uniform.

In this sense, non-pretensioned unbonded reinforcement is passively stressed only under structural deformation. In addition, the behaviour of beams strengthened with external unbonded reinforcement will result from a combination of flexural and tied-arch forms of structural action. Therefore, the typical calculation of flexural resistance based on traditional flexural theory is not valid.

Kothandaraman and Vasudevan (2010) tested four reinforced concrete beams which dimensions of 250 mm wide, 300 mm high, and 3000 mm long using single central point loading. Two control beams were built without external reinforcement while the other two beams included additional external reinforcing anchored at the ends of the beams. The ultimate tensile strength of the different sizes of reinforcement used ranged from 568 – 623 MPa. It was concluded that this technique could lead to considerable increases of approximately 70% in the moment capacity of the beam section. In addition, it was found that this method of strengthening reinforced concrete beams could be effective in enhancing ductile behaviour and crack control.

These investigations focused on the influence of unbonded reinforcement as a means to improve mechanical and physical properties of concrete beams. Results from these studies demonstrated possible improvements in the flexural capacity of the beam section ranging from 57% to 70%.

17
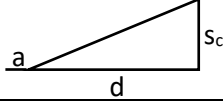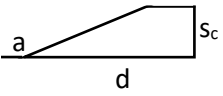
Relating these results to the current study, it would appear likely that the unbonded tension tie could be used to enhance the capacity of the masonry wall subjected to out-of-plane loading, as will be discussed in Chapter 3 and 4.

2.8 Summary

This Chapter presented a review of literature related to the flexural resistance of unreinforced walls and ways to enhance its out-of-plane resistance by taking advantage of the inherent compressive masonry capacity of masonry. One technique used in concrete elements to increase its flexural capacity and crack control has been introduced to demonstrate its relevance and applicability in masonry walls. It is well known that the lower flexural tensile strength of unreinforced walls under out-of-plane loading does not let the walls resist higher out-of-plane loads that may occur as a result of windstorms or earthquakes. Researchers revealed that this issue could be overcome using the arching action mechanism, pre-compressing the masonry walls, or through a prestressing technique.

Studies do not address the fact that non-prestressed unbonded reinforcement could be used to generate arching action in non-loadbearing unreinforced walls under simply supported conditions. The investigation discussed herein therefore includes an analysis of the use of unbonded reinforcement inserted in unreinforced walls. It has been observed that this mechanism restricts the vertical wall elongation resulting from out-of-plane loading. Walls with unbonded reinforcement have an inherent flexural capacity that could potentially be compared with the capacity of conventionally reinforced and grouted walls. The restoring wall capacity is also achieved since there is not a direct strain compatibility relationship between grout and reinforcement that prevents the wall from overcoming its brittle behaviour. The construction process of walls with unbonded reinforcement could be less time consuming that of conventionally reinforced and grouted walls. As a result, the overall cost of a project could therefore be reduced.

Table 2.1: Analytic forms for thrust force, and moment (McDowell et al.1956)

Range of R	Range of u	Stress distribution along contact area	$\dfrac{4P(u)}{s_c d}$	$\dfrac{4M(u)}{s_c d^2}$
$R \geq \dfrac{1}{2}$	$u \geq 0$			
$R < \dfrac{1}{2}$	$0 \leq u \leq 1 - \sqrt{1 - 2R}$		$\dfrac{2u}{R}(1-u)^2$	$\dfrac{8u}{3R}(1-\dfrac{5u}{4})(1-\dfrac{u}{2})^2$
$R < \dfrac{1}{2}$	$1 - \sqrt{1 - 2R} \leq u < \sqrt{2R}$		$4(1 - \dfrac{u}{2} - \dfrac{R}{2u})$	$4(1 + \dfrac{R}{2} + 3\dfrac{u^2}{4} - 2u - \dfrac{R^2}{3u^2})$

(a)

(b)

(c)

(d)

Figure 2.1: Wall support conditions: (a) ideal pin support along bottom edge of wall, (b) top ideal pin support, (c) realistic pin support along bottom edge of wall, and (d) top realistic pin support (Udey 2014).
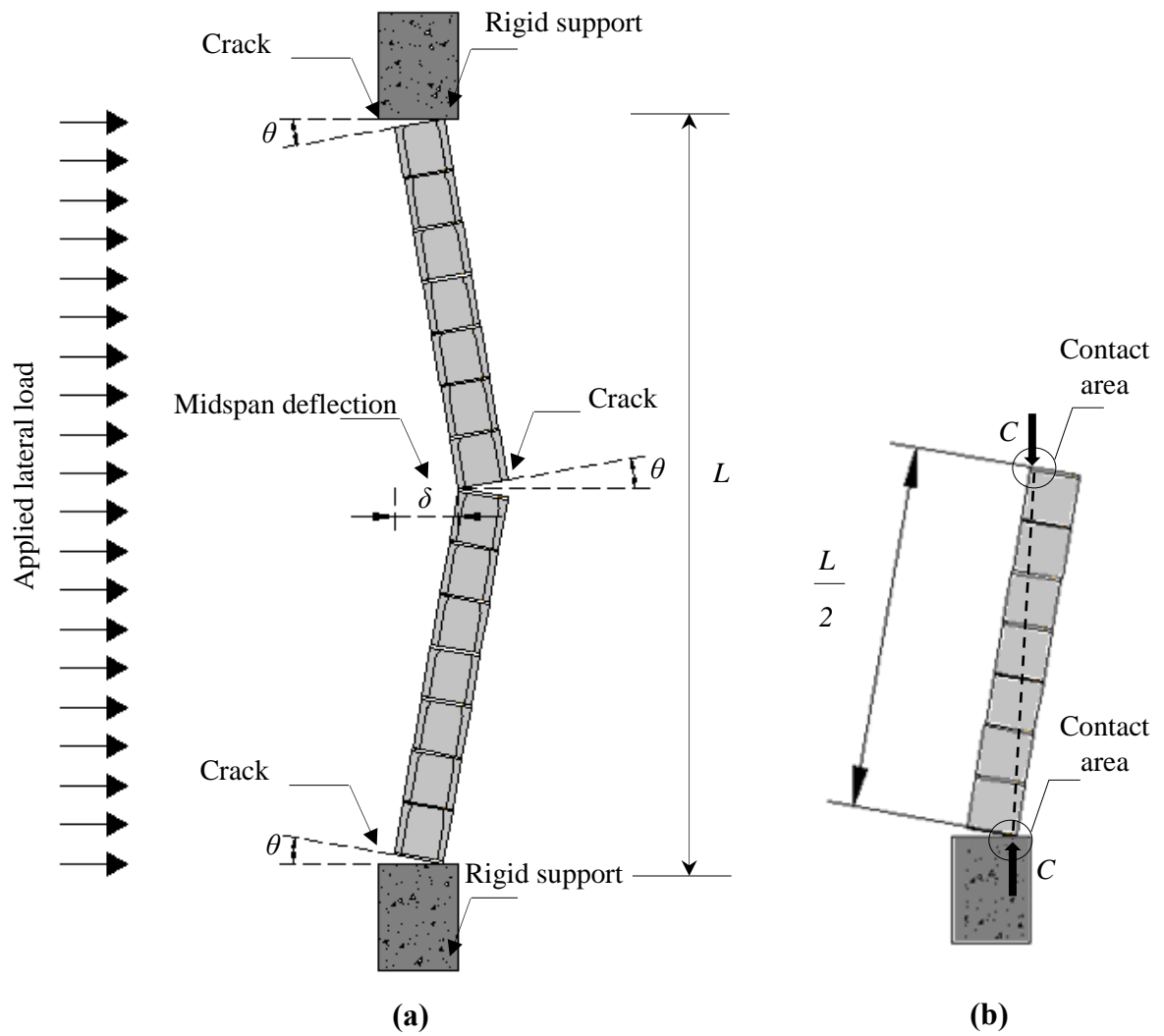
Figure 2.2: Arching mechanism in masonry walls: (a) deflected masonry wall, and (b) thrust force generated on the bottom masonry segment.
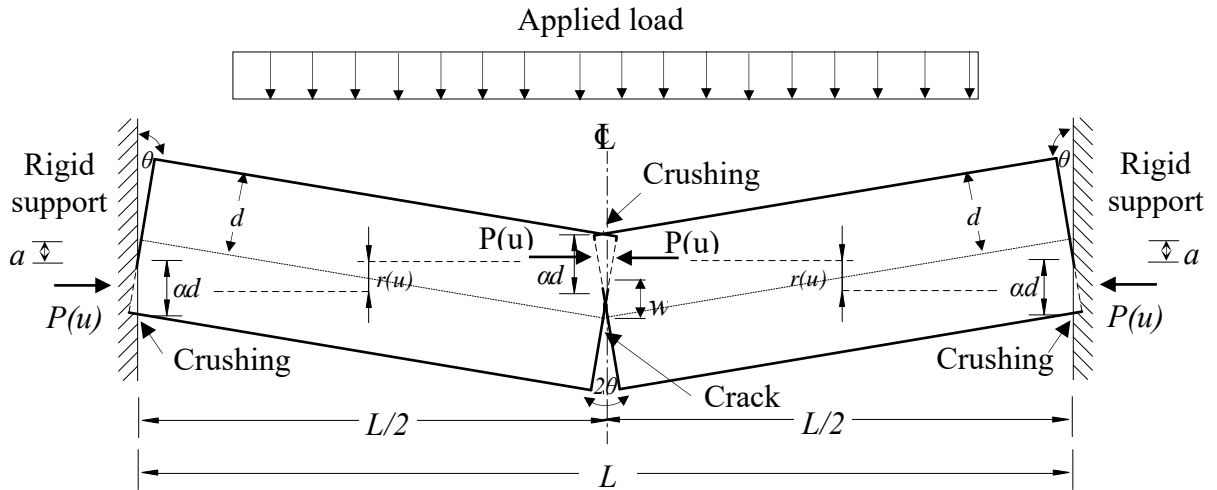
Figure 2.3: Idealized geometry of deformation of half of the span of a laterally restrained masonry beam (based on McDowell et al. 1956).
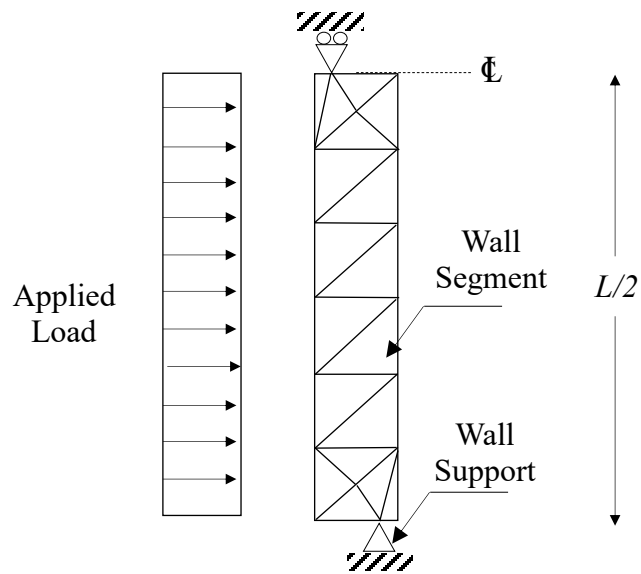
Figure 2.4: Strut model (based on Gabrielsen & Wilton 1974).
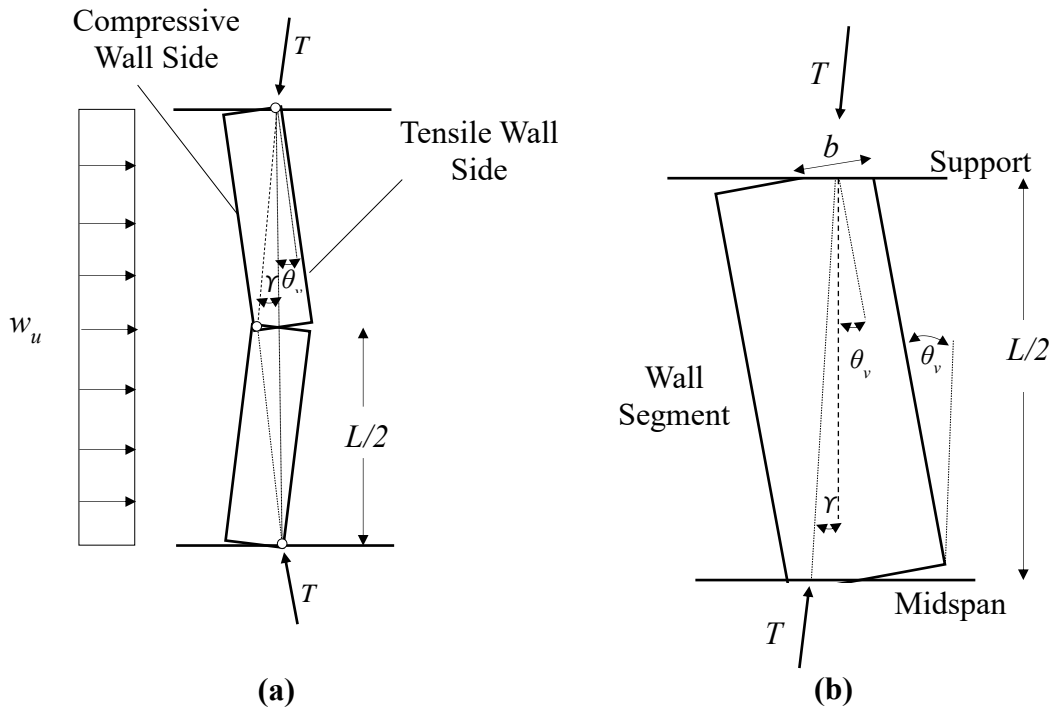
Figure 2.5: Idealized model for transverse arching action: (a) wall under out-of-plane pressure, and (b) top wall segment showing the geometry at the support (based on Abrams et al. 1996).
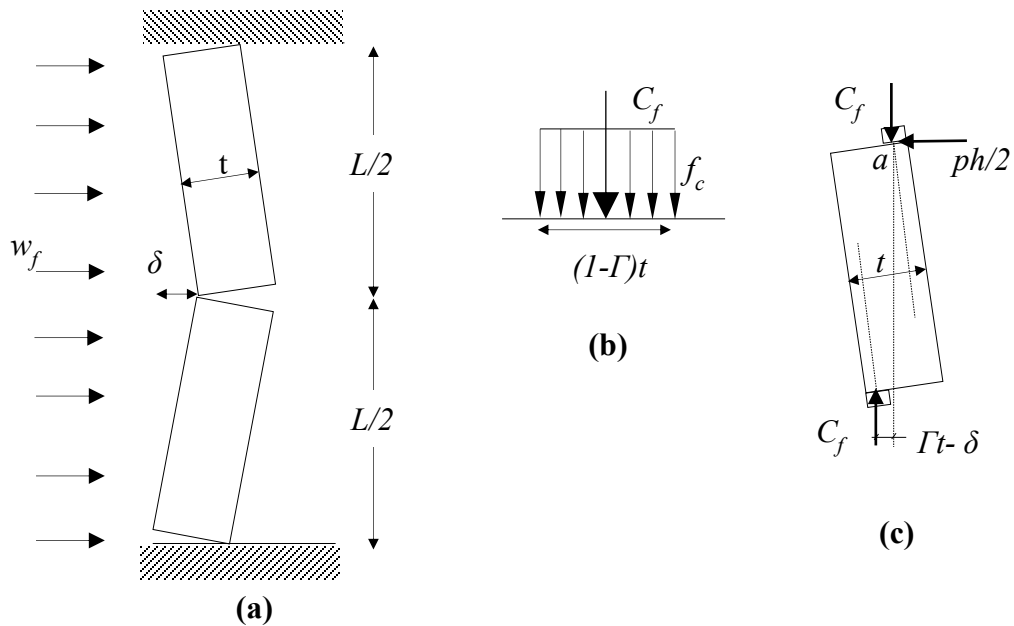
Figure 2.6: Three-hinged model for a deflected masonry wall: (a) wall subjected to out-of-plane pressure, (b) equivalent stress block of masonry, and (c) idealized wall segment model (based on Drysdale & Hamid 2005).
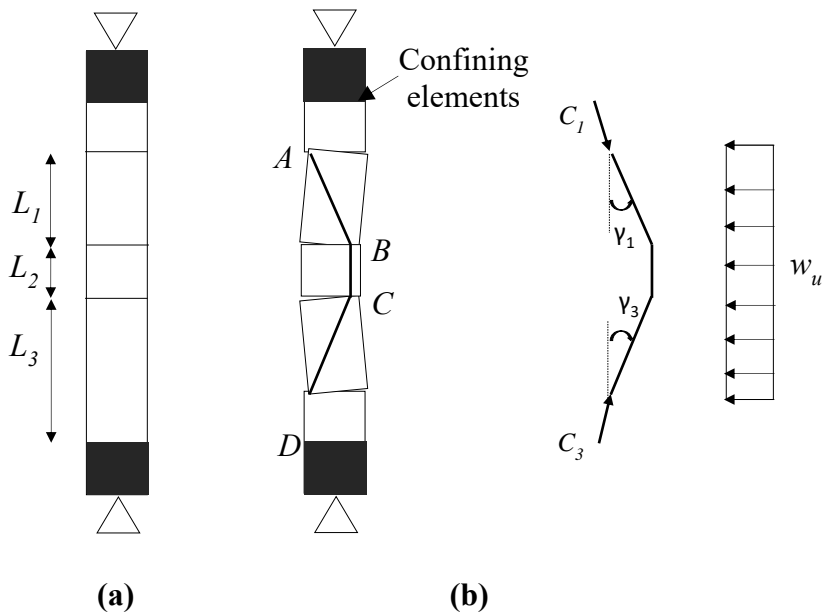
Figure 2.7: Strut method for computing the lateral wall pressure: (a) wall in its original position, and (b) equilibrium of horizontal forces on the wall (based on Varela et al. 2012).
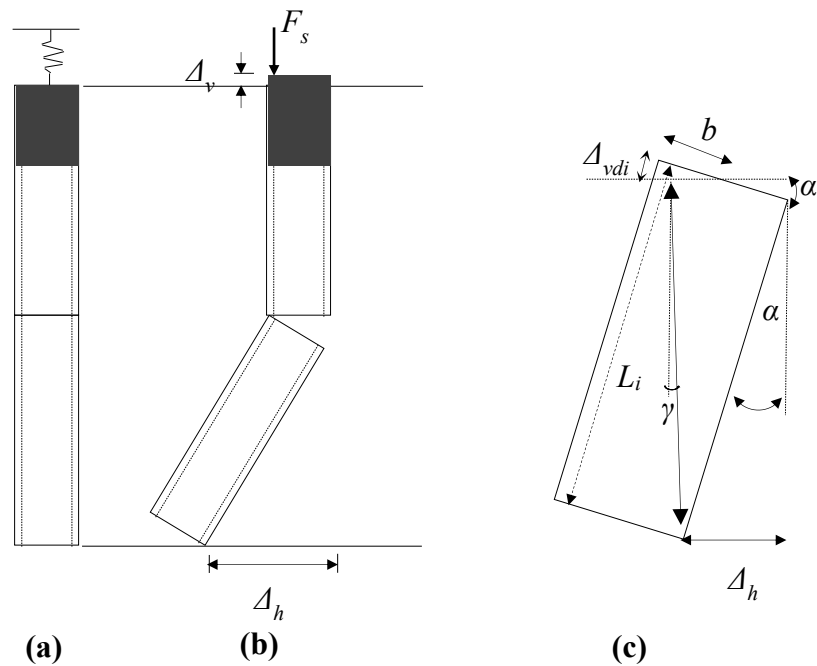
Figure 2.8: Spring-strut method: (a) wall showing a spring at the top representing the stiffness of the confining element, (b) wall in deflected position, and (c) geometry of the top wall segment (based on Varela et al. 2012).

Figure 2.9: Masonry wall test set-up (Griffith & Vaculik. 2005).
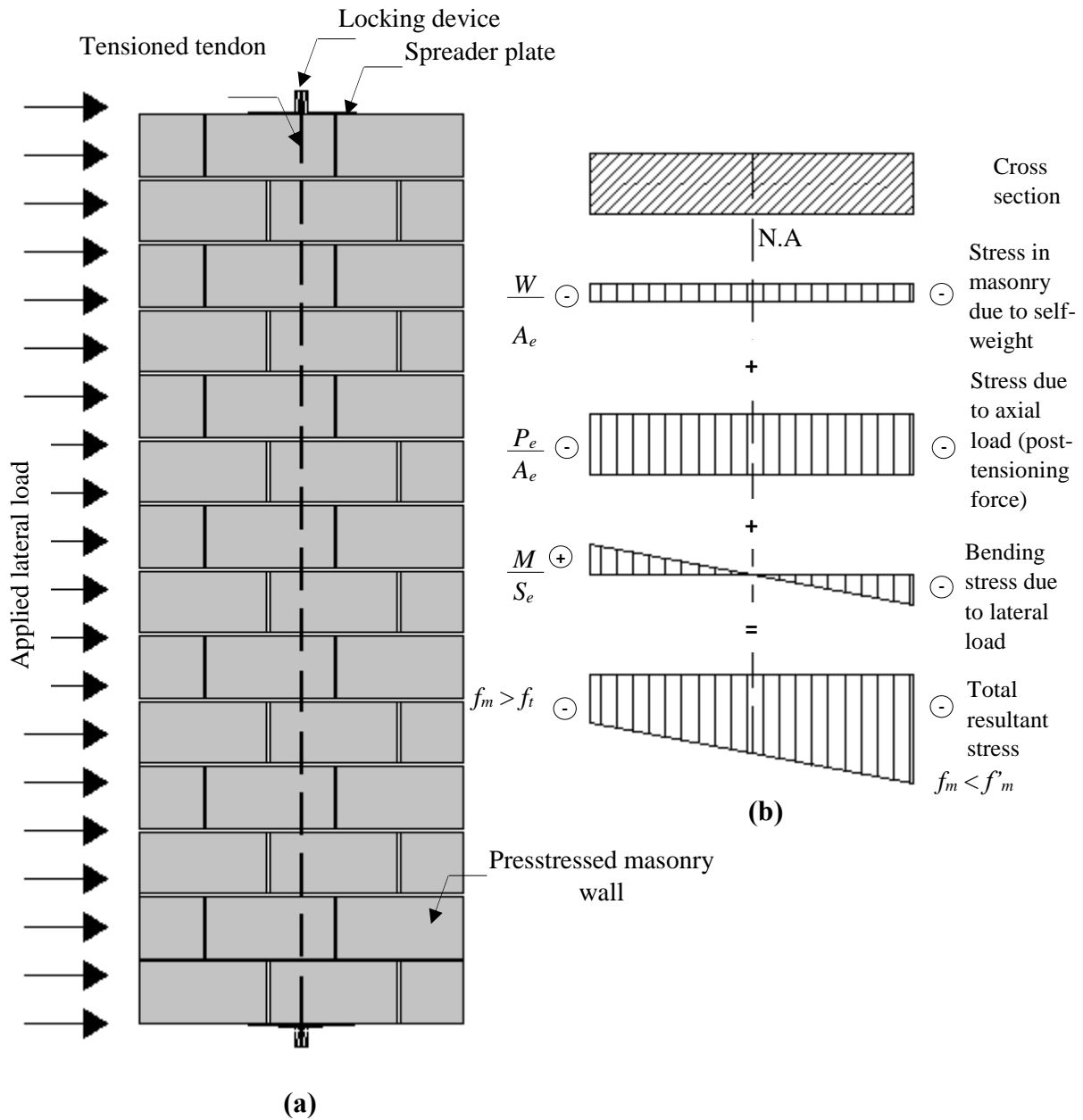
Figure 2.10: Prestressed masonry wall: (a) wall showing a prestressed tendon that is anchored at its ends using a locking device, (b) stress distribution in the masonry wall section (based on Curtin et al. 1989).
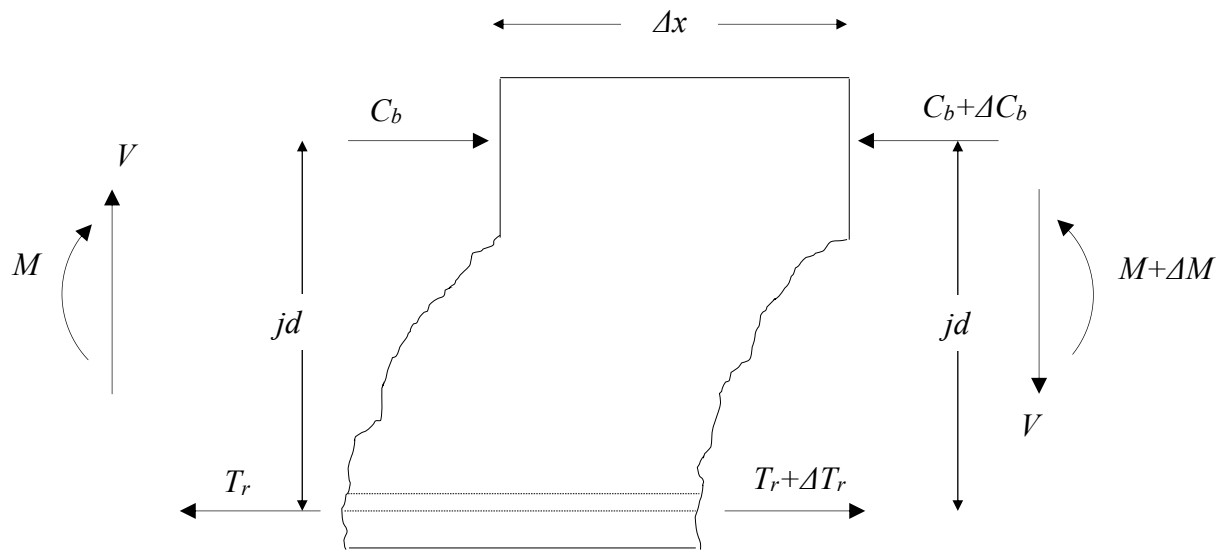
Figure 2.11: Segment of beam between two cracks (based on Wight & MacGregor 2009)

Chapter 3: Feasibility of Using Unbonded Reinforcement in Concrete Block Walls[1]

This Chapter presents the details of the specimen construction, instrumentation, and testing for an experimental program comprising 21 full-scale wall specimens. Two sets of control specimens, one consisting of unreinforced walls, and the other of conventionally reinforced and partially grouted walls, were included to allow for comparison with the ungrouted walls that included unbonded reinforcement. Since the test program was ongoing at the time that this manuscript was written, only results from the unreinforced and unbonded reinforced specimens are discussed in this Chapter. The test results presented here include visual observations of crack patterns and failure modes, load-deflection response, and ultimate capacity. Preliminary outcomes described herein comparing the walls with unbonded reinforcement to unreinforced walls suggest that this construction method is a promising alternative to more conventional systems. Results from the testing of the ungrouted walls which included unbonded reinforcement, and conventionally reinforced and partially grouted specimens are presented in Chapter 4.

3.1 Introduction

Unreinforced masonry walls cannot efficiently resist out-of-plane lateral loads such as those due to wind and earthquake since the resulting failure mode is generally governed by tensile cracking at mortar bed joints (Udey 2014). The inherently low tensile strength of the mortar, exacerbated by imperfect bond between the mortar and the concrete block units, severely limits the flexural capacity of such walls. As a result, the compressive strength of the concrete blocks is never fully realized.

The efficiency and flexural resistance of masonry walls can be significantly improved by providing longitudinal reinforcement in select block cells, with the reinforcement grouted in place to ensure strain compatibility with the surrounding cementitious materials (Drysdale & Essawy 1988). While the vertical span of unreinforced masonry walls is typically limited to a single storey, reinforced and partially grouted masonry walls can span much greater distances, making them

---

[1] A version of this chapter has been published as: Miranda H, Feldman, L.R., & Sparling B.F. (2016). Feasibility of using unbonded reinforcement in concrete block walls. Proceedings of the 2016 CSCE Annual Conference, London, ON. Retrieved from https:// ir.lib.uwo.ca.

more useful for open interior spaces such as building atriums or school gymnasiums. However, such construction methods are time consuming, increase project costs, and increase the risk of workplace injuries since they require workers to thread blocks up and over reinforcement that has already been grouted in place. The grout also substantially increases the dead load, with a fully grouted wall weighing approximately twice as much as a comparable ungrouted wall.

A novel solution was therefore sought to increase the out-of-plane flexural capacity of masonry walls while avoiding the disadvantages associated with conventionally grouted reinforcement. As such, an experimental investigation was conducted to study the use of non-prestressed, ungrouted and unbonded internal reinforcement in masonry walls to determine the resulting load-carrying capacity and serviceability characteristics. By anchoring the unbonded reinforcement at the top and bottom ends of the wall specimens, arching action can be engaged to resist the applied lateral loads and better utilize the compressive capacity of the masonry assemblage.

The experimental program was intended to provide a proof-of-concept validation for the use of unbonded reinforcement in masonry walls with well-defined loading and boundary conditions. Since it is recognized that the construction method employed herein would not be feasible in practice, further investigation will have to be undertaken to develop and evaluate a practical implementation strategy.

3.2 Experimental Program

A total of twenty-one concrete masonry block wall specimens were included in this experimental program with an explanation of the sample size determination included in Appendix A. All specimens were constructed with standard 200 mm concrete blocks laid in running bond by an experienced mason using standard Canadian construction practices. Three general categories of specimens were included: unreinforced walls, conventionally reinforced and partially grouted walls, and ungrouted walls that included unbonded reinforcement. The walls were tested to failure under monotonically increasing quasi-static lateral loading using a four-point loading system. The unreinforced and conventionally reinforced specimens served as control specimens that were used as benchmarks against which the performance of the wall specimens with unbonded reinforcement

could be compared. The following sections describe the construction, testing, instrumentation, and material properties used.

3.2.1 Specimen Details

Figure 3.1 shows the elevation and representative cross-sections for the wall specimens included in this investigation. All specimens were 14 courses high and two-and-one-half blocks wide (approximately 2.8 m tall by 1 m wide), and featured standard 10 mm concave tooled mortar joints. Six of the wall specimens were unreinforced, six were conventionally reinforced and partially grouted, while the remaining nine specimens featured unbonded reinforcement. Longitudinal reinforcement for both the conventionally reinforced and unbonded reinforced specimens consisted of 6.4 mm diameter deformed steel bars conforming to ASTM A1064/A1064M (ASTM 2016a).

All specimens were laid atop reinforced concrete grade beams to reproduce a support condition commonly encountered in practice, with a 10 mm mortar joint included between the grade beams and the first masonry course. The grade beams were 1700 mm long, extending beyond the block wall on each side, to allow the grade beams to be securely clamped to the laboratory strong floor during testing. Grade beams used for the unreinforced (Fig. 1(a)) and conventionally reinforced (Fig. 1(b)) wall specimens were 300 mm wide and 400 mm tall. These grade beams were longitudinally reinforced with four No. 15 bars, one located at each corner, and No. 10 stirrups at 300 mm on-centre. Appendix B presents the construction process for all concrete grade beams.

The grade beams used for the walls featuring unbonded reinforcement (Fig. 1(c)) had the same overall dimensions as those used for the other specimens, but required modifications to accommodate the dead-end anchors used to secure the unbonded reinforcement. For this purpose, two 200 mm tall x 200 mm long full-width blockouts were constructed at the bottom of the grade beams, each located 100 mm on either side of the centreline of the grade beam. The anchors bore against 240 mm x 153 mm x 9.7 mm thick steel plates embedded at the top of the blockouts; the anchor plates included a central 20 mm hole through which the wall reinforcing bars could pass. In addition, 20.9 mm diameter PVC ducts were cast into the grade beams directly above both anchor plates to allow the wall reinforcing bars to pass freely through the grade beam.

Modifications to the grade beam reinforcement required to accommodate the blockouts are illustrated in Figure 3.1(c).

The unreinforced wall specimens were constructed in a single lift and were ungrouted (see Figure 3.1(a)). The conventionally reinforced walls shown in Figure 3.1(b) were constructed in two lifts, with the first lift consisting of eight courses, and the second consisting of six courses. After the blocks for the first lift were placed, the reinforcing bars were placed in the first interior cell on either end of the wall specimens. The reinforced cells in the first lift were then grouted and allowed to cure for a minimum of 24 hours prior to erecting the second lift of masonry. Blocks in the second lift needed to be threaded over the reinforcing bars that were already grouted in place. Reinforced cells within the second lift were then grouted. The steel reinforcing bars were centered in the cells and held in place using welded wire mesh templates cast in the bed joints above the second, fourth, sixth, ninth, eleventh, and thirteenth masonry courses. Plywood strips with holes drilled through to accommodate the reinforcing bars were placed on top of the fully erected walls to further maintain the position of the reinforcing bars during placement of the second lift of grout and curing.

As shown in Figure 3.1(c), the configuration of the reinforcing bars for the nine wall specimens constructed with unbonded reinforcement was similar to that of the conventionally reinforced specimens, except that the reinforced cells were not grouted; instead, the reinforcing bars were anchored at the top and bottom ends of the wall using anchor chucks. In the absence of grout, one of the challenges was to maintain the position of the reinforcing bars in this specimen set, not just during construction, but also during testing, since the relative distance between the compression face of the wall and the reinforcing bars was a critical factor in determining the flexural resistance of the wall. As a result, more robust reinforcing spacers were required for these walls than the welded wire templates used in the conventionally reinforced specimens. Figure 3.2 therefore shows the 100 mm x 110 mm x 5 mm thick steel alignment plates that were placed horizontally in the bed joints above the second, sixth, eighth, and twelfth block courses. These plates had 12 mm diameter holes drilled at their centre to allow the reinforcing bars to pass through. To maintain the position of the alignment plates within the block cell, vertical 60 mm x 40 mm x 5 mm thick steel plates were welded to the underside of the horizontal plates 25 mm in from both ends such that the

31

vertical plates would fit fairly snugly adjacent to the face shell on either side of the cell when the alignment plate was seated within the block; the vertical plates also helped transfer to the block face shells any lateral loads generated by kinking of the reinforcing bars at the alignment plate locations during testing. Guide ropes were threaded up through the holes in the alignment plates as construction progressed so that the reinforcing bars could ultimately be pulled through the reinforced cells from the top end once the walls were constructed to their full height.

Prior to installation, the reinforcing bars for the unbonded specimens were instrumented with eight UFLA-1-11 120 Ω full bridge circuit metallic strain gauges (Tokyo Sokki Kenkyujo Co., Ltd.); pairs of gauges were located at 2500, 2600, 2700, and 2900 mm from the bottom of the wall or, in other words, at the level of the bed joints above the eleventh, twelfth, and thirteenth masonry courses. Wires connected to the strain gauges were threaded up through the reinforced cells and out the top of the specimen to be connected to the data acquisition unit.

To generate the required arching action in the walls with unbonded reinforcement once significant cracking and displacements had occurred, the compressive thrust force had to be transferred through the block webs from the loaded face of the wall at the crack located near mid-height to the unloaded face at the base of the wall (see Figure 3.3). The resulting potential for premature web failure near the base of the wall was mitigated in six of the nine unbonded specimens by fully grouting the bottom course of blocks; for purposes of comparison, the bottom course in the remaining three unbonded walls was left ungrouted. In the case of the six specimens with a grouted bottom course, the PVC tubing used in the grade beams was extended into the wall by a minimum of 200 mm so that the reinforcement could pass freely through the grouted first course. The grouted first course in those six walls was allowed to cure for a minimum of 24 hours prior to proceeding with the remainder of the wall construction. Since the top course of the wall bore more uniformly on the top support plate, web failure due to the action of the thrust force near the top support was deemed to be less of an issue, so that grouting of the top course was not done in any of the unbonded specimens.

Transverse reinforcement was not required in any of the specimens since the shear resistance of the specimens was calculated to be considerably greater than the appled shear at the predicted

flexural resistance based on CSA Standard S304-14 (CSA 2014d) and so would not govern. Once constructed, all specimens were cured in the laboratory for a minimum of 28 days prior to testing.

In preparation for testing, the walls were moved from their as-constructed position to the test bed, taking care to avoid cracking the specimens. Steel cross-beams were then placed over the grade beams on either side of the masonry wall and anchored to the strong floor in the Structures Laboratory. To simulate a roller support at the top of the wall capable of providing lateral restraint without generating a bending moment or axial force, a 100 mm x 460 mm x 25 mm steel plate was placed on top of the wall and connected to a rigid reaction frame by three horizontal steel rods that were pin-connected to lugs on the top plate at one end, and to the reaction frame at the other (see Figure 3.4); a layer of plaster was first applied to the top of the wall to ensure uniform contact. The horizontal reaction was provided by a 1.0 m long 75 mm x 75 mm x 5 mm structural angle bolted to the underside of the top plate and positioned with its vertical leg in secure contact with the unloaded face of the wall.

The roller support at the top of the wall was deemed to be a conservative approximation of the guide-angle supports typically used in practice for non-loadbearing walls. Binding of the wall within the guide-angle supports as the wall displaces laterally can generate compressive axial forces in the wall (Udey 2014) that would effectively supplement the arching action associated with the unbonded reinforcement. In a similar manner, moderate levels of superimposed axial loads applied at the top of a loadbearing wall would increase the resultant compressive force, thus complementing the arching behaviour. The boundary conditions at the base of the wall specimens (i.e. a mortar joint laid directly on a concrete grade beam), on the other hand, was representative of a detail typically employed in practice.

For specimens featuring unbonded reinforcement, the reinforcing bars were passed through 19 mm diameter holes drilled in the top plate and secured with the live-end anchor chucks that bore on the top plate, as well as with the dead-end anchor chucks positioned within the grade beam blockouts. Just prior to testing, the unbonded reinforcing bars were minimally stressed to an initial load of approximately 630 N (i.e. 3.6% of their actual yield force) to eliminate any slack in the bars and

so ensure that they would resist load from the start of testing. Reinforcement in the conventionally reinforced walls terminated at the top of the wall.

A typical test setup is shown in Figure 3.5. A single MTS^{TM} hydraulic actuator and a spreader beam assembly, centered at mid-height of the wall, was used to produce the four-point loading arrangement; the load points were vertically separated by 930 mm (i.e. the load points were located 465 mm on either side of the specimen mid-height), creating a constant bending moment zone in that region. The statically determinate spreader beam system was designed to ensure a symmetrical load distribution. Furthermore, the horizontal spreader beams at both load points extended the full width of the wall to produce uniform loading in the transverse direction. The load was applied under displacement control at a constant rate of 3 mm/min, except during the first test (specimen UR-1) for which the loading rate was set at 1 mm/min. In addition, six Linear Variable Differential Transducers (LVDTs) with a linearity error of ±0.35% were positioned on the unloaded face of each wall during the test to measure wall deformation and determine wall profiles. LVDTs are electro-mechanical devices that converts lineal motion to an electrical signal which is processed using a data acquisition system; therefore, the output is a linear measurement (i.e. millimeter) related to a specific location along the wall specimen.

3.2.2 Material Properties

Hollow concrete masonry units with frogged ends were obtained from a single batch of material via a local supplier. The concrete units were delivered to the Structures Laboratory well in advance of construction to allow for the block temperature to equilibrate with that of the laboratory. The 15 MPa standard concrete blocks measured 390 mm long x 190 mm wide x 190 mm high. Half blocks were produced by cutting whole blocks in two, thus ensuring all masonry units had the same material properties. The compressive strength of the blocks was determined by using the testing protocol in ASTM Standard C140/C140M-16 (ASTM 2016b). An average compressive strength value of 22.2 MPa (COV = 6.8%) was calculated using the net cross-sectional block area based on the results of six tests. Section C.1.1 in Appendix C shows the testing results of concrete blocks units in detail. Additionally, this section presents the procedure performed to obtain the compressive strength for the block units.

Mortar was prepared in the laboratory in accordance with CSA Standard A179-14 (CSA 2014b) using Type S mortar cement, and a 1:3 masonry cement-to-sand ratio. Nineteen mortar cubes were cast and tested in accordance with CSA Standard A179-14 (CSA 2014b). The average overall compressive strength for the mortar batches included in wall specimens tested thus far was 18 MPa with a coefficient of variation of 20%. A more detailed explanation of the mortar preparation and the mortar samples is provided in Section C.1.2 in Appendix C.

The grout was also prepared in the laboratory in accordance with CSA Standard A179-14 (CSA 2014b) and consisted of Type GU cement, aggregate with a maximum particle size of 10 mm, and a 5:1 aggregate to cement ratio by weight. A water-to-cement ratio between 0.95 and 1.00 was used in the batching process and the target slump value immediately following batching was 250 mm. The average result from the slump tests was approximately 231 mm. Thirty non-absorbent 75 mm diameter by 150 mm long grout cylinders (three from every batch of grout) were cast and tested in accordance with CSA Standard A179-14 (CSA 2014b). In addition, thirty absorbent 190 mm high x 100 mm wide grout prisms (three per grout batch) were cast and tested in conjunction with the wall specimens and tested in accordance with ASTM Standard C1019-16 (ASTM 2016c). The average compressive strength of the non-absorbent grout cylinders and absorbent grout prisms were 21.9 MPa (COV = 5.1%) and 13.4 MPa (COV = 4%), respectively. Section C.1.3 in Appendix C describes the material components for the grout preparation, the procedure to build the absorbent and non-absorbent companions, and their compressive strength results.

No. 10 and 15 Grade 400 hot-rolled reinforcing bars conforming to CSA Standard G30.18-9 (CSA 2014e) were used to reinforce the grade beams. Bars of each size were obtained from a single heat batch of material. Six samples of each bar size acquired from excess lengths of material were tested in accordance with ASTM Standard A370-16 (ASTM 2016d) to establish their material properties. The average yield strengths were 533 MPa (COV = 0.7%) and 464 MPa (COV = 1.8%) for the No. 10 and 15 bars, respectively.

Deformed steel bars with a diameter of 6.4 mm conforming to ASTM A1064/A1064M-16 (ASTM 2016a) were used to longitudinally reinforce the wall specimens, where applicable. These bars had a nominal yield stress of 515 MPa. Six samples of these bars were tested in accordance with

35

ASTM Standard A370-15 (ASTM 2015) to establish their average actual yield strength of 537 MPa (COV = 2.7%). Section C.1.4 in Appendix C shows the procedure used to obtain the yield strength, tensile strength, and Young's modulus of the deformed steel bar.

One standard ungrouted one-block-wide by three-course-tall prism was constructed alongside each unreinforced wall, as well as specimens containing unbonded reinforcement. One fully grouted prism of the same dimensions was constructed in conjunction with each conventionally reinforced and partially grouted wall specimen. Prisms were constructed and tested in accordance with CSA Standard S304-14 Annex D (CSA 2014d) with compressive strengths as reported in Table 3.1. Section C.2 in Appendix C presents the procedure for the construction of the masonry prisms associated with each wall specimen.

3.3 Discussion of Test Results

At the time of writing this manuscript, 12 of the 21 wall specimens had been tested: six unreinforced (UR) specimens, three specimens with unbonded reinforcement and no grouting in the first course of blocks (UB-U), and three specimens with unbonded reinforcement and grouting in the first course of blocks (UB-G). A summary of preliminary test results is presented in Table 3.1, including strength of the masonry prism associated with each wall specimen, the applied load at cracking, the ultimate load, and the midspan deflection at the ultimate load. In addition, plots of the total applied load versus midspan deflection for the wall specimens tested at the time that this manuscript was prepared are provided in Figure 3.6(a); a separate plot featuring only the unreinforced specimens is also included in Figure 3.6(b) for clarity due to the large difference in vertical scale between the unbonded reinforced (UB) and unreinforced (UR) wall plots. More detailed discussions of the test results are presented in the sections below.

3.3.1 Cracking, Deflections and Failure Modes

As suggested in Table 3.1, the initial cracking in the unreinforced walls occurred at relatively low applied load levels ranging from 0.28 – 0.49 kN. It should be noted that this first cracking load was detected based on observed discontinuities in the load-deflection plots, rather than by the identification of visible cracks. In all but one specimen (UR-2), the first visible crack appeared in the mortar joints within the constant moment region near mid-height (at the bottom of courses 7 –

10); specimen UR-2, on the other hand, exhibited a visible crack above of the first course of blocks prior to a second crack forming near mid-height. Somewhat surprisingly, only unreinforced walls UR-1 and UR-2 developed visible cracks at the base of the wall.

Figure 3.6(b) shows that five of the six unreinforced specimens exhibited a definite load-deflection plateau, maintaining load levels similar to the peak applied load over a displacement range that varied between approximately 7 – 18 mm prior to failure. Since an ideal pinned support at the base of the wall would have resulted in the creation of a collapse mechanism immediately after the formation of a mid-height crack (Udey 2014), this suggests that the grade beam support used in this study retained some minimal moment capacity after the initial formation of cracks, possibly as a result of the accumulation of mortar within the cells at the base of the wall and/or the resisting couple created by the wall self-weight as the vertical support reaction shifted from the middle of the wall to the unloaded face as the base of the wall rotated under load. For all of the unreinforced wall tests, the failure condition was defined as the point at which the MTS^{TM} load control system detected a sudden drop in load-carrying capacity, rather than by total collapse of the wall.

As indicated in Figure 3.6(a), the first wall tested with unbonded reinforcement (UB-U1) exhibited much higher displacements and a lower apparent load-carrying capacity than the remaining five unbonded specimens. This was attributed to the fact that the system used to anchor the grade beam to the strong floor was not sufficiently rigid, allowing the grade beam to rotate appreciably; this rotational flexibility may have also contributed to the lack of visible cracking at the base of the unreinforced specimens, as noted above. For subsequent tests of walls with unbonded reinforcement, a more rigid anchorage system was implemented that appeared to adequately restrain the grade beam. This proved to be an important factor in improving the performance of the unbonded reinforced walls since it forced a sizable crack to form at the base of the wall, as well as near mid-height, thereby increasing the rate at which strain was induced into the unbonded reinforcement with increasing wall displacements.

For the remaining five wall tests featuring unbonded reinforcement, the initial visible cracks appeared in a mortar joint on the unloaded face of the wall within the constant moment region, followed by a crack at the base of the wall on the loaded face of the wall. As shown in Figure

3.6(a), the load carrying capacity of those specimens then continued to increase at an approximately constant rate with increasing wall displacements until large lateral displacements in the range of 30 – 60 mm had been attained. At this point, the mortar joint cracks near mid-height and at the base of the wall were both excessively large (12-17 mm); in addition, the wall segments above and below the mid-height crack were noticeably inclined (approximately 2 to 3° with respect to the vertical).

The tests were terminated prior to collapse of the wall when the MTS^{TM} loading system detected a sudden drop in load-carrying capacity. Although the cause of the drop in capacity could not be determined precisely, it is speculated that there may have been shear-related slippage at the mid-height cracked mortar joint brought about by large axial loads in the increasingly inclined wall segments on either side of the crack. It should be noted, though, that crushing was not observed in the mortar joints or blocks at that point, and that the average strain in the unbonded reinforcement was below (or, in the case of specimen UB-G3, just above) the nominal yield strain. Furthermore, upon unloading, the walls returned very nearly to their initial undeformed position, with the cracks closing to the point where they were hardly visible. When an attempt was made to reload specimen UB-U1 after the initial failure and unloading, it was found that the wall specimen exhibited a stiffness comparable to its post-cracking response in the initial load cycle.

3.3.2 Lateral Load-Carrying Capacity

It is evident from Table 3.1 and Figure 3.6(a) that the addition of unbonded reinforcement substantially increased the lateral load-carrying capacity of the masonry walls considered in this experimental program as compared to similar unreinforced walls. Specifically, the average ultimate applied load resisted by the walls featuring unbonded reinforcement was 356% higher than that for the unreinforced specimens; in making this comparison, specimen UB-U1 was excluded due to the issues related to support anchorage flexibility, as discussed above. It is also interesting to note that the ultimate condition in the walls with unbonded reinforcement appeared to be limited as much by geometric considerations (large crack widths and the slope of the cracked wall segments) as by material strength.

In the wall specimens featuring unbonded reinforcement without grouting in the bottom course, no evidence of premature failure or distress was observed in the webs of the lower block courses due to transfer of the thrust force from the loaded to the unloaded face under arching action. The slight increase in capacity and stiffness seen in the unbonded specimens with a grouted first course (particularly UB-G2 and UB-G3), as compared to those with an ungrouted first course (UB-U2 and UB-U3) may be attributed more to an improvement in the alignment of the unbonded reinforcing bars over the first course due to the presence of the grout than to any strengthening effect that the grout had upon the webs. It can therefore be concluded that, for the wall configurations considered in this program, that grouting of the first course was not necessary to avoid web-related failures under arching action.

3.4 Summary and Conclusions

An experimental program was undertaken at the University of Saskatchewan to investigate the use of unbonded, non-prestressed reinforcement in concrete masonry block walls in order to enhance resistance to out-of-plane lateral loads. When the test program was ultimately completed, a total of 21 full-scale wall specimens were tested to failure: six unreinforced specimens, six conventionally reinforced and partially grouted specimens, and nine specimens with unbonded reinforcement. Preliminary results from tests of the six unreinforced walls, along with six of the nine walls featuring unbonded reinforcement were presented in this chapter.

The inclusion of unbonded, non-prestressed reinforcement was found to produce a dramatic increase in both the lateral load-carrying capacity and ductility of the wall specimens. For the wall configurations considered in the study to date, the average lateral capacity of the walls was seen to increase by 356%, while the average lateral displacement at failure increased by 690%, as compared to those of unreinforced companion specimens. Since the strain, and hence the resisting force, in the reinforcing steel was largely governed by the displaced geometry of the wall specimens (i.e. rigid-body rotation of the wall segments after cracking near mid-height and at the base), it can be expected that walls with the same thickness but higher slenderness ratios will experience similar increases in bending moment capacity with the addition of unbonded reinforcement, albeit at higher lateral displacements; however, that would have to be verified by further testing. It was evident, though, that the tensile action of the unbonded reinforcement greatly

enhanced the lateral stability of the walls considered in this study, even at very large lateral displacements, since the walls invariably returned to a straight configuration immediately after the load was removed.

Due to the potential benefits associated with the elimination of the need for grouting, including lower wall self-weight and improved constructability, the use of unbonded, non-prestressed reinforcement appears to hold significant promise based on the outcomes of this study. While this study was intended primarily as a proof-of-concept investigation, future research will be required to address the development and evaluation of methods by which unbonded reinforcement can be effectively incorporated into masonry walls in practice.

Table 3.1: Preliminary test results

Specimen ID	Prism Strength (MPa)	Measured Cracking Load (kN)	Ultimate Load (kN)	Midspan Deflection at Ultimate Load (mm)
Unreinforced:				
UR-1	22.3	0.28	1.49	1.6
UR-2	21.9	0.37	2.32	0.4
UR-3	21.2	0.49	1.60	16.7
UR-4	19.4	0.37	1.42	0.6
UR-5	18.4	0.35	1.75	18.1
UR-6	20.2	0.35	1.12	3.5
Average:	20.5	0.37	1.62	6.8
COV (%):	6.7	18.5	22.8	110.9
Unbonded:				
UB-U1	23.2	1.77	4.35	85.5
UB-U2	20.6	0.75	6.89	62.0
UB-U3	21.4	1.54	6.80	58.0
UB-G1	19.7	1.69	8.51	39.2
UB-G2	20.2	1.69	7.49	52.9
UB-G3	20.6	2.27	7.27	56.6
Average:*	20.5	1.59	7.39	53.7
COV (%):*	2.7	30.7	8.3	14.6

* Excluding specimens UB-U1 as this grade beam was not appropriately anchored to the laboratory floor.
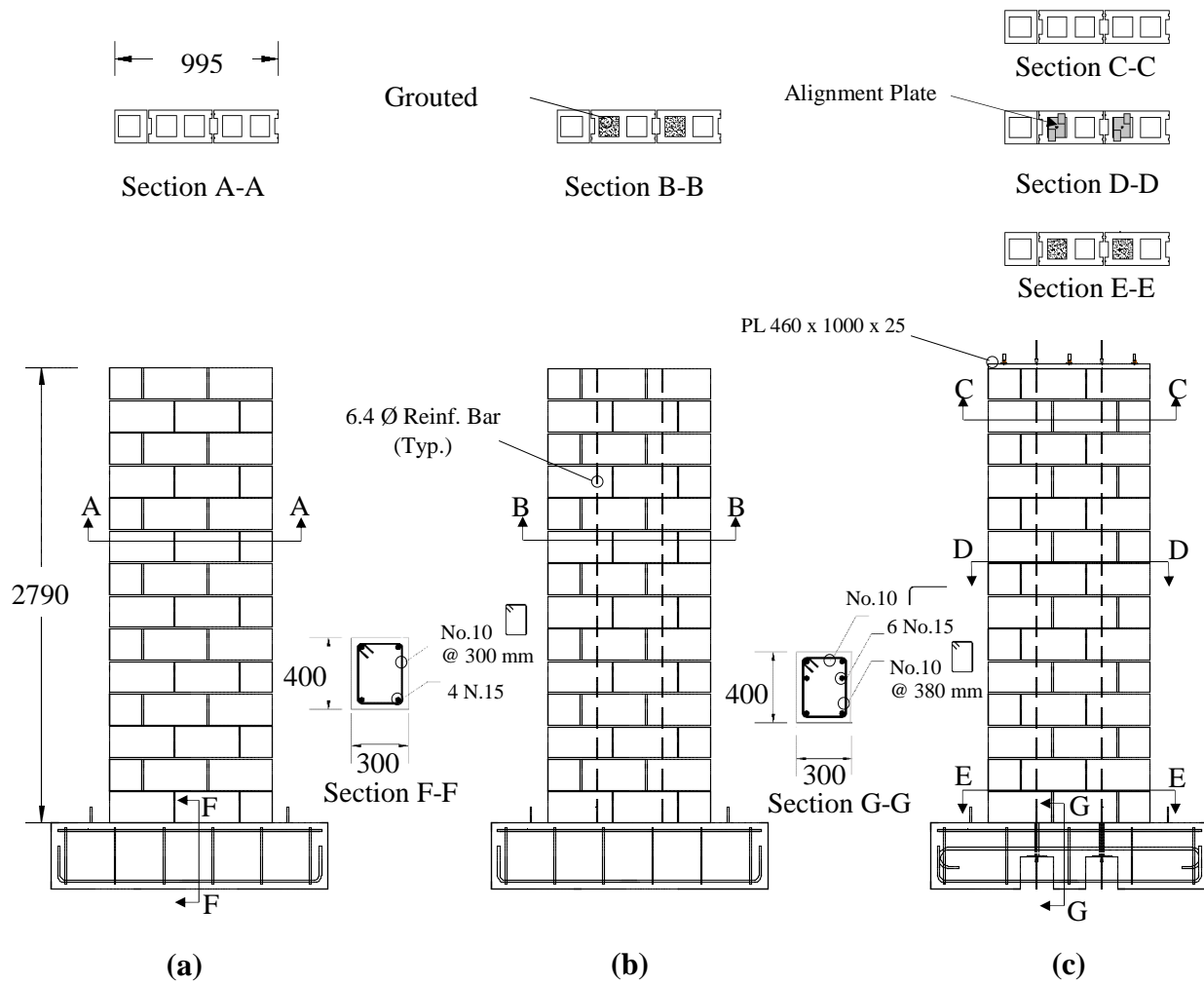
Figure 3.1: Cross-section and elevation of the wall specimens: (a) unreinforced walls, (b) conventionally reinforced and grouted walls, and (c) walls with unbonded reinforcement. (dimensions in mm).
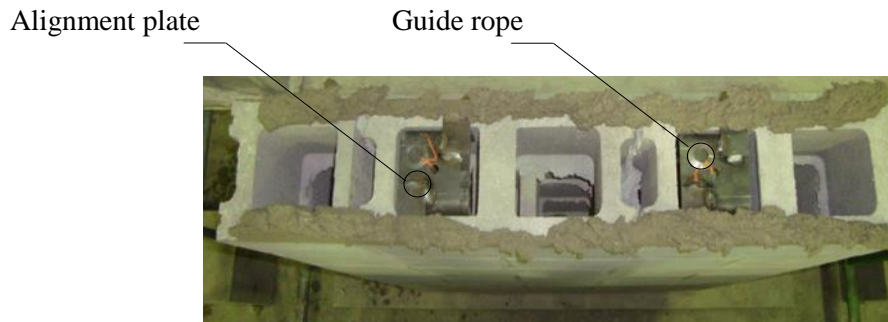
Figure 3.2: Reinforcement alignment plates used in specimens with unbonded reinforcement: restraints fabricated from steel plates embedded within the wall section
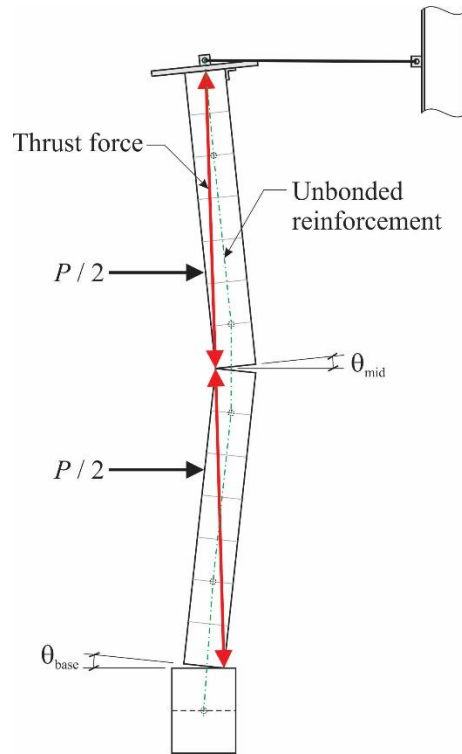
Figure 3.3: Schematic of wall with unbonded reinforcement in displaced position showing thrust forces.
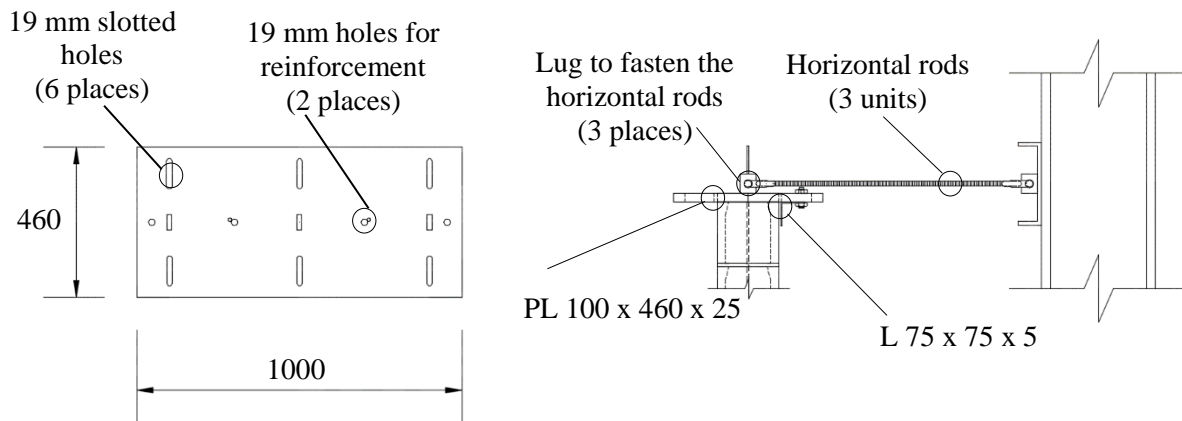
Figure 3.4: Top wall support, showing plan view of top plate and an elevation of the entire support assembly (dimensions in mm).
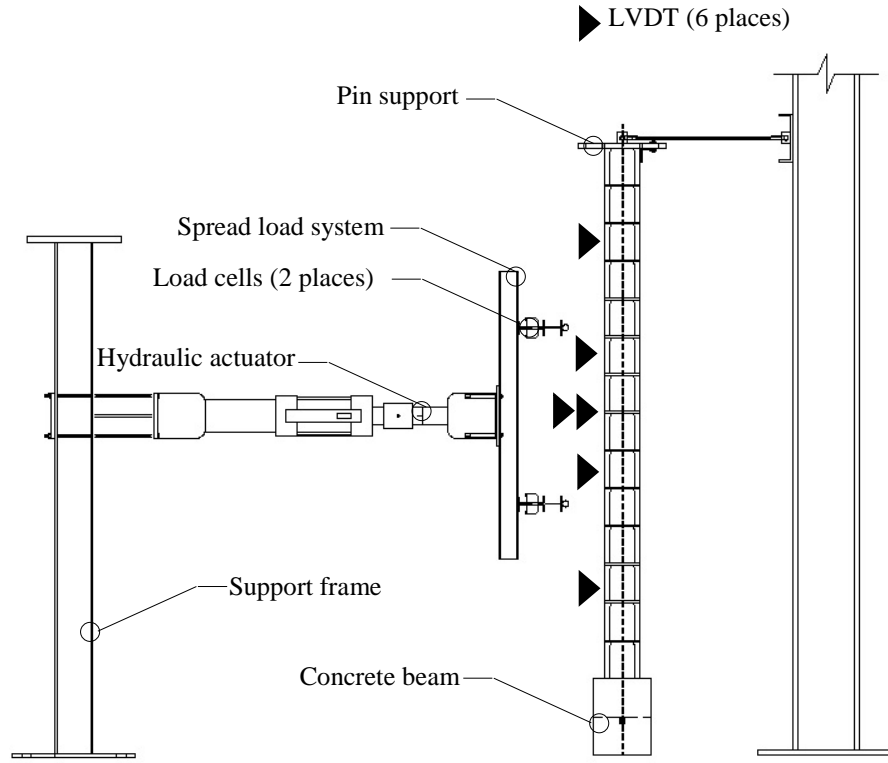
Figure 3.5: Schematic of loading arrangement and LVDT placement.

(a)   **(b)**
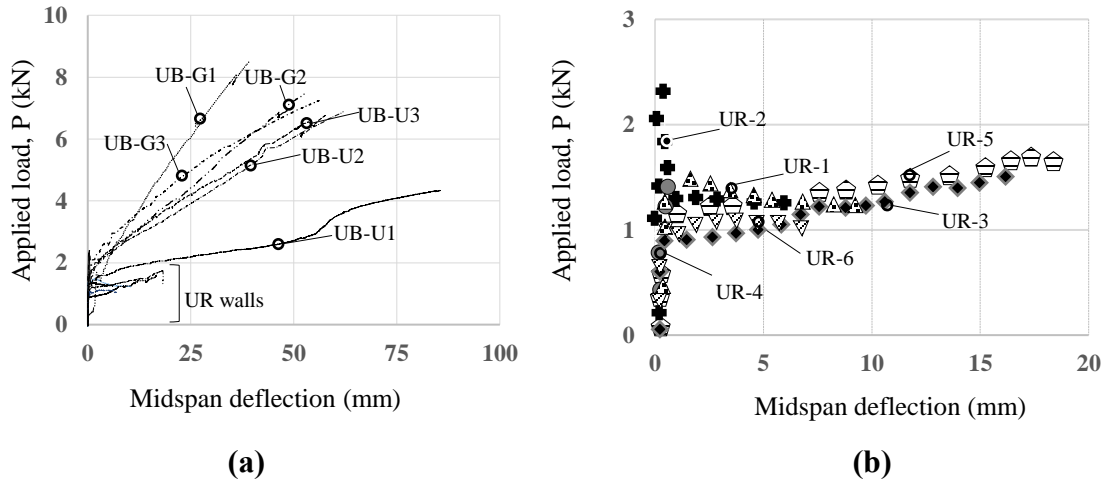
Figure 3.6: Applied lateral load versus midspan lateral displacement plots: (a) all wall specimens; and (b) unreinforced wall specimens only.

Chapter 4: Proof of Concept Investigation of Unbonded Reinforcement in Concrete Block Masonry[2]

This chapter presents a brief description of the construction procedure and testing of three types of masonry wall specimens: unreinforced walls, partially grouted and conventionally reinforced walls, and ungrouted walls with unbonded reinforcement. Material properties based upon the results of testing companion specimens are also presented. Results presented in this chapter include the analysis of strain contours and crack patterns as recorded using a digital image correlation system. Cracking loads, ultimate load capacity, mid-height deflection at the ultimate load, deflection profiles, crack locations and strain contours were analyzed, and compared with those results obtained from control unreinforced and conventionally grouted and reinforced walls. The development of an analytical model that reasonably captures the load-deflection response of walls where unbonded reinforcement is also included.

4.1 Introduction

Unreinforced masonry walls cannot effectively and efficiently resist out-of-plane loading that occurs as a result of wind or earthquakes, as failure is typically initiated by tensile cracking of mortar bed joints well before the compressive strength of the concrete blocks is realized (Udey 2014). The flexural resistance of concrete block walls can be markedly increased by providing longitudinal reinforcement in select block cells, and grouting these cells to ensure strain compatibility between the bars and the surrounding cementitious materials (Drysdale & Essawy 1988). Reinforced concrete block walls constructed in this manner can typically span at least two stories, in contrast to the limited single story capacity of unreinforced walls, and so are often used in the construction of school gymnasiums and building atriums. However, the use of grout as needed for the construction of these walls increases their self-weight, and requires an additional trade on-site. Project cost, construction time, and the likelihood of workplace injuries also increase as masons are typically required to lift blocks up and over reinforcement that has already been

---

grouted in place. The cost-competitiveness of masonry construction may therefore benefit from the development of construction techniques that can minimize the need for grouting.

Post-tensioned masonry construction, as one example of a system that reduces the need for grouting, has been the subject of numerous studies. The load-deflection behaviour of grouted and ungrouted prestressed wall panels was accurately modelled by Devalapura (1995). Graham and Page (1995) calculated the ultimate capacity of post-tensioned walls using Phipps' (1993) approximation for unbonded reinforcement. Bean Popehn et al. (2007) analysed the behaviour of slender post-tensioned masonry walls and determined that the maximum flexural resistance was relatively insensitive to the magnitude of the prestress force. Others (e.g. Korany and Drysdale 2006) focused on the flexural rehabilitation of masonry walls using external CFRP rope reinforcement. While all of these studies showed that the strength and serviceability characteristics of post-tensioned reinforcement are generally favorable, such construction methods require specialized skilled labor and high strength materials that increase the construction cost of the resulting elements. An extended literature review is provided in Chapter 2.

A novel, potentially cost-effective approach to achieve reasonable load-carrying capacity in masonry walls that has yet to be fully explored involves the use of unbonded reinforcement that is only minimally stressed, but anchored at the top and bottom of a masonry wall. This would allow for a grout-free structural system that relies upon arching action to resist the flexural effects resulting from out-of-plane loads, making more effective use of the compressive capacity of the masonry assembly. To this end, a proof-of-concept experimental study of concrete block masonry walls with unbonded reinforcement and well-defined loading and support conditions was conducted to evaluate their flexural capacity and serviceability. Results of these wall tests were compared to those of both unreinforced, and conventionally reinforced and partially grouted walls with otherwise similar geometry. Recognizing that the construction methods used for the walls with unbonded reinforcement as described herein would not be feasible on site, a follow up study is planned to establish and evaluate a more practical construction technique.

4.2 Experimental Investigation

Detailed information related to the geometry, construction, and testing of specimens was originally reported by Miranda et al. (2016) but is briefly described herein for comprehensiveness. All walls were constructed with standard 200 mm concrete blocks laid in running bond by an experienced mason following conventional Canadian construction practices, and were two and a half blocks wide and 14 courses tall. A total of 21 walls were included in the experimental program, which consisted of three sets of specimens: the unreinforced walls (UR) shown in Figure 4.1(a), the partially grouted and conventionally reinforced (PGR) walls shown in Figure 4.1(b), and the ungrouted walls with unbonded reinforcement (UB) shown in Figure 4.2. While the focus of the experimental investigation related to the ungrouted walls that contained unbonded reinforcement, the other two test series were constructed as controls for comparative purposes. A total of six replicates were constructed for each of the two control sets while nine ungrouted walls with unbonded reinforcement were constructed. The PGR and UB test series were reinforced with 6.4 mm (D5) deformed steel bars conforming to ASTM A1064/A1064M-16 (ASTM 2016a), with one full-length bar located in the first interior cell on either side of the wall specimen, as shown in Figures 4.1(b) and 4.2. Transverse reinforcement was not required in any of the walls since the shear resistance did not govern. All specimens were cured for a minimum of 28 days in their as-constructed position prior to testing.

All specimens were constructed on 300 mm wide by 400 mm high by 1700 mm long reinforced concrete grade beams to reproduce a realistic support condition at the base of the walls. Designers would typically model such supports, for the case of the UR and PGR walls, as being pinned. The grade beams were intentionally cast wider than the walls above so that they could be clamped at both ends to the laboratory strong floor during testing (Figure 4.3). Section G-G in Figure 4.2 shows that two full-width blockouts that were 200 mm tall by 200 mm long were required to accommodate the dead-end anchors used to develop the reinforcing bars in the unbonded specimens. The anchors bore against a steel plate cast into the concrete grade beam above these blockouts; the steel bearing plates contained a central 20 mm diameter hole through which the reinforcement could pass. Twenty-one millimeter diameter PVC ducts were cast into the grade beam above these anchor plates to serve as a bond breaker between the concrete and the reinforcing bars. Allowing the reinforcement to extend into the grade beam provided for the formation of a

third hinge in the UB walls, one hinge was located at the top and mid-height region; the third hinge location resulted in additional elongation of the reinforcement as the expected crack between the grade beam and the first block course widened. It was hypothesized that this geometry would increase the resulting flexural resistance of the UB walls. Some rotational stiffness provided by this support condition for the UB wall series was also anticipated.

It was recognized that out-of-plane deflections incurred by the UB walls would change the alignment of the reinforcing bars within these specimens such that the lever arm between the bars and the centroid of the compressive force would be reduced, resulting in a decrease in the walls' flexural resistance. As such, it was deemed important to maintain the alignment of the reinforcing bars at mid-depth of the specimen, as was accomplished by using structural steel alignment plate assemblies shown in Section E-E in Figure 4.2; these plates were installed in the bed joints above the 2nd, 6th, 8th, and 12th block courses. These alignment plate assemblies had 12 mm diameter holes pre-drilled at their centres to allow the reinforcing bars to pass through. A second concern related to the UB walls was whether the block webs in the bottom course of the wall would have adequate capacity to transfer the compressive thrust force to the unloaded wall face. Six specimens were therefore constructed with a fully grouted bottom course (denoted as UB-G walls), with 20.9 mm diameter PVC ducts cast in to serve as a bond breaker between the reinforcement and the surrounding grout (Section F-F in Figure 4.2), while the remaining three specimens were constructed without any grout (denoted as the UB-U walls). Just prior to testing, the reinforcing bars in the UB test series were clamped to an electric wire rope hoist and minimally stretched until bars reached an average strain of 9.10×10^{-5} mm/mm (i.e. 18.7 MPa) to eliminate any slack in the bars and ensure that they would resist load from the start of testing.

4.2.1 Material Properties

Table 4.1 shows the material properties of the masonry assemblage and reinforcing steel as determined from tests of companion specimens. These included compression tests of the concrete block units, grouted and ungrouted masonry prisms, grout cylinders and prisms, and mortar cubes. Results of tests of the reinforcing bars, bond wrench tests, and slump tests of the grout used in the PGR and UB-G walls are also presented. Individual results of the wall companion specimens, masonry prisms, and reinforcement companion specimens are presented in Appendix C.

Hollow concrete units with flat and frogged ends were obtained from a local supplier and were 390 mm long by 190 mm high and 190 mm wide. Half blocks were cut from the standard concrete units in the laboratory to ensure that all blocks used in each wall had the same material properties. The average value of compressive strength, as reported in Table 4.1, resulted from tests of six standard units using the protocol included in ASTM Standard C140/C140M-16 (ASTM 2016b) and CSA A165-14 (CSA 2014a) and are based on the net cross-sectional area of the units.

Type S mortar was prepared in the laboratory in accordance with CSA Standard A179-14 (2014b). The mortar was batched using a 1:3 ratio of mortar cement to sand by volume. Mortar cubes were cast and tested for each batch prepared in accordance with CSA Standard A3000-13 (2013).

High slump grout was used to fill the block cells in the PGR and UB-G walls and was prepared using Type GU cement, aggregate with a maximum size of 10 mm, and a 5:1 aggregate-to-cement ratio by weight. The grout was prepared in the laboratory in accordance with CSA Standard A371-14 (CSA 2004c). A water-to-cement ratio of between 0.95 and 1.0 was used to achieve a target slump of 250 mm; Table 4.1 shows that an average 231 mm as-measured slump was attained. Non-absorbent grout cylinders, 75 mm in diameter by 150 mm long, as well as 100 mm wide x 100 mm long x 190 mm high absorbent grout prisms were cast and tested for each grout batch in accordance with ASTM Standard C1019-16 (ASTM 2016c).

Compressive strength test results from one block wide by three course tall masonry prisms were obtained. Grouted prisms were used to estimate the compressive strength of the masonry assemblage for the PGR and UB-G walls while ungrouted prisms were used to estimate the compressive strength of the UR, UB-U and upper courses of UB-G walls. All prisms were tested in accordance with CSA Standard S304-14 Annex D (CSA 2014d) at an initial loading rate of approximately 1 kN/s. Controls were adjusted such that the prism failed within the next 2 minutes after the load gauge showed one-half of the expected maximum load for the masonry prism.

Six excess lengths of the reinforcement were tested in accordance with ASTM Standard A370-16 (ASTM 2016d) to establish their mechanical properties. The yield strength, as reported in Table 4.1, was based on a 0.2% offset approach given that the material was cold drawn.

4.2.2 Testing and Instrumentation

The reinforcing bars in the UB walls were instrumented with strain gauges which were located at the level of the bed joints above the 11th, 12th, and 13th masonry courses. These strain gauges were affixed to the bars prior to their installation in the walls. Wires connected to the strain gauges were threaded up the block cells and out the top of the specimens so that they ultimately could be connected to the data acquisition unit.

Once ready for testing, wooden bracing was used to secure each wall and prevent damage as it was moved from its as-constructed position to the test bed. Bolts were used to fix a wood frame to the concrete grade beams supporting the wall; straps secured to the moveable lift in the laboratory were connected to hooks built into the reinforcing cage in the grade beam supporting the wall so that the wall could be lifted and moved to the test bed. Figure 4.3 shows that steel beams resting on the grade beam on either side of the wall were then bolted through the laboratory strong floor. A steel plate pin-connected to three horizontal rods (Figure 4.3) was erected at the top of the wall to serve as an ideal roller support, with the rods also pin-connected to the reaction frame that was used for testing; a layer of plaster was placed between the top of the wall and the underside of the steel plate.

Six linear variable differential transducers (LVDTs) were used to instrument the loaded face of the specimen such that a deflected profile could be established at different load levels. Data were sampled from the LVDTs at a rate of 16-20 Hz during wall testing with a linearity error of ±0.35%.

A digital imaging correlation system (DICS) was then set up as shown in Figure 4.4 to obtain deformation and strain contours as experienced by the walls during testing. Walls were first painted white, followed by the application of a 35% density random black speckle pattern with individual marks ranging in size from 3 to 6 mm (Figure 4.4). Two stereo vision recording systems were set up. One system (camera system 1 as shown in Figure 4.4) included two digital cameras (resolution of each = 2,448 pixels x 2,048 pixels with 1.4/8 mm and 1.4/17 mm lenses) that were set up to process images of the unloaded face of the wall (north). A second system (camera system 2 as shown in Figure 4.4) with two digital cameras was used to record images of one side (west)

50

face for each wall. The resolution of the cameras used in the second system was similar to that of camera system 1. Figure 4.4 also shows that four LED (light-emitting diode) lamps were used to illuminate the wall surfaces being recorded by the digital imaging correlation system. The DICS was calibrated prior to each wall test using a 56 mm calibration grid to ensure the maximum error score did not exceed 0.03. A detailed explanation of the setup of the DICS is presented in the Appendix D.

Once instrumented, walls were tested under four-point loading as shown in Figure 4.3. A single 250 kN actuator was operated in displacement control to apply load to a spreader beam system at a rate of 3 mm/min. The spreader beam system allowed the single point load from the actuator to be transferred to two horizontally distributed line loads on the wall, located 465 mm above and below the specimen mid-height and extending the full width of the front (i.e. loaded) face of the specimen. One load cell (static error band of ±0.04%) was affixed to both the upper and lower load point to confirm that loading was shared equally. Tests of the UB wall series were terminated prior to the collapse of the walls at a load slightly less than that predicted to cause yielding of the reinforcement. Loading of walls in other test series continued until failure.

4.3 Experimental Results

Table 4.2 presents the primary results of experimental testing as will be described in this section. Observations of physical distress, applied load versus mid-height deflection, strain contours as captured by the digital imaging correlation system, and deflection profiles for the walls will be discussed.

4.3.1 Cracking, Deflection, and Failure Modes

Initial cracking loads, P_{cr}, as reported in Table 4.2, were established based upon discontinuities identified in the load versus midspan deflection curves obtained for the specimens rather than from visual observations made during testing. Table 4.2 shows that the first cracking load was relatively similar for the UB and UR walls but somewhat greater for the PGR walls given that the reinforced cells in the PGR walls were grouted, thus increasing their moment of inertia in comparison with the other wall sets. The observed difference between the average cracking load for walls with unbonded reinforcement that had their first course grouted (i.e. the UB-G wall series) and UB

walls contain any grout (i.e. the UB-U wall series) was not of a sufficient magnitude to confident state that there was a significantly statistical difference between them.

Table 4.2 also shows the locations of observed cracks for each specimen listed in the order that they appeared. All cracks occurred within the mortar joints; these joints are numbered from the bottom (i.e. with the 1st joint located between the concrete grade beam and the first block course) to the top of the wall. Theoretically, all walls should fail when a three-hinged mechanism forms. Given that the support at the top of the wall was designed to be an ideal roller and so allowed rotation to occur freely, two cracks in each wall were expected: one at the base of the wall, and one within the constant moment region between load points. Results reported in Table 4.2 show that this was indeed the general case. Further, Table 4.2 indicates that the first crack appearing in the wall was typically on the unloaded face within the constant moment region between load points, and generally occurred slightly above mid-height of the wall (i.e. the 8th mortar joint) within either the 9th or 10th mortar joint. All of mortar joints 6 through 10 were located between points of applied load and so would be subject to the same bending moment and hence stress at the extreme tensile fibre at a given magnitude of load application. It would be the weakest of these joints, due to a number of possible construction related factors, such as the strength of the mortar batch and whether or not the mortar had been retempered, that would be subject to cracking first. Further, whereas the top support was designed to model an ideal roller condition, some restraint at the bottom of the wall was provided by the mortar joint between the grade beam and the first block course. As a result, the midspan crack tended to shift toward the upper half of the wall. The second crack that formed at the bottom of the wall on the loaded face occurred either in the mortar joint between the grade beam and the first block course, or in the joint between the lowest two block courses.

Four of the walls showed cracks appearing at three locations (Table 4.2): two walls in each of the UB-G and PGR wall series. Two of the cracks in each of the walls from the UB-G test series occurred within the constant moment region, likely reflecting the similar strengths of those two joints. The third crack in the two walls in the PGR test series occurred in the shear span above the constant moment region and, though less expected given the lower tensile stress demand in this

region, is believed to have occurred again due to weakness in the mortar joints where these cracks occurred.

Finally, Table 4.2 shows the location of the cracks on the wall specimens. It was observed during testing that the width of the cracks in the constant moment region as measured on the unloaded wall surface at the maximum load level, Δ_{mid}, for the UB test series are significantly wider than for the PGR wall series. Figure 4.5 also relates to serviceability, and shows the deflected profile of representative UB (Figure 4.5(a)) and PGR (Figure 4.5(b)) walls at the maximum load level as recorded by the LVDTs used the instrument all specimens during testing. As a result, while the load carrying capacity of the UB walls approached that of conventionally grouted and reinforced construction, their serviceability behaviour differed: the lateral deflection and crack width at mid-height as attained by the UB walls were significantly greater than those measured for the PGR walls. Walls with unbonded reinforcement, if used in practice, would therefore likely be limited to indoor environments where water ingress would not be a significant concern. A beneficial characteristic of the UB walls, though, was that all cracks were observed to close immediately and lateral deflections along the wall height were essentially eliminated upon removal of the applied load. This reflects the restoring action of the tensile force in the unbonded reinforcement, adding inherent stability to the wall, and counteracting slenderness effects generated by gravity loads. As such, unbonded reinforcement may represent a viable option for enhancing the out-of-plane resistance of interior walls subjected to seismic loads: the inherent stability and reduced mass would be beneficial, and serviceability issues would be of less concern.

4.3.2 Lateral Load Carrying Capacity

Figure 4.6 shows the applied load versus mid-height deflection for all walls included in the experimental investigation. The curves can generally be classified in one of three categories, based upon the construction type of the wall (i.e. UR, UB, or PGR). The ungrouted and unreinforced (UR) walls achieved the lowest cracking and maximum loads, with deflections corresponding to the maximum load being roughly 46% and 11% of the average values corresponding to the PGR and UB walls, respectively. The partially grouted and conventionally reinforced walls (PGR) achieved the greatest value of average maximum load, which was 5.75 and 1.23 times those calculated for the UR and UB walls, respectively; however, it should be noted that the test of UB

walls were terminated prior to anticipated yielding of the reinforcement. Figure 4.6 also shows that the PGR walls exhibited post-peak behaviour with the load dropping off with increased midspan deflection following attainment of the maximum load.

A review of Figure 4.6 also shows that there is no appreciable difference in the applied load versus mid-height deflection of the two sets of walls containing unbonded reinforcement (i.e. between the UB-U and UB-G test series). Following cracking, all walls in the UB test series exhibited mid-height deflections that increased in an approximately linear manner with increasing applied load. The maximum load attained by these specimens, at the time that testing was halted, was significantly greater than for the UR walls and about 82% of that attained, on average, for the PGR test series. Figure 4.6 shows that Specimen UB-U1 experienced larger mid-height deflections for a given applied load level in comparison to others in the UB test series. Rotation of the grade beam used to support this specimen was observed during testing that was attributed to the lack of rigidity of the anchoring system used to secure this grade beam to the laboratory strong floor. A more rigid anchoring system was used for all other specimens in the UB test series; as a result, wall UB-U1 was identified as a physical outlier. For this reason, data for specimen UB-U1 was excluded from the calculation of average values and coefficients of variation for the test results reported in Table 4.2.

Figure 4.7 shows the strain contour plots obtained from the digital imaging correlation system for a representative wall from each of the three test series as the maximum load was approached; the loaded face of the wall is positioned on the right side of these figures. The colors in the figure represent different ranges of strain magnitudes, ε, as shown in the legend associated with each wall; here, it should be noted that the legend associated with each strain contour plot is non-linear. Figure 4.7 shows that high tensile strain concentrations, as characterized by the concentrated regions of red orange and yellow, occurred at crack locations as noted in Table 4.2 for walls UR-2 (Figure 4.7(a)), UB-U2 (Figure 4.7(b)), and PGR-5 (Figure 4.7(c)). Further, the uniform grey region in the top fifth as shown for wall PGR-5 in Figure 4.7(c) resulted from the fact that the digital imaging correlation system was not able to capture the strain measurements in this region of this wall.

The unreinforced wall shown in Figure 4.7(a) and the wall with unbonded reinforcement shown in Figure 4.7(b) both show some variation in strain along the entire wall height, with strain magnitudes shown in Figure 4.7(c) for the partially grouted and conventionally reinforced wall being more consistent throughout (i.e. less pronounced color changes are apparent). This observation is consistent with the load-carrying behaviour as expected for the walls: the reinforced cells in the PGR walls are grouted and so allow stresses and strains to be transferred between the reinforcing bars and the surrounding cementitious materials along the entire wall height. A narrow tension zone is apparent on the loaded face of the wall as indicated by the red, yellow, and green contours on the right face of the PGR wall in Figure 4.7(c); however, it is believed that this zone would be wider for the reinforced cell itself which is located in the first interior cell, while the digital correlation system could only capture strain contours on the exterior faces of the specimen. Figure 4.7(a) shows that some strain variation was observed in the UR walls, particularly along the face shell on the loaded (left) surface of the walls. This may be attributed to flexural action in the blocks between mortar joints.

Perhaps the most revealing aspect in Figure 4.7(b) are strain contour patterns that suggest the presence of arching action in the UB wall, a finding that is consistent with the predominant load resisting mechanism for these specimens. Compressive struts, shown in pink/violet, appear to develop from the applied load point on the right side (i.e. loaded wall face) of the wall to the left side (i.e. unloaded wall face) at the top and bottom wall supports. These compressive struts exhibit roughly uniform magnitudes of stress and strain along the wall height, as would be expected based on arching action theory. Strain contours at specific displacements within the elastic range for all individual specimens using the two camera systems are provided in Appendix E.

4.4 Analytical Results

An analytical model was developed to estimate the applied load versus mid-height deflection of the UB wall series by assuming the formation of a three-hinge mechanism in each wall as shown in Figure 4.8(a). Hinge locations were assumed to occur in the mortar joint between the concrete grade beam and the first block course (Point A), at mid-height of the wall (i.e. between the 7th and 8th block courses – Point B^*), and at the top support (Point C^*) regardless of the actual crack locations as observed for each specific wall. The two resulting wall segments (bottom half shown

in Figure 4.8(b) and top half shown in Figure 4.8(c)) were assumed to remain straight and inextensible and so undergo rigid body rotations. It was also assumed that the steel rods that made up part of the upper support assembly were permitted to rotate but remained inextensible. The reinforcing bars in the wall were modelled as behaving in a perfectly elastic-plastic manner with a yield strength of 563 MPa and a modulus of elasticity of 205 GPa, as reported in Table 4.1. As a calibration exercise, different assumptions regarding to the hinge locations and material behaviour of reinforcing bars were made to investigate the influence of those assumptions on wall behaviour; the results using the various assumptions were compared to determine the accuracy of the analytical model, as shown in Appendix F. The model described here was found to generate accurate results, while remaining relatively straightforward to implement.

Once a value of mid-height deflection δ was selected, standard trigonometric relationships could be established to calculate the coordinates of the following points in their as-deflected position: the centreline of each of the four reinforcing alignment locations (labelled as Points 1 to 4 in Figure 4.8(a)), the centroid of the top plate forming part of the upper support assembly (i.e. Point C^* as shown in Figures 4.8(a) and (b)), and Point B^* which represents the contact point between the upper and lower wall segments once the three-hinge mechanism had formed. Additionally, the magnitude of the following angles (Figure 4.8(a)) could also be calculated: that between the top surface of the concrete grade beam and the bottom course of the wall, $\Delta\theta_{AB}$; the angle of inclination between the bottom surface of the 8th block course and the horizontal, $\Delta\theta_{BC}$; the angle of inclination β between the horizontal and the line segment connecting Point B^* and Point D that represents the connection point between the rods forming part of the upper support assembly and the test frame; and α, the angle between the line segment connecting Points B^* and D and the centroidal axis of the top wall segment in its deflected position.

Forces could be calculated once the geometry of the wall in its deflected position was established. The strain, stress, and force in the reinforcing bars could be determined from the final length of the bars in the deflected wall, which was calculated based on the resulting segment lengths between successive sets of alignment plates, the segment length between the dead end anchor at the underside of the concrete blockout in the grade beam (Point E) and the first alignment plate, and the 4th alignment plate and the top support (Point C^*). The amount of prestress provided to the

reinforcement in any particular specimen was then added to the force in the reinforcement resulting from its elongation. Further, the horizontal, F_{six}, and vertical, F_{siy}, forces caused by the reinforcing bars bearing against the alignment plates, where i is an integer between 1 and 4 representing a specific alignment plate, could be calculated. The internal force in the rods forming part of the upper support assembly, R_{rod}, could also be calculated once the final coordinates of Point $C*$ had been established.

Force equilibrium of the bottom (Figure 4.8(b)) and top (Figure 4.8(c)) wall segments thus allowed for the calculation of the applied load, P, corresponding to the selected value of mid-height wall deflection, δ. The self-weight of the bottom, W_{D_bot}, and top, W_{D_top}, wall segments were assumed to act at the centroid of the respective segments in their final, deflected position. The weight of the top support assembly, W_{pl}, equal to 0.95 kN, was assumed to act at the centroid of this plate in its deflected position. Similarly, the weight of the grout in the first block course (not shown in Figure 4.8(b)) was assumed to act at the centroid of the bottom block course in its deflected position.

The procedure as outlined in the previous paragraphs was repeated numerous times, varying the input value of the mid-height wall deflection, to allow for a plot of applied load versus mid-height deflection to be established.

Figures 4.9 and 4.10 show a comparison of the applied load versus mid-height deflection curves as derived analytically and measured experimentally for the UB-U and UB-G wall series, respectively. Table 4.3 further presents a comparison of the tension force per reinforcing bar and the maximum applied load measured during testing and calculated analytically at the value of mid-height deflection corresponding to the as-tested maximum load. Table 4.3 shows that the analytical model typically under-estimated the force per reinforcing bar, with percentage errors ranging from -41.1% for UB-G1 to +3.60% for UB-U2. Results from the analytical model also tended, on average, to under-estimate the maximum applied load, with percentage errors ranging from -38.1% for UB-G1 to +14.5% for UB-G5. However, Figures 4.9 and 4.10 show that the model reproduces the general trends in the as-tested data reasonably well following cracking. In most cases (i.e. Walls UB-U3, UB-G2, UB-G3, UB-G4, UB-G5, and UB-G6) the model under-

estimates the as-tested load values in the earlier stages of displacement; however, the slope of the as-tested curve decreases in later stages for a number of walls (UB-U3, UB-G4, UB-G5, and UB-G6) which results in the analytical model over-estimating the maximum applied load for five out of the nine walls tested by an amount ranging from 0.735% (UB-U3) to 14.5% (UB-G5).

4.5 Summary and Conclusions

This paper presents the results of an experimental investigation consisting of a total of 21 large-scale concrete block masonry walls. All walls were two and a half blocks wide and 14 courses tall. Nine of the walls featured conventional reinforcement placed in ungrouted cells, but anchored at their top and bottom ends: six of these specimens had all blocks in the first course grouted, while the remaining three specimens were completely ungrouted. The aim of the work was to conduct a proof-of-concept program of a wall system that eliminates the need for grout in reinforced masonry, thereby potentially improving cost-effectiveness and ease of construction. The remaining 12 specimens were used as controls, with six of these specimens being unreinforced, and the other six specimens being conventionally reinforced and partially grouted. The study was limited to walls subject to out-of-plane loading, applied as four-point loading, used to simulate wind and seismic effects. Axial loading was not applied. An analytical model based upon the deflected wall geometry assuming the formation of a three-hinge mechanism was developed in an attempt to estimate the applied load versus mid-height deflection of walls featuring unbonded reinforcement.

The following significant conclusions and observations were identified:
1.   The load-deflection behaviour of walls with unbonded reinforcement appeared to be insensitive to whether or not the first course was grouted, suggesting that transfer of the resulting thrust forces through the block webs of ungrouted walls was sufficient.
2.   Crack widths that developed in the constant moment region for walls with ungrouted reinforcement were significantly wider than those observed for conventionally reinforced and partially grouted walls. However, these cracks closed immediately upon unloading and walls returned to their undeflected, vertical position. Due to the internal tensile force in the reinforcement, walls with unbonded reinforcement therefore exhibit an inherent stability that renders them less susceptible to slenderness effects; however, if used in practice, such walls would generally need to be limited to indoor exposure where water

ingress would not be an issue. The inherent stability and lower mass of walls with unbonded reinforcement may be advantageous with respect to the out-of-plane strength of interior walls subjected to seismic loading, particularly since serviceability is not as critical under those conditions.

3. Fully grouting the bottom course of the walls containing unbonded reinforcement increased the cracking load, on average, by 1.7 times that recorded for specimens when the bottom course was left ungrouted.

4. Walls with unbonded reinforcement had approximately 4.7 times the lateral-load carrying capacity as compared to unreinforced walls.

5. Strain contour plots as captured by the digital imaging correlation system confirmed the expected load-carrying mechanism for all three wall test series. Strain concentrations were evident in the face shells of the unreinforced walls, as the material concentrated at the extreme tension and compression faces would resist the internal moment imposed by the four-point lateral loading. A reasonably consistent strain distribution was noted for partially grouted and conventionally reinforced walls given that the grout allowed strains and stresses to be transferred between the reinforcing bars and the surrounding cementitious materials along the entire wall height. Compression struts with reasonably uniform strain magnitudes were observed for walls with unbonded reinforcement, and extended from the two load points on the loaded specimen face, to the adjacent support on the unloaded specimen face.

6. An analytical model assuming the formation of a three-hinge mechanism was found to match experimentally obtained load versus mid-height deflection data reasonably well throughout the entire post-cracking range.

7. It is acknowledged that the construction of walls with unbonded reinforcement, as described herein, cannot be reasonably reproduced in practice. It is recommended that a construction technique for such walls that can be readily implemented on-site be devised.

Table 4.1: Material properties as obtained from tests of companion specimens

Material Property	# of Specimens	Average Value	COV[a]	Representative of
Compressive strength of concrete block units	6[b]	22.2 MPa	7.4%	All walls
Compressive strength of ungrouted masonry prisms	21[c]	20.5 MPa	8.1%	All walls
Compressive strength of grouted masonry prisms	7	13.4 MPa	10%	PGR and UB-G walls
Flexural tensile strength of the masonry assemblage[d]	21	0.06 MPa	71%	All walls
Slump test of grout	10	231 mm	4.1%	PGR and UB-G walls
Compressive strength of non-absorbent grout cylinders	30	21.4 MPa	25%	PGR and UB-G walls
Compressive strength of absorbent grout prisms	30	19.2 MPa	4.7%	PGR and UB-G walls
Compressive strength of mortar cubes	192	18.0 MPa	16%	All walls
Ultimate tensile strength of reinforcement	6	612 MPa	1.7%	PGR and UB walls
Yield strength of reinforcement	6	563 MPa	5.1%	PGR and UB walls
Modulus of elasticity of reinforcement	6	205000 MPa	7.1%	PGR and UB walls

[a]COV = Coefficient of Variation
[b]As measured from 3 flat-ended and 3 frogged ended blocks
[c]Excludes result from Wall UB-U1
[d]As measured from bond wrench tests

Table 4.2: Summary of experimental test results

Specimen ID[a]	P_{cr} (kN)	P_{max} (kN)	Δ_{mid} at P_{max} (mm)	Crack Locations[b]
Unreinforced				
UR-1	0.284	1.49	1.62	2nd & 8th
UR-2	0.368	2.33	0.390	2nd & 11th
UR-3	0.674	1.60	16.7	9th & 2nd
UR-4	0.367	1.42	0.623	11th & 2nd
UR-5	0.353	1.75	18.1	9th & 2nd
UR-6	0.350	1.12	3.46	10th & 2nd
Average =	0.399	1.62	6.81	
COV (%) =	34.6	25.1	122	
UB-U1[c]	1.77	4.35	85.5	10th & 1st
UB-U2	0.754	6.89	62.0	9th & 1st
UB-U3	1.55	6.79	57.8	9th & 1st
Average[d] =	1.15	6.84	59.9	
COV (%)[d] =	48.7	1.02	4.94	
UB-G1	1.69	8.51	39.2	9th, 1st & 10th
UB-G2	1.70	7.49	52.9	9th, 1st & 10th
UB-G3	2.27	7.27	56.6	11th & 1st
UB-G4	1.83	6.91	66.8	11th & 1st
UB-G5	2.02	7.54	77.4	10th & 1st
UB-G6	2.11	9.45	114	8th & 1st
Average =	1.94	7.86	67.8	
COV (%) =	12.2	12.0	38.6	
PGR-1	6.37	9.08	14.7	9th, 1st & 14th
PGR-2	5.68	9.51	14.2	9th & 1st
PGR-3	4.92	8.99	21.5	9th & 1st
PGR-4	5.40	9.47	15.4	9th & 1st
PGR-5	3.12	9.17	12.1	9th & 1st
PGR-6	3.82	9.69	10.8	9th, 1st & 12th
Average =	4.89	9.32	14.8	
COV (%) =	24.8	2.98	25.2	

[a]The letters preceding the hyphen in the specimen ID are used to represent the general specimen type with UR representing ungrouted and unreinforced walls, UB representing walls with unbonded reinforcing bars, and PGR signifying partially grouted and conventionally reinforced walls; the letter following the hyphen, included only for the UB specimen series, denotes whether the first (i.e. bottom) course of these walls is grouted (G) or ungrouted (U); and the subsequent numbers indicates the replicate number within the test series.

[b]Crack locations are listed in the order that they were observed to have appeared and represent the mortar joint number from bottom to top of the wall (i.e. 1st is the mortar joint between the concrete grade beam and the bottom block course in the wall and the 14th represents the joint between the top and next to top block courses in the wall).

[c]Specimen identified as a physical outlier as described in the text.

[d]Values calculated excluding results from specimen UB-U1

Table 4.3: Comparison of the analytical and as-tested results for wall with unbonded

reinforcement

Specimen ID[a]	$(T_{max})_{test}$ (kN)	$(T_{max})_{model}$ [b] (kN)	% Error	$(P_{max})_{test}$ [c] (kN)	$(P_{max})_{model}$ (kN)	% Error
UB-U1[d]	n/a	n/a	n/a	4.35	n/a	n/a
UB-U2	11.1	11.5	+3.60	6.89	7.24	+5.08
UB-U3	12.5	10.6	-15.2	6.80	6.85	+0.735
UB-G1	12.2	7.19	-41.1	8.51	5.27	-38.1
UB-G2	10.8	9.72	-10.0	7.49	6.48	-13.5
UB-G3	16.3	10.1	-38.0	7.27	6.63	-8.80
UB-G4	16.8	12.2	-27.4	6.91	7.62	+10.3
UB-G5	20.5	14.5	-29.3	7.54	8.63	+14.5
UB-G6	22.0	18.1	-17.7	9.45	9.75	+3.17

[a]The letters preceding the hyphen in the specimen ID are used to represent the general specimen type with UR representing ungrouted and unreinforced walls, UB representing walls with unbonded reinforcing bars, and PGR signifying partially grouted and conventionally reinforced walls; the letter following the hyphen, included only for the UB specimen series, denotes whether the first (i.e. bottom) course of these walls is grouted (G) or ungrouted (U); and the subsequent number indicates the replicate number within the test series.

[b]T_{max} is maximum tension force in the reinforcement while

[c] P_{max} is the maximum applied load on the wall specimen.

[d]Specimen identified as an outlier as described in the text.
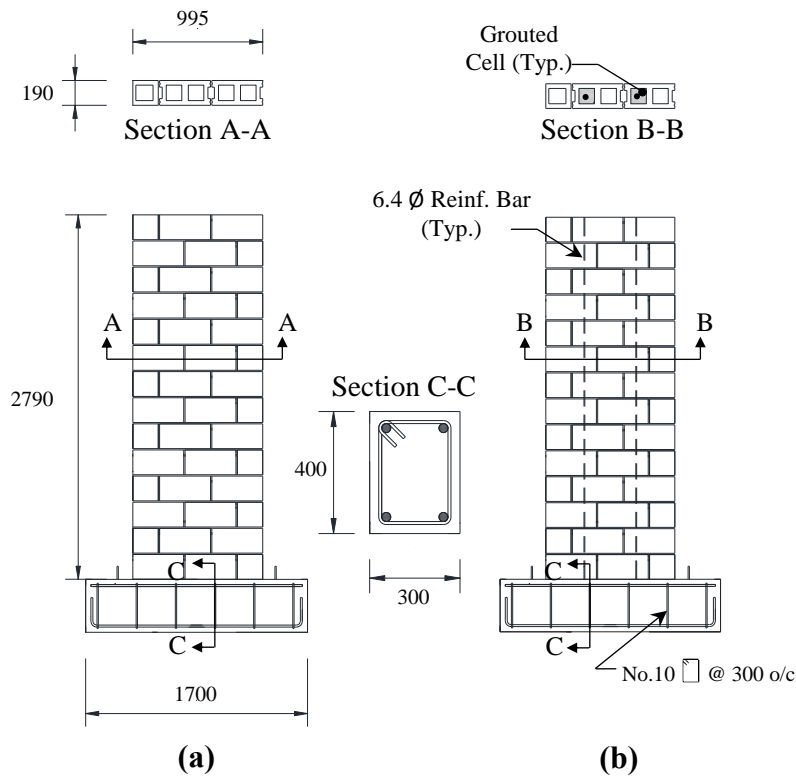
Figure 4.1: Control specimen geometry: (a) unreinforced and ungrouted walls, and (b) partially grouted and conventionally reinforced walls (dimensions in mm).
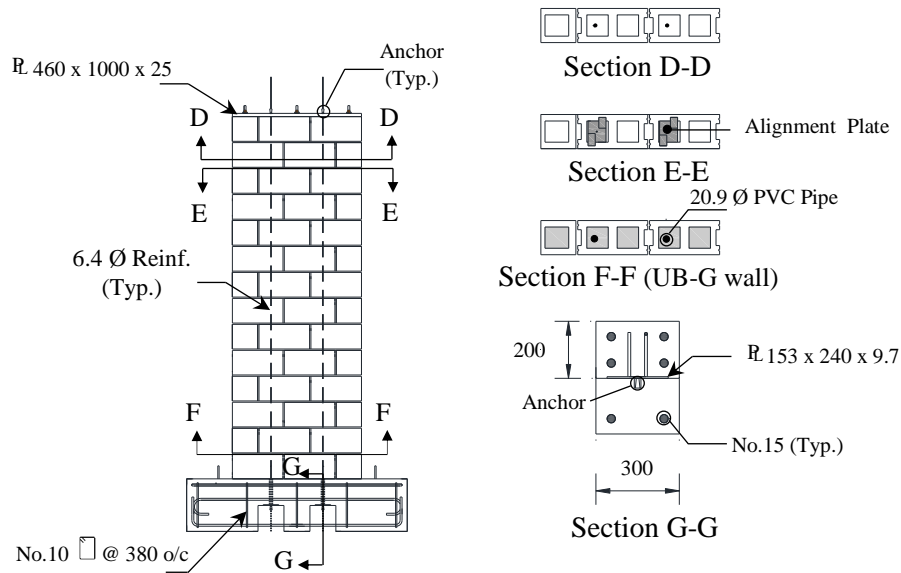
Figure 4.2: Geometry of ungrouted walls with unbonded reinforcement (dimensions in mm).

63
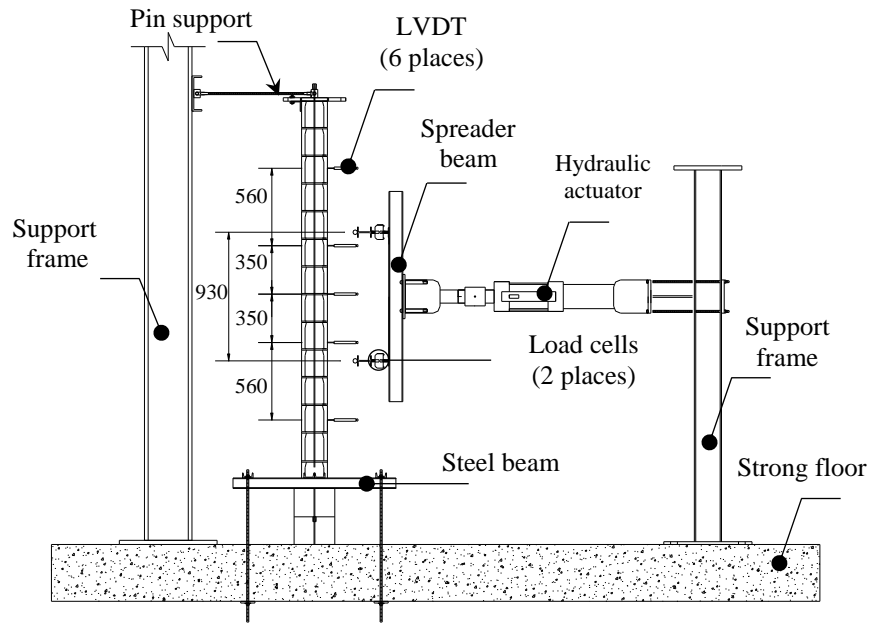
Figure 4.3: Lateral view of the test frame, LVDT locations, and top and bottom supports (dimensions in mm).
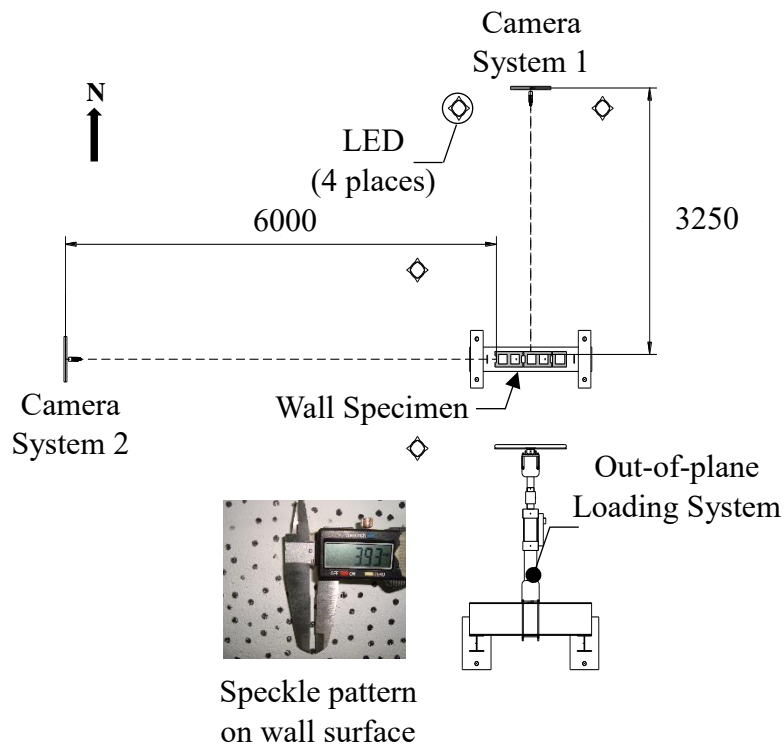
Figure 4.4: Digital imaging correlation system setup (dimensions in mm).
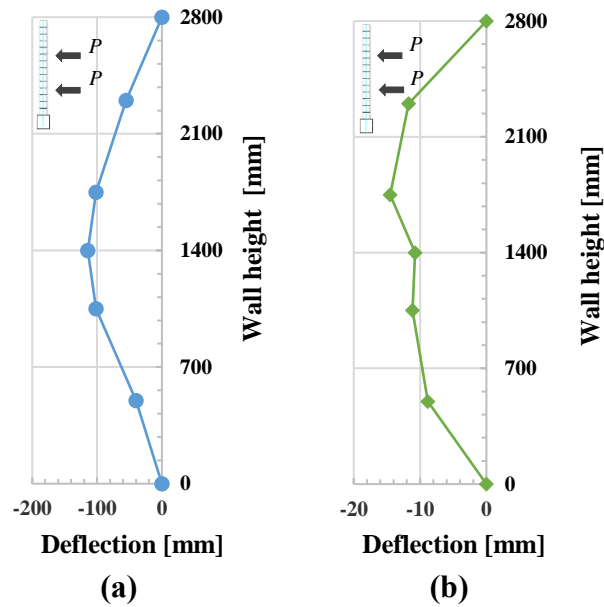
Note: The horizontal scale for the two plots differs due to the significantly different deflections as measured for walls in the different series

Figure 4.5: Lateral deflection profiles for representative walls at the maximum load level: (a) UB wall, and (b) PGR wall.
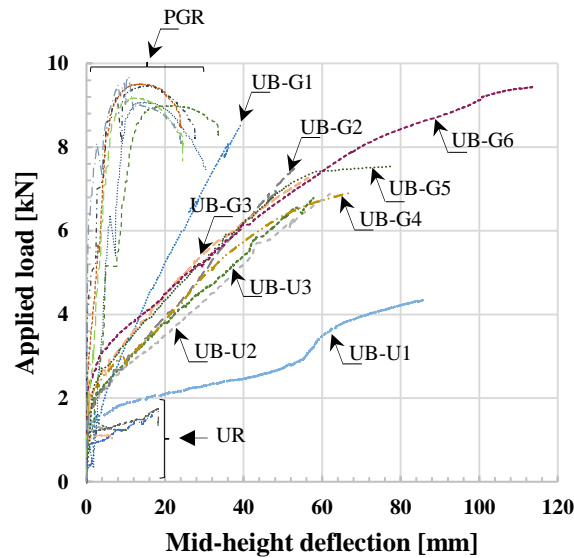
Figure 4.6: Applied load versus mid-height deflection curves for all walls.
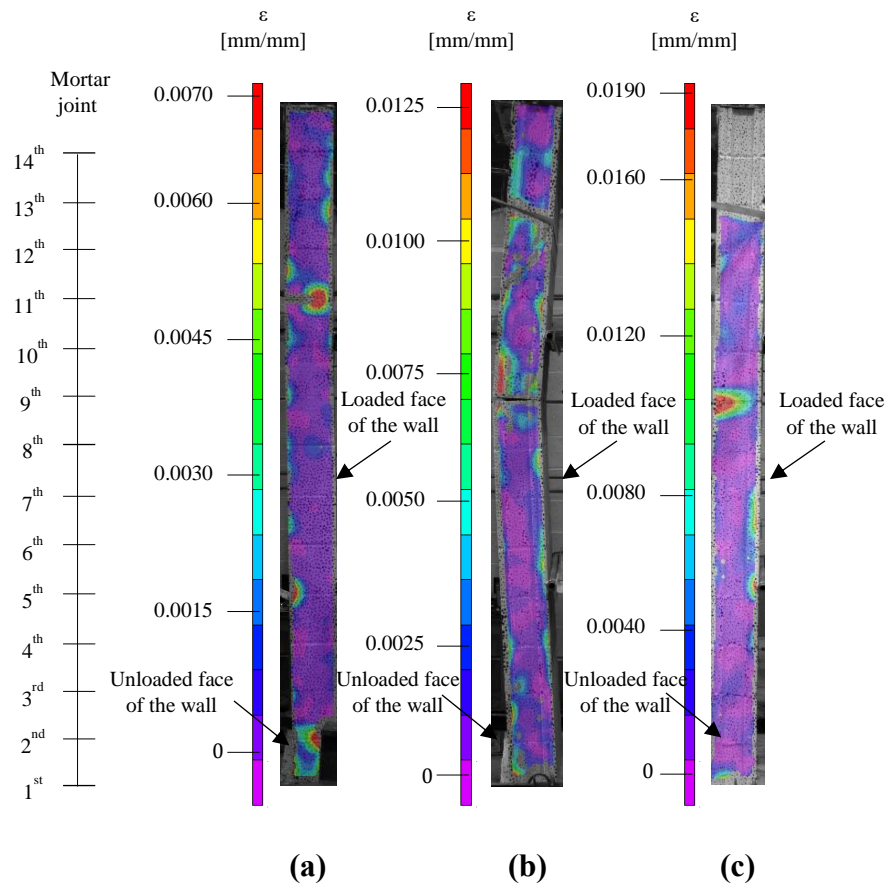
Figure 4.7: Strain contours as measured using the digital imaging correlation system for representative walls: (a) UR wall (UR-2), (b) UB wall (UB-U2), and (c) PGR wall (PGR-5).
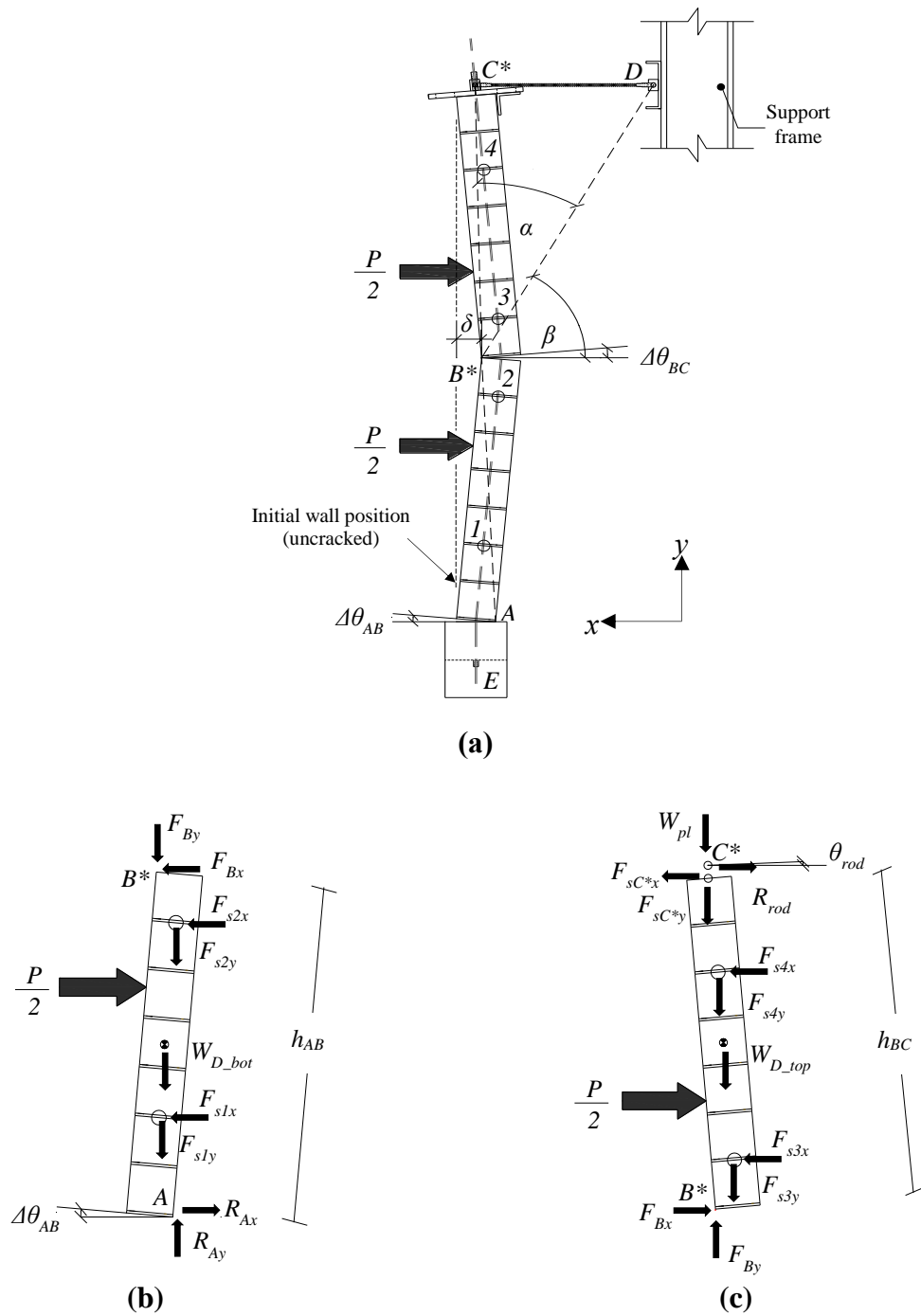
Figure 4.8: Analytical model used to estimate the mid-height wall deflection: (a) assumed wall geometry following cracking, (b) free-body diagram of the bottom half of the wall, and (c) free-body diagram of the top half of the wall.
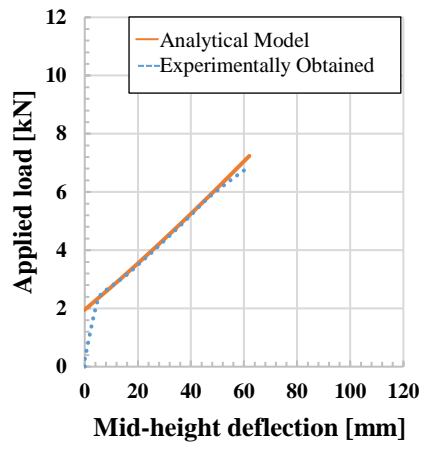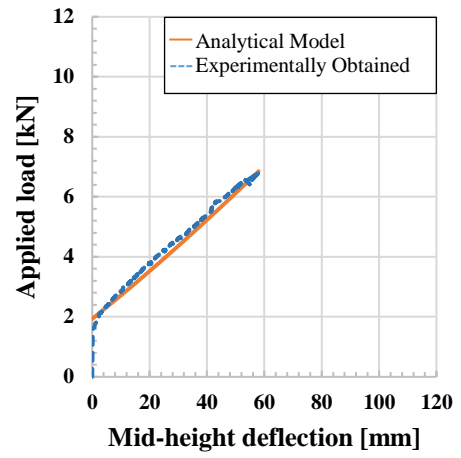
Figure 4.9: Comparison between analytical models and experimental results: (a) UB-U2 wall, and (b) UB-U3 wall
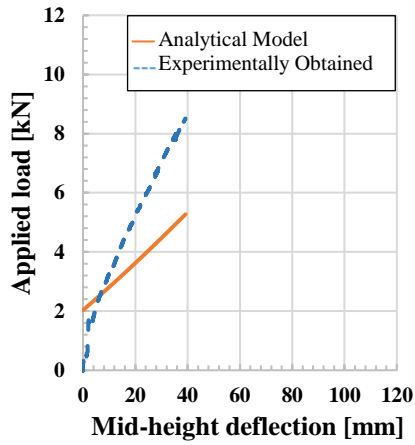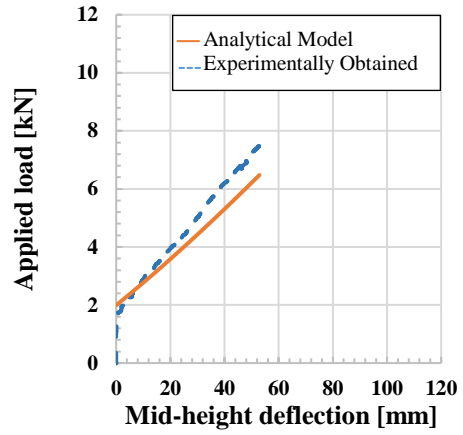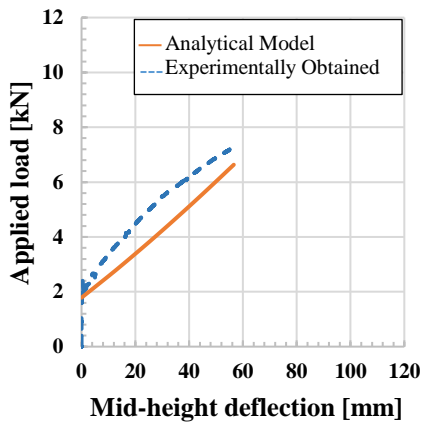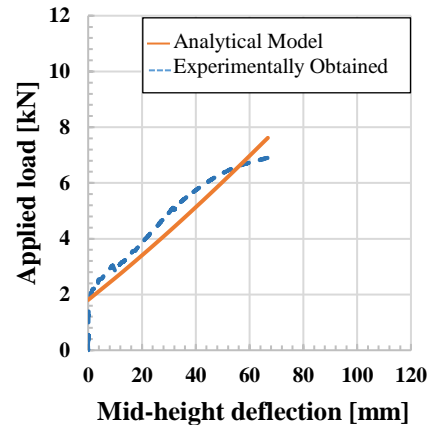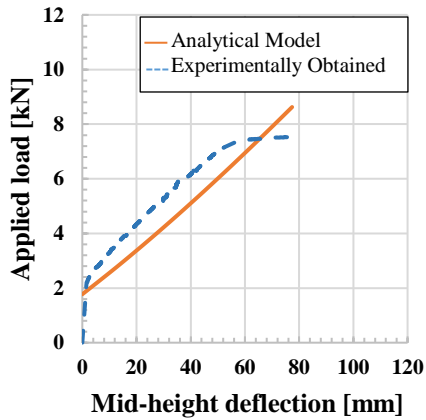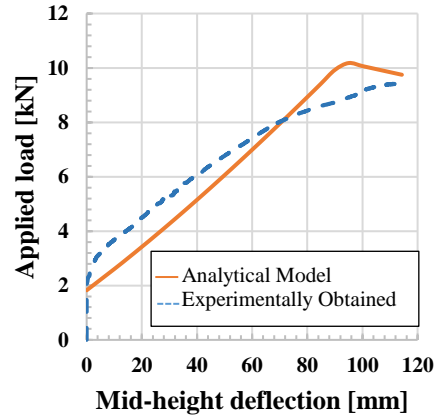
Figure 4.10: Comparison between analytical models and experimental results: (a) UB-G1 wall, (b) UB-G2 wall, (c) UB-G3 wall, (d) UB-G4 wall, (e) UB-G5 wall, and (f) UB-G6 wall.

Chapter 5: Summary, Conclusions and Recommendations

This Chapter includes a summary, conclusions, and recommendations gained from this study that was conducted in the Structures Laboratory of the University of Saskatchewan. Minimally stressed ungrouted reinforcement was used in concrete block walls to achive reasonable resistance to out-of-plane loads while minimizing their cost, construction time, and self-weight. The literature review, methodology, results from physical tests, comparison of outcomes between walls with unbonded reinforcement and control specimens, as well as a numerical model study, were described in the previous Chapters.

5.1 Summary

An innovative masonry wall system making use of arching action to resist out-of-plane loads was presented and analyzed in this research program. A total of twenty-one wall specimens were built and subjected to quasi-static out-of-plane loading. The behaviour of walls with unbonded vertical reinforcement that were anchored at their top and bottom ends was compared to those of unreinforced and ungrouted walls, and partially grouted and conventionally reinforced walls that were used as control specimens. Unreinforced, and partially grouted and conventionally reinforced walls were built using common field practices, while the walls with unbonded reinforcement introduced several nonconventional features that enabled the development of arching action within the walls. A total of six replicate unreinforced and ungrouted walls, six replicate partially grouted and conventionally reinforced walls, and nine ungrouted walls with unbonded reinforcement were built by an experienced mason. The unbonded wall test series was divided into two groups: six of these walls featured a grouted first course, while no grout was used in the remaining three specimens. These two subsets were included to investigate the ability of ungrouted blocks to transfer the arching thrust force to the bottom support.

Walls were designed considering a realistic bottom support consisting of a grade beam, and an ideal roller joint connection at their top end. Two types of concrete grade beams were used: a set of conventional rectangular concrete beams for the unreinforced and conventionally reinforced walls, and a set of modified beams featuring two blockouts to facilitate the anchorage of the

unbonded reinforcement. The ideal roller connection at the top of the walls was replicated by connecting a steel plate set on top of the walls to the support columns using three horizontal rods that were pin-connected at both ends.

The out-of-plane behaviour of the walls with unbonded reinforcement was assessed on the basis of a visual assessment of damage, the measured cracking load, maximum load capacity, the mid-height deflection at critical stages, and strain contours as obtained using a digital image correlation system. These results were compared with those obtained for the control specimens. Companion specimens were tested to obtain the mechanical properties of all constitutive materials. An analytical model was also developed that allowed for a comparison of the load-deflection curves with those obtained experimentally. The following sections provide a summary of the findings and conclusions derived from this research program.

5.2 Conclusions

5.2.1 Comparison of the performance of ungrouted walls with unbonded reinforcement and the control specimens

Cracking Behaviour

The first observable crack in the walls with unbonded reinforcement appeared within the constant moment region, while the location of the first crack in most of the unreinforced walls was located somewhere outside of the constant moment region. The joint in which cracking occurred was dependent upon the tensile strength of the mortar and the quality of the bond between the mortar and the concrete block units. Mortar residue accumulated in the bottom course block cells during the construction phase of the ungrouted and unreinforced walls and may have increased the effective rotational restraint at the bottom of some of the walls. Walls with unbonded reinforcement showed a cracking load that was 287% higher, on average, than that for the unreinforced walls. However, these walls had an average initial structural stiffness of 17.6 kN/mm, which was 19% lower than that of the ungrouted and unreinforced walls.

All partially grouted and conventionally reinforced walls initially behaved in a consistent manner, exhibiting first cracking within the constant moment region. This behaviour may be attributed to the the presence of grout that increases the overall moment of inertia of the wall and reduces the relative importance of the mortar bond strength. Walls with unbonded reinforcement showed a measured cracking load that was 68% lower, on average, than that for the partially grouted and conventionally reinforced walls. Partially grouted and conventionally reinforced walls had an average initial structural stiffness of 18.3 kN/mm which was 4% higher than walls with unbonded reinforcement.

Lateral Load Carrying Capacity

Walls with unbonded reinforcement exhibited an improved maximum flexural capacity that was 354%, on average, higher than that recorded for the ungrouted and unreinforced walls. A sudden drop in the lateral-load carrying capacity and the collapse of ungrouted and unreinforced walls occurred once maximum load was attained, while tests of walls with unbonded reinforcement was halted prior to failure. The formation of cracks at the ends and at midspan appeared to increase the lateral-load carry capacity of the walls with unbonded reinforcement by causing elongation of the reinforcement. Three cracks (i.e. within the constant moment region, at bottom and top of the wall) in walls with unbonded reinforcement created an essentially rigid body mechanism that enhanced the out-of-plane wall capacity.

The ultimate lateral load-carrying capacity of walls with unbonded reinforcement was not attained since those tests were terminated prior to failure due to limitations associated with the actuator stroke. Test results, at the stage that the actuator was stopped, showed that the measured maximum load for lateral load-carrying capacity was approximately 18% lower than those recorded for partially grouted and conventionally reinforced walls. The ultimate capacity of the walls with unbonded reinforcement may therefore be somewhat larger than indicated by test results. Additionally, their load-carrying capacity following cracking showed continuous growth as the lateral deflection increased, compared to the results of partially grouted and conventionally reinforced walls which exhibited an extended yield plateau.

Lateral Deflection

Observed mid-height deflections of the walls with unbonded reinforcement was, on average, 838% higher than those for unreinforced walls at maximum load conditions. The crack width at mid-height of the unreinforced walls at the maximum applied load level was smaller than at observed in the walls with unbonded reinforcement during testing. However, the unbonded reinforcement kept the wall segments together and stable, which enabled the development of significant cracks accompanied by large out-of-plane deflections. As mentioned previously, cracks widths on the wall surface positively affected the resisting capacity of the walls with unbonded reinforcement by causing additional elongation of the reinforcement.

Walls with unbonded reinforcement had an average mid-height deflection that was 331% higher, on average, than partially grouted and conventionally reinforced walls at maximum load conditions. Therefore, the lack of bond between the reinforcement and surrounding grout appeared to delay the rate at which the reinforcement could be fully engaged in resisting the applied loads.

Wall Stability

The walls with unbonded reinforcement resisted premature collapse as crack widths increased, unlike unreinforced walls that became unstable at large deflections. Furthermore, the walls with unbonded reinforcement were observed to return to their original position once the out-of-plane loading was removed during the test. This reflected the restoring action of the tensile force in the reinforcement, adding inherent stability to the wall with unbonded reinforcement, and counteracting slenderness effects produced by gravity loads. In contrast, ungrouted and unreinforced walls collapsed almost immediately following first cracking, while partially grouted and conventionally reinforced walls experienced permanent lateral deformation. Ungrouted and unreinforced, and partially grouted and conventionally reinforced walls therefore exhibited a condition of unstable equilibrium once displaced from their original position since the lateral deformation encouraged, rather than resisted, further displacement.

5.2.2 Influence of the unbonded reinforcement on measured strain

A Digital Image Correlation System was used to collect data that allowed for strain contours for all wall series to be mapped at various load levels. Comparisons were made between the walls with unbonded reinforcement and the control wall specimens.

Unreinforced walls exhibited large strain variations in the mortar joints, where cracks would form, with low tensile values observed at early stages of the loading. The brittle behaviour of these walls meant that strain contours rapidly changed such that tension in the mortar joints became near zero once the crack was formed, while strain contours in the wall segments showed very small magnitudes of compression strain in the post-cracking stage. In contrast, partially grouted and conventionally reinforced walls displayed the highest tensile strain values observed within the linear range. A more consistent strain distribution was observed as the ultimate load was approached for partially grouted and conventionally reinforced walls in comparison with those observed for walls with unbonded reinforcement since strains and stresses were transferred between the reinforcement and the grout along the wall height.

Strain variations in the mortar joints within the linear range prior to cracking were greater for walls with unbonded reinforcement than those for unreinforced walls. Once a horizontal crack formed, the strain contours indicated the generation of compression in the upper and lower wall segments. The walls with unbonded reinforcement showed the highest compression strain values when the crack widths increased since the unbonded reinforcement and the concrete grade beam restrained the vertical movement of the top and bottom of the wall, respectively. The presence of compressive struts in the walls with unbonded reinforcement were noted that extended along of the upper and lower wall segments. As the out-of-plane loading increased, the compressive strains in the walls with unbonded reinforcement increased: 1) within the bottom concrete block course, 2) within the top concrete block course, and 3) within the block courses adjacent to the mid-height crack. The formation of compressive struts within the wall was consistent with the assumption that arching action was the primary mechanism resisting lateral load in the walls with unbonded reinforcement.

5.2.3 Accuracy of the analytical model for ungrouted walls with unbonded reinforcement

Results of the developed analytical model were compared with the as-measured data for the walls tests with unbonded reinforcement. The model was developed based on assumptions regarding the

physical characteristics of the walls (dimensions, mass, etc.), formation of hinges at the ends and near mid height of the wall, and rigid-body rotation of the wall segments.

Comparison between the maximum loads (at the maximum observed mid height deflection) as obtained from testing and those resulting from the analytical model showed that the analytical model generally underestimated the as-measured ultimate loads. Results showed that the predicted values ranged from -38.1% to 14.5% of the experimental values. Using measured material properties for the reinforcing bars, the analytical model was able to reproduce the slopes of the experimental load-deflection curves in the post-cracking region, as well as provide a reasonable description of the overall experimental wall behaviour.

5.3 Recommendations for future research

A literature review revealed limited information related to alternative load resisting mechanisms for non-prestressed and ungrouted block walls with unbonded reinforcement. While the research program described herein demonstrated the potential for such a system, further research is required to demonstrate that unbonded reinforcement is a practical alternative that can be reasonably constructed on site to resist out-of-plane loading by engaging an arching mechanism. Such a wall system would be suitable to resist out-of-plane loads resulting from wind pressure or earthquakes. Even though walls with unbonded reinforcement might not be suitable for use in exterior walls due to serviceability concerns, these walls could help reduce the number of fatalities associated with the collapse of interior walls. In order to make this option feasible, construction details for walls with unbonded reinforcement must be improved to include effective and easily implemented anchorage for the vertical reinforcement. The placement and vertical alignment of the reinforcement within the cell core in a practical manner are also issues requiring further investigation.

Factors that could be considered in a subsequent study are listed below:

- Using a lateral top support similar to those used on-site, such as employing clip angles connected to an overhanging beam;

- The use of open-end concrete block units to facilitate the placement of the unbonded reinforcement during the construction of the masonry walls. Blocks that feature one or two open ends, such as "H" blocks, may provide a simpler method for the installation of the reinforcement;

- Reinforcement that is anchored at the bottom and top of the wall, and mechanically spliced within the wall will facilitate its installation. For example, the lower segment might be a steel dowel embedded into the concrete grade beam, while the upper segment could be anchored in a bond beam formed the top course of the wall, and mechanically connected to the dowel; and

- Alternate methods for aligning the reinforcing within the cells, such as partially or fully grouting selected cells while ensuring that the reinforcement remains unbonded.

References

Abrams, D. P., Angel, R., & Uzarski, J. (1996). Out-of-plane strength of unreinforced masonry infill panels. *Earthquake Spectra*, *12*(4), 825-844.

Abou-Zeid, B. M., El-Dakhakhni, W. W., Razaqpur, A. G., & Foo, S. (2010). Response of arching unreinforced concrete masonry walls to blast loading. *Journal of Structural Engineering*, *137*(10), 1205-1214.

Al-Menyawi, Y.M. (2001). *Concrete block masonry construction* (Doctoral dissertation). Texas Tech University, Lubbock, TX.

ASTM. (2016a). *Standard specification for carbon-steel wire and welded wire reinforcement, plain and deformed, for concrete* (ASTM A1064/A1064M-16). ASTM International, West Conshohocken, PA.

ASTM. (2016b). *Standard test methods for sampling and testing concrete masonry units and related units* (ASTM C140/C140M-16). ASTM International, West Conshohocken, PA.

ASTM. (2016c). *Standard test method for sampling and testing grout* (ASTM C1019-16). ASTM International, West Conshohocken, PA.

ASTM. (2016d). *Standard test methods and definitions for mechanical testing of steel products* (ASTM A370-16). ASTM International, West Conshohocken, PA.

ASTM. (2010). *Standard test methods for measurement of masonry flexural bond strength* (ASTM C1072-10). ASTM International, West Conshohocken, PA.

Anderson, C. (1984). Arching action in transverse laterally loaded masonry wall panels. *Structural Engineering, 62*(1), 12.

Bean Popehn, J.R., Schultz, A.E, & Drake, C.R. (2007). Behavior of slender, posttensioned masonry walls under transverse loading. *Journal of Structural Engineering*, *133*(11): 1451-1550. doi: 10.1061/(ASCE)0733-9445(2007)133:11(1541)

Cairns, J., & Rafeeqi, S. F. A. (2002). Analysis of reinforced concrete beams strengthened by external unbonded bars. *Magazine of Concrete Research*, *54*(2), 141-153.

Cairns, J., & Zhao, Z. (1993). Behavior of concrete beams with exposed reinforcement. *Proceedings Institution of Civil Engineers, Structures and Building*, *99*(2), 141-154.

Cintron, R., & Saouma, V. (2008). *Strain measurements with the digital image correlation system Vic 2D* (CU-NEES-08-06). Colorado, USA: The George E Brown, Network for Earthquake Engineering Simulation.

Correlated Solutions. (2010). *Vic 3D: Reference Manual*. Retrieve from: http:// www.CorrelatedSolutions.com.

CSA. (2014a). *Standards on concrete masonry units* (CAN/CSA-A165 Series-14 R2014). Canadian Standards Association, Mississauga, ON.

CSA. (2014b). *Mortar and grout for unit masonry* (CAN/CSA-A179-14). Canadian Standards Association, Mississauga, ON.

CSA. (2014c). *Masonry construction for buildings* (CAN/CSA A371-14). Canadian Standards Association, Mississauga, ON.

CSA. (2014d). *Design of masonry structures* (CAN/CSA S304-14). Canadian Standards Association, Mississauga, ON.

CSA. (2014e). *Carbon Steel Bars for Concrete Reinforcement* (CAN/CSA G30.18-09 R2014). Canadian Standards Association, Mississauga, ON.

CSA. (2013). *Cementitious materials compendium* (CAN/CSA A3000-13). Canadian Standards Association, Mississauga, ON.

CSA. (2009). *Sieve analysis of fine and coarse aggregate* (CAN/CSA A23.2-2A-09). Canadian Standards Association, Mississauga, ON.

Curtin W.G., Shaw G., Beck J.K., & Howard J. (1989). *Design of post-tensioned brickwork*. The Bick Development Association. Woodside House, Winkfield.

Devalapura, R.K. (1995). *Development of prestressed clay brick masonry walls* (Doctoral dissertation), The University of Nebraska, Lincoln, NE.

Dawe, J. L., & Aridru, G. G. (1992). Post-tensioned concrete masonry walls subjected to uniform lateral loadings. *Proceedings of the 6th Canadian Masonry Symposium,* 201-212.

Drysdale, R. G., & Essawy, A. S. (1988). Out-of-plane bending of concrete block walls. *Journal of Structural Engineering*, *114*(1), 121-133.

Drysdale, R. G., & Hamid, A. A. (2005). *Masonry structures: Behavior and design*. Ontario, Canada: Canadian Masonry Design Centre.

Gabrielsen, B., & Wilton, C. (1974). *Shock tunnel tests of arched wall panels* (URS Report No. URS-7030-19). California, USA: URS Research Company.

Giffith, M., & Vaculik, J. (2005). *Flexural strength of unreinforced clay brick masonry walls*. Paper presented at the 10th Canadian Masonry Symposium, Alberta, Canada. Retrieved from http://www.canadamasonrydesigncentre.com/download/10th_symposium/4c-2.pdf

Graham, K.J., & Page, A.W. (1995). The flexural design of post-tensioned hollow clay masonry. *Proceedings of the 7th Canadian Masonry Symposium*, Hamilton, ON, 12 pp.

Hendry, A. W. (1973). The lateral strength of unreinforced brickwork. *The Structural Engineer*, *51*(2), 43-50.

Hamid, A. A., & Drysdale, R. G. (1988). Flexural tensile strength of concrete block masonry. *Journal of Structural Engineering*, *114*(1), 50-66.

Korany, Y., & Drysdale, R. 2006. Rehabilitation of masonry walls using unobtrusive FRP techniques for enhanced out-of-plane seismic resistance. *Journal of Composites for Construction*, *10*(3), 213-222. doi: 10.1061/(ASCE)1090-0268(2006)10:3(213)

Kothandaraman, S., & Vasudevan, G. (2010). Flexural retrofitting of RC beams using external bars at soffit level–An experimental study. *Construction and Building Materials*, *24*(11), 2208-2216.

Liebenberg, A. C. (1966). *Arch action in concrete slabs*. National Building Research Institute, Council for Scientific and Industrial Research.

Miranda, H., Feldman, L.R., & Sparling, B.F. (2016). Feasibility of using unbonded reinforcement in concrete block walls. *Proceedings of the 2016 CSCE Annual Conference* (electronic compendium), London, ON, 10 pp.

McDowell, E. L., McKee, K. E., & Sevin, E. (1956). Arching action theory of masonry walls. *Journal of the Structural Division*, *82*(2), 1-8.

Page, A. W. (1979). A non-linear analysis of the composite action of masonry walls on beams. *Proceedings of the Institution of Civil Engineers*, *67*(1), 93-110.

Phipps, M.E. (1993). The principles of post-tensioned masonry design. *Proceedings of the 6th North American Masonry Conference*, Philadelphia, PA, 11 pp.

Rodríguez, R., Hamid, A.A., & Larralde, J. (1998). Flexural behavior of post-tensioned concrete masonry walls subjected to out-of-plane loads. *ACI Structural Journal*, *95*(1), 61-70.

Sutton, M., Orteu, J., & Schreier, H. (2009). *Image correlation for shape, motion and deformation measurements*. New York, USA: Springer Nature.

Tabbakhha, M., & Deodatis, G. (2017). Effect of uncertainty of tensile strength of mortar joints on the behavior of masonry walls under lateral loads. *Journal of Structural Engineering*, *143*(2). 04016166.

TMS, ACI, & SEI. (2013). *Building code requirements and specification for masonry structures with commentaries* (TMS 402-13/ ACI 530-13/ ASCE 5-13). Masonry Standards Joint Committee, Boulder, CO.

Thomas, F. G. (1953). The strength of brickwork. *The Structural Engineer*, *31*(2), 35-46.

Udey, A. (2014). *Realistic wind loads on unreinforced masonry walls* (M.Sc. thesis), University of Saskatchewan, Saskatoon, SK.

Varela-Rivera, J., Moreno-Herrera, J., Lopez-Gutierrez, I., & Fernandez-Baqueiro, L. (2012). Out-of-plane strength of confined masonry walls. *Journal of Structural Engineering*, *138*(11), 1331-1341.

Wight, J., & MacGregor J. (2012). *Reinforced concrete: Mechanics and design (Vol 6)*. Upper Saddle River, NJ: Prentice Hall.

Zhou, P., & Goodson, K. (2001). Subpixel displacement and deformation gradient measurements using digital image/speckle correlation. *Society of Photo-Optical Instrumentation Engineers*, *40*(8), 1613-1620.

Appendix A: Sample Size Determination

Presented herein is the determination of the required number of specimens constructed at the Structures Laboratory for this research program. A statistical analysis was undertaken to identify the sample size needed to establish the statistical significance of experimental results. The statistical parameters were determined based on variability data taken from previous studies. Specifically, an analysis was carried out to determine the number samples required to make inferences about comparison between the out-of-plane behaviour of unreinforced wall specimens (UR), conventionally reinforced and partially grouted wall specimens (PGR), and ungrouted wall specimens with unbonded reinforcement (UB).

A.1 Sample Size Determination

It was determined that at least six replicate specimens for each set of walls would be required to show a statistically significant difference between two populations at the 90% of confidential level (i.e. using a two-tailed student test) with a minimum 10% difference between their mean values, assuming a COV of 8% for the critical responses. Statistical values were determined based on previous research conducted in the University of Saskatchewan by Udey (2013), while the statistical procedures to identify outliers is presented at the end of this section. As discussed in Chapter 3, an additional three unbonded reinforced wall specimens with a slightly modified design (i.e. the first course was ungrouted, whereas the remaining six walls with unbonded reinforcement featured a fully grouted first course) were also tested. Therefore, a total of twenty-one wall specimens were included in this study.

Assumed number of unreinforced wall specimens type 1, N_1:	$N_1 = 6$
Degrees of freedom, d.o.f.:	$\text{d.o.f} = 2n - 2 = 10$
Expected coefficient of variation in each specimen type, C.O.V:	$\text{C.O.V.} = 0.08$
Mean out-of-plane force resistance in specimen type 1, X_1 (arbitrarily set):	$X_1 = 100 \, \text{N}$
Standard deviation in specimen type 1, σ_1:	$\sigma_1 = X_1 * \text{C.O.V} = 8$
Assumed number of unreinforced wall specimens type 2, N_2:	$N_2 = 6$

Mean out-of-plane force resistance in specimen type 2, X_2 $X_2 = 110$ N
(based on an expected difference of 10% between the mean
values of the two specimen types):

Standard deviation in specimen type 2, σ_2: $\sigma_2 = X_2 * C.O.V = 8.8$

Difference between the mean values, X_d: $X_d = X_1 - X_2 = 10$

"t" value calculation in accordance with the student "t" test $t = 2.059$
(Equation A.1)

$$\dfrac{(X_d)}{\sqrt{\dfrac{\sigma_1^2(N_1\text{-}1)+\sigma_2^2(N_2\text{-}1)}{N_1+N_2\text{-}2}\left(\dfrac{1}{N_1}+\dfrac{1}{N_2}\right)}} \qquad [A.1]$$

The level of confidence for $t = 2.059$ with 10 degrees of freedom from a two-tailed student "t" table is equal to 92%. Therefore, six replicate specimens are sufficient to demonstrate a statistically difference between two populations at the 90% confidence level with a minimum 10% difference between their mean values.

Appendix B: Concrete Grade Beam Design and Construction

This appendix presents the design considerations and construction process for the concrete grade beams used in this study. Design considerations were formulated to meet the requirements established in CSA A23.3-14 (CSA 2014) and to overcome the constraints resulting from space availability within the test frame. Modifications were made to the series of grade beams used for specimens including the unbonded reinforcement. The concrete grade beams were built using ready-mix concrete from a local supplier.

B.1 Design

The grade beams were constructed to simulate a realistic pinned support that was formed by placing the first course of masonry blocks on the concrete bases using a standard mortar joint. The ready-mix concrete was supplied by a local company, and had an actual average compressive strength of 24 MPa resulting from test of three cylinders for every delivery. As shown in Figure B.1 to B.3, the concrete grade beams were 1700 mm long, and 300 mm wide x 400 mm tall. The length of the grade beams was extended beyond each side of the wall specimens to allow steel beams used to clamp the grade beam to the test floor. Two No.10 liftings lugs were included in the reinforcing cage to facilitate the transportation of the wall specimens to the test frame location.

Grade beams for the UB wall specimens were longitudinally reinforced with six No. 15 bars, and No. 10 stirrups at 380 mm on-center, as shown in Figure B.1 and Section A-A in Figure B.2(a). These grade beams required two openings of 200 mm x 200 mm to accommodate the anchor chucks for the vertical reinforcement. Section B-B in Figure B.2(b) shows a typical grade beam section used for the UB wall specimens which included a 240 mm x 153 mm x 9.7 mm steel plate to prevent crushing underneath the concrete beam, and a 20.9 mm PVC pipe to allow the reinforcement to pass through the beam. Two No. 10 anchors were welded on the plate top surface to prevent any misalignment of the PVC pipe during concrete placement, as illustrated in Figure B.2(c).

Figure B.3 illustrates a typical grade beam for the UR and PGR wall specimens. Section C-C in Figure B.3 shows that four No. 15 bars served as longitudinal reinforcement, and six No. 10

stirrups with a 135° hook served as the transverse reinforcement. All the grade beams featured a concrete cover of 40 mm and an effective depth of 342.5 mm.

B.2 Construction

Twelve concrete grade beams were built in the laboratory as typical supporting bases for UR and PGR walls using Grade 400 steel bars, timber formwork, and ready-mixed concrete. First, the formwork was built using 2 in x 4 in x 10 ft lumber and 7/16 in x 48 in x 8 ft oriented strand board. Second, the steel bars were bent assembled hand according to the design using a steel bending machine. The reinforcement cage was then assembled, as shown in Figure B.4(a). Prior to pouring the concrete, a debonding agent was applied to formwork surface and the steel cage was placed inside the form using plastic support chairs to ensure proper concrete cover. Figure B.4(b) presents a typical grade beam after concrete was placed. Grade beams were cured for a minimum of 28 days prior to removal of the formwork.

Nine concrete beams with two pre-formed openings were built as supporting bases for the UB wall specimens using similar materials to those used for typical grade beams. Rigid foam insulation was cut used to form a 300 mm x 200 mm x 200 mm blockout, that was inserted in the steel cage, as shown in the Figure B.5(a). The steel cage in this type of grade beam featured six No. 15 longitudinal steel bars, five No. 10 closed stirrups, and two lifting lugs. Two 153 mm x 240 mm x 9.7 mm steel plates with two No.10 anchors were integrated into the steel cage to allow for their transportation from that location where they were cast to the test bed. Additionally, two 20.9 mm PVC pipes were placed on the top of the steel plate surfaces to allow the unbonded reinforcement to pass through the entire grade beam. A wooden template was used to keep the PVC pipes in their desired locations during placing and curing as presented in Figure B.5(b). The grade beams were removed from the formwork following the 28 days curing period.
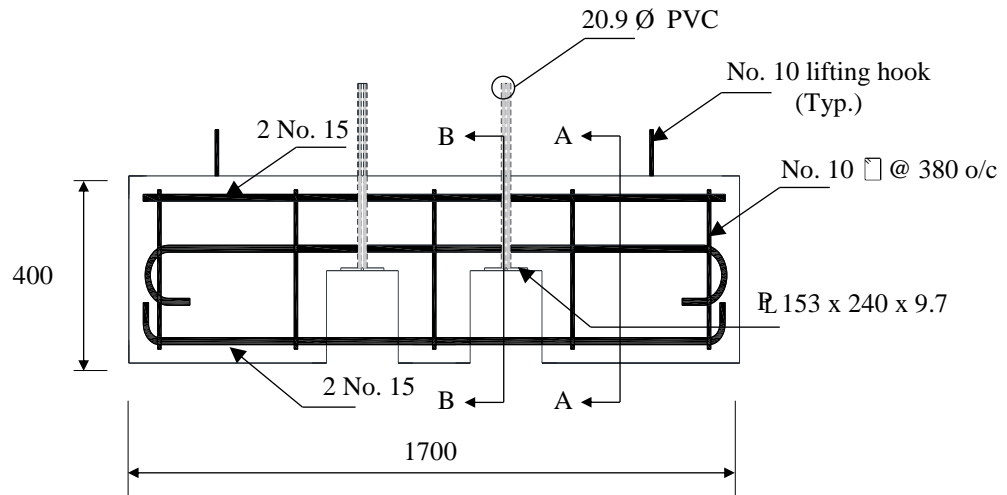
Figure B.1: Typical concrete grade beam for UB walls (dimensions in mm).

Section A-A

(a)

Section B-B

(b)

(c)
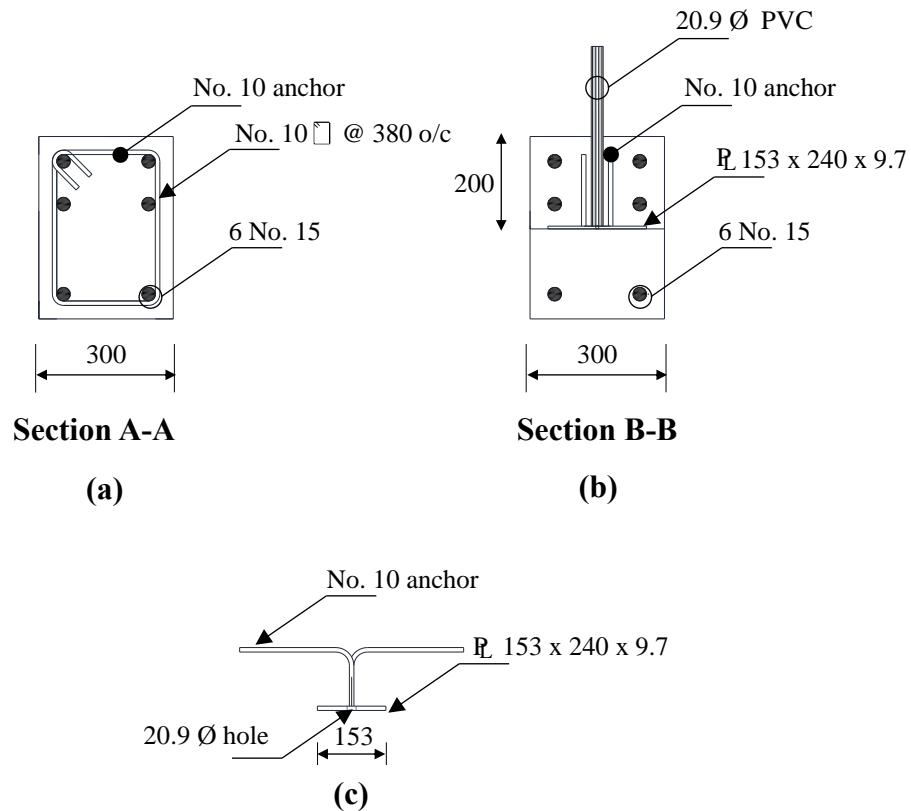
Figure B.2: Concrete grade beam sections: (a) section A-A, (b) section B-B, and (c) steel plate details (dimensions in mm).
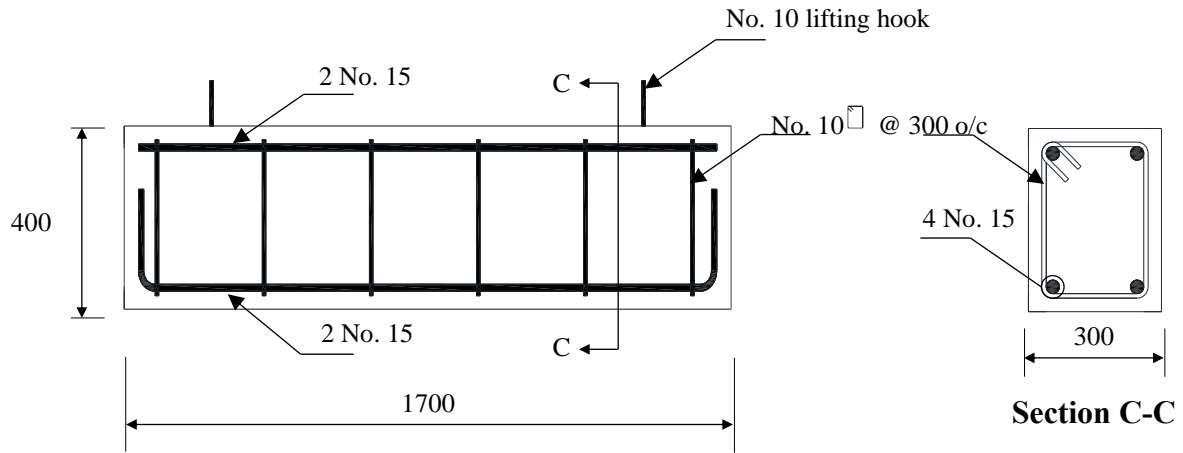
Figure B.3: Typical concrete grade beam for UR and PGR walls (dimensions in mm).

(a)   **(b)**

Figure B.4: Grade beam construction for UR and PGR walls: (a) reinforcing steel cage, and (b) wooden form and grade beam after concrete placement.

(a)   **(b)**

Figure B.5: Grade beam construction for UB walls: (a) reinforcement cage with insulation foam, and (b) wooden form, hard board template, and grade beam during curing.

Appendix C: Wall Companion Specimens and Masonry Prisms

This appendix shows individual test results for all masonry block companion specimens, masonry prisms, and reinforcement companion specimens tested in this research program, as discussed in Section 4.2.1. The concrete block units were randomly selected to be tested and used to build a series of masonry prisms, while reinforcement samples were acquired from the respective steel batches. Mortar cubes, grouted cylinders and grouted prisms were built in parallel with each wall construction.

C.1 Wall Companion Specimens

C.1.1 Concrete Block Units

Six block specimens were measured to accurately determine their section properties. Resulting measurements are reported in Table C.1. Three flat blocks and three frogged ended blocks were selected and labelled by the letters A through C. Dimensions were taken using a digital calipers and measured to the nearest 0.01 mm. Figures C.1(a) and (b) show the plan view and transversal sections of the frogged end blocks with measured dimensions of 190.32 mm x 188.61 mm x 389.50 mm, while flat ended blocks had measured dimensions of 190.91 mm x 188.80 mm x 389.33 mm. The selected concrete block units were in compliance with the minimum thickness of faceshell and webs, and with the permissible variations in dimensions, as prescribed in CSA Standard A165-14 (CSA 2014a). Sections A-A and B-B show the typical block elevation showing the presence of flared and tapered webs.

Three frogged end blocks and three flat end blocks were tested in compression to verify the compressive strength of the concrete block units. Absorptive tests also were performed on six additional concrete blocks to determine the average net cross-sectional area in accordance with the ASTM Standard C140/C140M-16 (ASTM 2016b), and CSA A165-14 (CSA 2014a). Figure C.2(a) shows a concrete block unit that was submerged in water for 24 hours. The block units were then weighed using a digital scale and placed into an oven at 110° C for not less than 24 hours, as shown in the Figure C.2(b). The weight of the units was accurately measured in 1 gram increments. Table C.2 summarizes the absorptive and compression test results of twelve block specimens showing the results from the absorptive and compression tests conducted at laboratory.

Figure C.3 shows the compressive strength test of a block unit which was performed in accordance with ASTM Standard C140/C140M-16 (ASTM 2016b). A 2000 kN Amsler Beam Bender was used to test the concrete block units; the data was collected via a data acquisition system. The load, measured using a load cell, was evenly distributed on the block unit using a steel spreader beam, steel plate, and fibre board. Data was recorded using a data acquisition system with a sampling frequency of 10 Hz. The mean compressive block strength was determined based on the resulting ultimate load and the average net cross-sectional area, as obtained from the absorptive test.

C.1.2 Mortar Preparation and Mortar Cube Specimens

Mortar was prepared in the Structures Laboratory using a mortar mixer. A dry 25 L bucket and an industrial scale were used to measure the components of the mixture. One full bucket of water, two full buckets of sand and two 17 kg mortar cement bags were added into the main container, as presented in the Figure C.4(a). One full bucket of sand was poured into the mixture in small portions of approximately 5 kg after two minutes of having started this process.

Retempering of the mortar was allowed to keep the mortar workable during the construction of the wall specimens. This practice was performed on a mortar board by the experienced mason using a trowel and adding small quantities of water into the mortar pile. Use of a mortar batch for more than two hours was not permitted to ensure proper consistency of materials in specimen construction.

Figure C.4(b) shows that six 50 mm mortar cubes were cast from each mortar batch, in accordance with CSA Standard A179-14 (CSA 2014b). A total of 192 mortar cubes were cast from 32 mortar batches. The mortar cubes were demoulding following 24 hours of curing in ambient conditions.

An Instron DX600 Universal Testing Machine was used to test the mortar cubes in compression at a constant load rate of 10 kN/min, as shown in Figure C.5. Mortar cubes were coded based on the mortar batch number. The associated mortar cubes were tested in parallel with the respective wall test. Partner[TM] computer software was used to control the test machine and record the data. The mortar cubes were tested until failure in accordance with CSA Standard A179-14 (CSA 2014b) with results shown in Table C.3.

C.1.3 Grouting Preparation and Companions

High-slump grout was prepared using a 5:1 aggregate-to-cement ratio with a maximum aggregate size of 10 mm, Lafarge Type GU hydraulic cement, and water. Coarse and fine aggregate was pre-mixed by Lafarge and delivered to the Laboratory. Three 3500 g aggregate samples were used to establish that the coarse to fine aggregate ratio was 2:2-2/5 by volume as required by CSA Standard A179-14 (CSA 2014b). The aggregate gradation of the coarse and fine aggregate was performed in compliance with the procedure defined in CSA Test Method A23.2-2A (CSA 2009) as show in Tables C.4 to C.6.

Three 17.1 L buckets of aggregate and one 22.8 L bucket of water were used for the preparation of each grout batch. Components were mixed using a mechanical mixer (Figure C.6(a)) which was previously moistened with tap water. One full bucket of water and six buckets of pre-blended aggregate were initially added while the drum rotated. Two bags of cement were then added to facilitate the water-cement reaction and to bind the components of the mixture. The drum slope was then increased approximately 20 degrees and three more buckets of pre-blended aggregate were poured. Approximately six liters of water were added slowly until the grout reached a uniform consistency suggesting visible workability. At this time, the grout was ready to be transported and placed without excessive segregation. At least two slump tests (Figure C.6(b)) were performed to verify that the mixture had achieved a high-slump grouting which varied from 210 mm to 240 mm, in accordance with CSA Standard A179-14 (CSA 2014b).

A series of non-absorbent cylinders and absorbent prisms were cast for each grout batch. Three non-absorbent cylinders for each batch were made using 150 mm tall cylinders in accordance with CSA Standard A179-14 (CSA 2014b), and three absorbent prisms were prepared according to ASTM Standard C1019-16 (ASTM 2016c) for each grout batch. The companion specimens were allowed to cure for a minimum of 28 days. Plastic sheets were used to cover the specimens during the curing period. A total of thirty non-absorbent grout cylinders and thirty absorbent grout prisms were cast from the ten grout batches.

Figure C.7(a) and (b) show the Instron DX600 Universal Testing Machine that was used to test the non-absorbent grout cylinders and absorbent prisms. The load was applied at a constant rate of

15 MPa/min. Both ends were capped with sulfur to ensure an even surface once the grout cylinders were removed out from the molds. Grout cylinders and prisms were tested within 24 hours of testing the corresponding wall specimen. Tables C.7 and C.8 show the data recorded by the data acquisition system.

C.1.4 Reinforcing Bar Companion Specimens

Grade 400 steel reinforcing bars were used for the fabrication of the concrete grade beam reinforcement cages used in the concrete grade beams. No. 10 and No.15 reinforcement was delivered in 6 m lengths by a local supplier in one batch. The reinforcement was cut to the required dimensions using a hand saw and bent according to the design.

Grade 515 deformed steel wire, 6.4 mm in diameter, was used as longitudinal reinforcement in the PGR and UB walls. This reinforcement was cut and straightened into of 3.5 m lengths from the same coil by the supplier prior to delivery. Once at the laboratory, the reinforcement was stored in a dry climate controlled environment.

As a result, the reinforcement was tested in conformance with ASTM Standard A370-16 (ASTM 2016d) using the Instron DX600 Universal Testing Machine; the results are shown in Table C.9. Six samples were tested to evaluate their tensile properties. Figure C.8 shows the test set-up for the tensile tests. Data was sampled at a rate of 0.2 kN/s to determine the yield strength, ultimate tensile strength, and modulus of elasticity, while LVDTs and strain gauges were placed with a 50 mm (2 in) gauge length on the Grade 515 reinforcement to determine their axial extension, with stress and strain data was collected from the tensile test. Properties such as yield strength, ultimate strength, strain and modulus of elasticity were determined from the plots and used as input to the analytical model.

C.2 Masonry Prisms

Two masonry prisms were constructed for each UR and UB wall specimen: one ungrouted three-course prism was constructed for compression testing, and one two-course high prism was constructed for bond wrench testing. Three masonry prisms were made for each PGR wall specimen, with one two-course prism used for bond wrench testing, and two three-course prisms

92

used for compression testing. One of three-course prisms was fully grouted whereas another prism was ungrouted. The prisms were constructed following construction of first eight courses of the corresponding wall, using the same mortar batches used in the midspan region of the wall.

Prisms were built in a stacked bond pattern with 10 mm thick bed joints. The three-course prism dimensions were 390 mm x 190 mm x 590 mm, whereas the two-course prisms were 390 mm high. Prisms were stored under the same climatic condition as the corresponding wall specimens and covered with plastic sheets to prevent moisture loss. Prisms were tested within 24 hours of the corresponding wall specimen.

C.2.1 Compression Tests of the Masonry Prisms

Figure C.9 shows a compression test of a typical masonry prism. A total of twenty-one ungrouted and six grouted masonry prisms were tested using the 2000 kN Amsler Beam Bender in accordance with CSA Standard S304-14 Annex D (CSA 2014d). A constant loading rate of 1 kN/s was used for testing all masonry prisms. Readings were acquired using a load cell with a static error band of ±0.05. Load was applied to the top surface of the masonry prism, and uniformly distributed using a steel plate, spreader beam, and fibre board. The mean compressive prism strength was determined based on the average maximum loading and the average net cross-sectional area for each type of masonry prism (i.e. frog ended and flat ended block). Results are presented in Table C.10 and C.11.

Vertical deformation of the three-course prisms was measured using two 50 mm stroke linear variable differential transducers (LVDTs with an error of ±0.35%) located 400 mm apart. Two 3 mm steel angles were glued onto the block face shell to support the LVDTs. Data from the load cell and LVDTs were recorded at a rate of 1 Hz by a data acquisition system using LabVIEW software. LVDTs were removed from the test frame prior the failure of the prism to avoid any damage.

C.2.2 Bond Wrench Test

Figure C.10 shows the bond wrench apparatus that was used to test twenty-one two-course prisms. Testing was conducted in accordance with CSA Standard S304-14 Annex D (CSA 2014d). This

apparatus was a modified version of the apparatus described in ASTM Standard C1072-10 (ASTM 2010) due to the dimensions of the actual concrete blocks used in this experimental program. The lower and upper blocks were clamped to test the mortar joint between them once the masonry prism was in the support frame. A load cell with a static error band of ±0.04 was then attached to the loading arm. A hydraulic piston was then used to apply a uniform load at a rate of 1 mm/min. The data was recorded used a data acquisition system and Lab View software at a sampling rate of 4 Hz. Results are shown in Table C.12.

Table C.1: Block dimensions testing results

Block Type	Specimen	Width[a] [mm]	Height[b] [mm]	Length[b] [mm]	Face Shell Thickness[b] [mm]	Web Thickness[d] [mm]
Frogged	A	190.28	189.37	389.5	33.19	27.37
Frogged	B	190.27	188.04	389.5	33.35	27.34
Frogged	C	190.41	188.41	389.5	33.77	27.53
Average =		190.32	188.61	389.5	33.44	27.41
Flat	A	190.98	187.84	389	33.60	30.76
Flat	B	190.70	189.07	389.5	33.36	30.68
Flat	C	191.06	189.48	389.5	33.58	31.13
Average =		190.91	188.80	389.33	33.51	30.86

[a] Average result from top and bottom block faces.
[b] Average result from front and back block faces.
[c] Average results from front and back face shells located on the block bottom face.
[d] Average result from three locations along the block web located on the block bottom face.

Table C.2: Block unit testing results

Block Type	Specimen	Moisture Content [%]	Oven-Dry Density [kg/m^3]	Average Net Area [mm^2]	Compressive Strength [MPa]
Frogged	A	16.3	1615	47067	23.1
Frogged	B	16.1	1610	47522	24.5
Frogged	C	11.3	1675	46464	21.9
Average =		14.6	1633	47018	23.2
COV (%) =		19.5	2.24	1.13	6.94
Flat	A	17.3	1618	47933	22.2
Flat	B	13.8	1646	47502	21.5
Flat	C	19.7	1637	47159	19.6
Average =		16.9	1634	47531	21.1
COV (%) =		17.6	0.86	0.82	7.86

Table C.3: Mortar cube compressive strength testing results

Batch #	Compressive Strength[a] [MPa]						Average Compressive Strength [MPa]
	A	B	C	D	E	F	
1	22.1	17.6	22.4	21.9	19.9	22.0	21.0
2	22.0	23.9	22.8	21.5	20.8	20.6	21.9
3	11.9	11.8	11.7	11.9	12.1	12.9	12.1
4	21.8	21.2	21.9	21.3	20.7	20.6	21.2
5	19.1	19.1	19.9	16.4	18.0	17.0	18.3
6	18.8	18.8	19.6	18.2	19.0	19.2	18.9
7	19.3	19.9	18.5	18.5	19.1	18.8	19.0
8	15.7	19.1	19.7	20.4	20.1	19.8	19.1
9	12.4	12.8	11.4	11.9	12.1	12.5	12.2
10	16.3	19.0	18.7	16.9	15.7	19.5	17.7
11	13.9	13.4	14.7	14.5	14.6	15.7	14.5
12	23.8	21.2	23.9	17.4	19.4	22.4	22.1
13	17.4	15.4	18.1	16.8	16.1	17.1	16.8
14	21.4	19.3	23.1	21.4	21.3	21.9	21.4
15	23.8	22.6	26.1	28.5	28.8	30.2	27.5
16	22.9	25.5	23.8	24.2	22.7	26.8	24.3
17	14.8	14.6	14.6	15.2	14.3	15.8	14.9
18	19.4	20.7	22.4	23.9	20.3	21.3	21.3
19	15.9	15.1	15.3	15.6	16.0	15.9	15.6
20	16.9	17.1	16.9	17.1	16.5	14.9	16.6
21	19.0	17.2	18.0	18.6	16.1	16.6	17.6
22	18.7	19.1	21.2	20.3	19.5	20.4	19.8
23	16.9	17.3	15.8	15.4	15.6	13.9	15.8
24	14.0	13.2	13.4	15.9	14.7	16.9	14.7
25	19.3	16.8	16.8	16.7	18.6	19.4	17.9
26	18.3	15.8	19.5	17.6	17.4	18.0	17.7
27	15.1	16.5	16.3	16.4	16.9	18.3	16.6
28	19.8	16.9	18.7	18.5	17.6	18.9	18.4
29	15.9	16.6	15.4	17.1	16.9	18.0	16.6
30	16.3	17.1	17.2	17.9	17.4	15.5	16.9
31	15.7	16.8	16.4	16.7	16.9	16.2	16.4
32	21.5	18.9	19.9	19.2	19.5	21.0	20.0
Average =							18.0
COV (%) =							16.0

[a] Mortar cube specimens for each mortar batch were labelled by a positive integer number and the letters A through F.

Table C.4: Aggregate gradation of the fine aggregate used in the grout mix

ISO sieve size	Fine aggregate (sand),% passing			CSA A179-14 requirements
	Sample 1	Sample 2	Sample 3	
14 mm	--	--	--	--
10 mm	--	--	--	--
5 mm	100	100	100	100
2.5 mm	88	89	89	90 – 100
1.25 mm	80	80	79	85 – 100
630 μm	58	51	47	65 – 95
315 μm	13	10	10	15 – 80
160 μm	4	3	4	0 – 35

Table C.5: Aggregate gradation of the coarse aggregate used in the grout mix

ISO sieve size	Fine aggregate (sand),% passing			CSA A179-14 requirements
	Sample 1	Sample 2	Sample 3	
14 mm	100	100	100	100
10 mm	81	82	80	85 – 100
5 mm	21	19	18	10 – 30
2.5 mm	9	9	8	0 – 10
1.25 mm	0	0	0	0 – 5
630 μm	--	--	--	--
315 μm	--	--	--	--
160 μm	--	--	--	--

Table C.6: Aggregate gradation of the fine aggregate used in the mortar mix

ISO sieve size	Fine aggregate (sand),% passing			CSA A179-14 requirements
	Sample 1	Sample 2	Sample 3	
14 mm	--	--	--	--
10 mm	--	--	--	--
5 mm	100	100	100	100
2.5 mm	99	99	99	90 – 100
1.25 mm	98	97	97	85 – 100
630 μm	91	89	86	65 – 95
315 μm	39	37	26	15 – 80
160 μm	14	13	10	0 – 35

Table C.7: Non-absorbent grout cylinder compressive strength testing results

Batch #	Compressive Strength[a] [MPa]			Average Compressive Strength [MPa]
	A	B	C	
1	23.5	21.3	21.1	22.0
2	26.6	6.6	30.3	28.5
3	18.24	18.4	26.7	18.3
4	33.8	22.9	23.6	23.3
5	26.7	18.5	13.1	15.8
6	29.3	32.7	29.4	30.5
7	21.1	19.2	18.3	19.6
8	23.6	19.4	16.5	21.5
9	22.1	15.4	9.1	12.3
10	25.2	19.5	21.8	22.2
Average =				21.4
COV (%) =				25.4

[a] Mortar cube specimens for each mortar batch were labelled by a positive integer number and the letters A through C.

Table C.8: Absorbent prism compressive strength testing results

Batch #	Compressive Strength[a] [MPa]			Average Compressive Strength [MPa]
	A	B	C	
1	14.1	13.2	12.8	13.4
2	16.8	20.9	20.1	20.5
3	17.2	19.5	18.6	18.4
4	19.3	21.8	19.3	20.1
5	18.4	17.7	20.6	18.9
6	18.0	19.8	14.8	18.9
7	17.9	14.8	17.1	17.5
8	8.8	17.0	21.7	19.3
9	18.4	20.6	19.4	19.5
10	20.5	19.7	18.2	19.5
Average =				19.2
COV (%) =				4.70

[a] Mortar cube specimens for each mortar batch were labelled by a positive integer number and the letters A through C.

Table C.9: As-tested mechanical properties of the reinforcement

Bar diameter [mm]	Sample[a]	Yield Strength [MPa]	Ultimate Tensile Strength [MPa]	Young's Modulus [GPa]
	A[b]	---	---	---
	B	602	621	219
	C	578	619	208
	D	553	613	219
6.4	E	528	594	191
	F	552	611	189
	Average =	562	612	205
	COV (%) =	5.08	1.72	7.12

[a] Reinforcement samples were labelled by the letters A through F.
[b] Instron DX600 Testing Machine stopped at the beginning of the test and data was not recorded.

Table C.10: Compressive strength testing results of the ungrouted masonry prisms

Ungrouted Prisms	Compressive Strength [MPa]
1	22.3
2	18.4
3	21.2
4	19.4
5	21.9
6	20.2
7[a]	---
8	20.6
9	21.4
10	19.7
11	20.2
12	20.6
13	17.4
14	20.0
15	23.9
16	18.4
17	22.3
18	22.6
19	19.8
20	20.9
21	18.2
Average =	20.5
COV (%) =	8.10

[a] Excludes results from UB-U1 wall.

Table C.11: Compressive strength testing results of the grouted masonry prisms

Grouted Prisms	Compressive Strength [MPa]
1	12.0
2	12.5
3	11.9
4	14.5
5	13.4
6	14.5
7	15.3
Average =	13.4
COV (%) =	10.0

Table C.12: Flexural tensile strength of the masonry assemblages

Masonry Prism[a]	Corresponding Wall	Flexural Strength [MPa]	Masonry Prism	Corresponding Wall	Flexural Strength [MPa]
1	UR-1	0.12	12	UB-G3	0.04
2	UR-2	0.02	13	UB-G4	0.03
3	UR-3	0.06	14	UB-G5	0.10
4	UR-4	0.05	15[b]	UB-G6	---
5	UR-5	0.02	16	PGR-1	0.06
6	UR-6	0.02	17	PGR-2	0.08
7[b]	UB-U1	0.04	18	PGR-3	0.05
8[c]	UB-U2	---	19	PGR-4	0.03
9[c]	UB-U3	---	20	PGR-5	0.08
10	UB-G1	0.00	21	PGR-6	0.06
11	UB-G2	0.15			
Average =					0.06
COV (%) =					71

[a] Masonry prisms for each wall were labelled by a positive integer number.

[b] Excludes results from UB-U1 wall.

[c] Physical outlier.
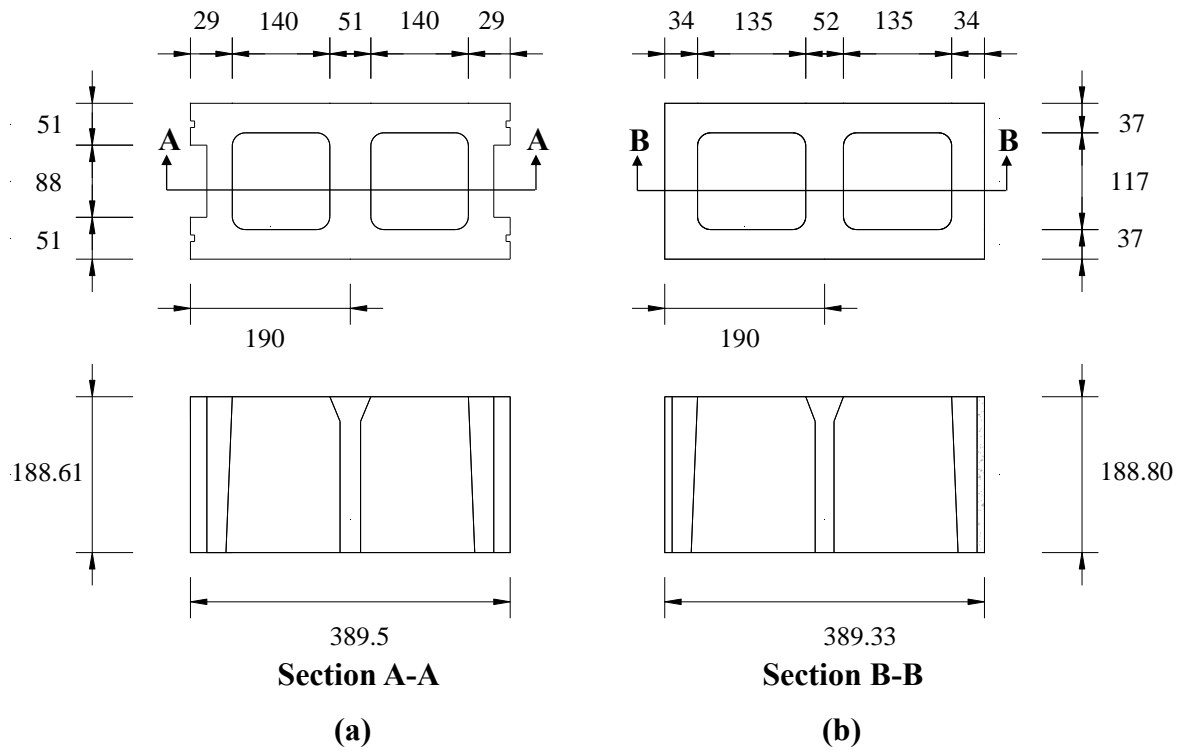
Figure C.1: Standard concrete block measuring dimension: (a) frogged end block, and (b) flat end block (dimensions in mm).

Figure C.2: Absorption test: (a) submerged block unit, and (b) oven drying of units.

101
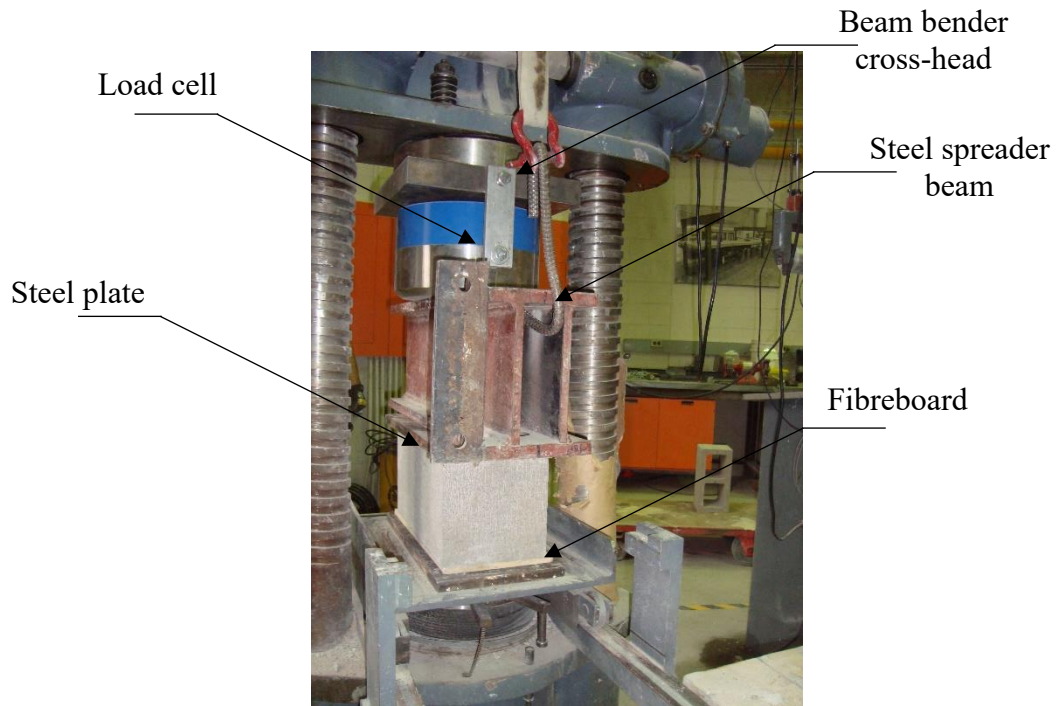
Figure C.3: Concrete block compression test.

| (a) | (b) |

Figure C.4: Procedure of mixing mortar and preparing companion specimens: (a) mortar preparation using a mortar mixer, and (b) mortar cube preparation.

(a)

Figure C.5: Mortar cube testing.

(a)   **(b)**

Figure C.6: Grout preparation: (a) grout preparation, and (b) slump test.

(c)   **(d)**

Figure C.7: Compression tests for the companion specimens: (a) non-absorbent grout cylinder, and (b) absorbent grout prism.

Figure C.8: Reinforcing test set-up.
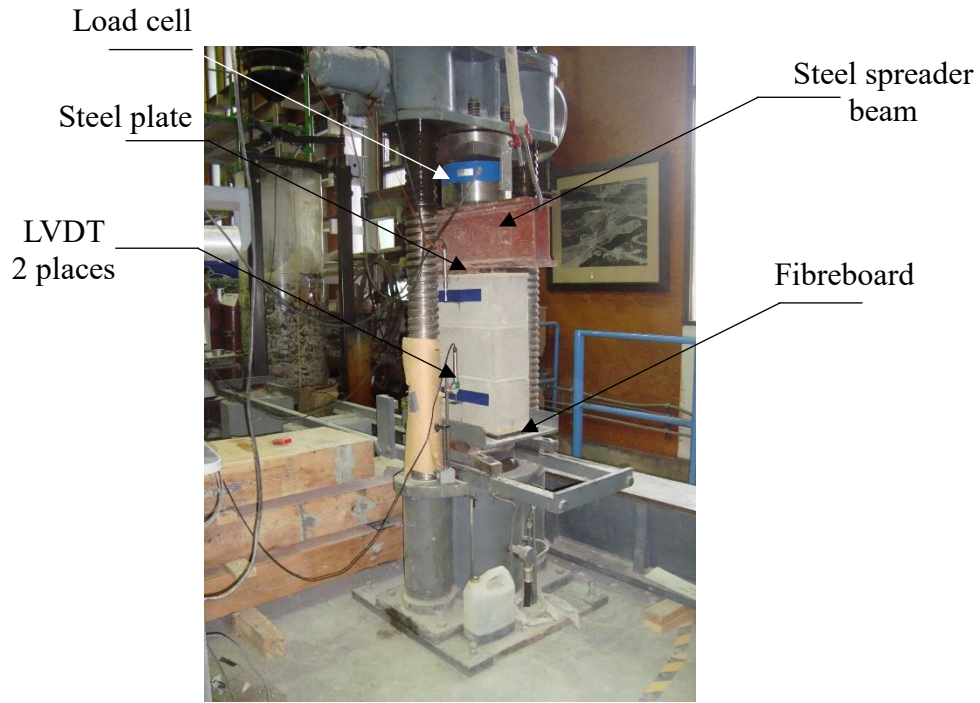
Figure C.9: Masonry prism test.
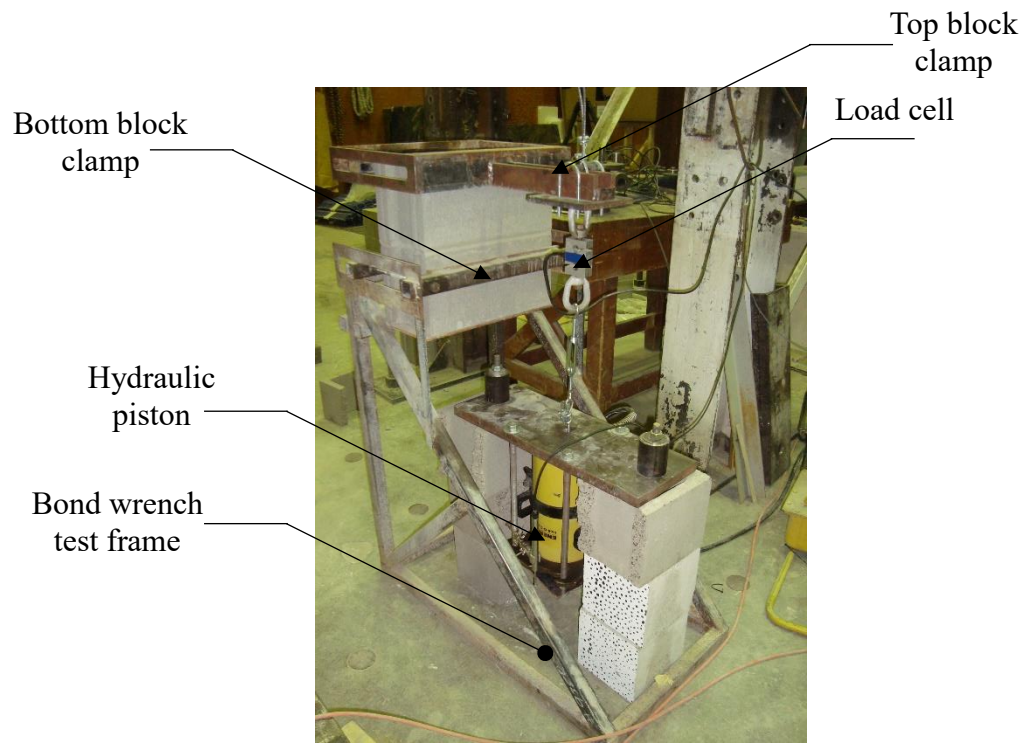
Figure C.10: Bond wrench test.

Appendix D: Setup of the Digital Image Correlation System

Full scale testing of UR, UB and PGR walls subjected to out-of-plane loading was conducted at the University of Saskatchewan. The test measurements included a series of digital monochromatic images of the unloaded face and one lateral side face of the walls that were acquired using a set of cameras. These images were used to determine the wall deformation state through a correlation system once the load was applied. A Digital Image Correlation System (DICS) was used to evaluate the strain contours and crack locations. The DICS is an emerging technique that uses an optical method to provide full-field displacements and strain measurements at any point inside an area of interest, as well as crack propagation by comparing images of the specimen surface. This system uses a reference speckle as initial location to evaluate its movement on the surface. However, a single speckle is not a unique signature of a position; hence, neighbouring speckles are also used. Such a group of speckles is called a subset. The average value of all speckles in a subset will then be shown. Each subset is taken out from the appropriate speckle pattern so that displacements may be traceable. To do that, speckle patterns should contain bright white and dark black areas with an appropriate speckle size, which was determined through a relationship between the geometry and size of the specimen, and the resolution of the cameras. This appendix focuses on the steps to prepare the specimens, set up the cameras, and display the data obtained after running the test.

D.1 Equipment Installation

The calibration of the DICS includes: choosing the appropriate lenses, calculating the dot size for the speckle pattern, preparing the specimen surface, setup of the cameras, and verification of the calibration through the use of a three dimensional software (Vic 3D) which is based on the principle of digital image correlation. Initially, it is important to determine the field of view of the wall and the distance between the wall and the cameras. An effective visualization of the wall was obtained using appropriate lenses since this is the main means to obtain information for the system. The lenses for the system were chosen considering the wall height and the available space in the Laboratory. Four digital cameras with a pixel resolution of 2,448 x 2,048 and equipped with 1.4/8 mm and 1.4/17 mm Schneider lenses were grouped in two systems, with two cameras each, to

capture the out-plane behaviour of the walls because this project required the analysis of the crack mapping and displacement measurements on large-scale specimens.

System 1 was setup to take readings of the unloaded face of the wall whereas the System 2 was positioned pointing the cameras at one of the wall sides (190 mm thick). Due to the space limitations of the Laboratory, System 1 used two digital cameras having two 1.4/8 mm lenses and spaced 170 mm apart to obtain an acceptable stereo angle. A crossbar with the two system cameras was secured to a tripod and positioned at 3250 mm from the unloaded wall surface. System 2 included two digital cameras with similar resolution and equipped with 1.4/17 mm lenses. Those lenses allowed for targeting the full-field of one lateral side of the wall specimen. The cameras were set 500 mm apart and situated at 6000 mm from the reference wall surface.

D.2 Determination of the Speckle Size

For this research, a speckle pattern is defined as the group of speckles or dots having a unique shape with a random position, and contained in a determined surface area, while the speckle size deals with the largest speckle dimension taken from its extremes edges. The speckle pattern plays a high importance role since the quality of the results depends on the appropriate shape, size, and dimension of the speckle, the density of its pattern, and the contrast between the speckle and the wall surface background color. An appropriate speckle pattern on the wall surface allowed the Vic 3D to be able to detect and estimate displacements and deformation with adequate accuracy.

The horizontal support for each camera system was oriented 90º degrees with respect to the horizontal to capture most of the wall details. Each wall specimen was then painted with an appropriate dot or speckle size. The wall dimensions and the digital image resolution of the camera were related to find an appropriate mm to pixel ratio (Cintron & Saouma 2008) that led to the selection of speckle sizes between 2 to 5 pixels (Zhou & Goodson 2001). The primary goal was to obtain the maximum numbers of speckles without affecting the density of the speckle pattern on the wall surface (where density is defined as the relationship between the dark black and bright white areas on a measurable surface).

Considering a rectangular aspect ratio image resolution of 1.20, the pixel space represented on a wall image for this research was 1.15 mm/pixel, which shows the quantity of space represented by a pixel in a wall image. A computed minimum allowable speckle size of ~3.5 mm was obtained in accordance with the recommendations provided by Sutton et al. (2009). Medium and large speckle sizes featured dimensions of ~5 mm and ~6 mm, respectively.

A series of speckle pattern templates were then fabricated by hand using 1005 mm x 270 mm plastic sheets, lengths of 2 in x 4 in timber members, and a printed paper with speckles randomly generated using a computer software package. The speckles featured polygonal shapes which were drawn using a circumscribed circle with radius that ranged from 1.5 to 3 mm. A drill was used to make holes in the plastic according to the paper template. The plastic templates were then removed from the wooden frame and verified to ensure the holes on the plastic meet the required dimensions.

Figure D.1(a) presents the unloaded and lateral faces of the wall painted white after cleaning and removing any debris using a brush. Figure D.1(b) shows a speckle template affixed to the specimen once the white paint had dried. Black paint was then applied using a 3 in. x 3/8 in. high-density polyester roller as displayed in Figure D.1(c). A high contrast and high-quality pattern was therefore achieved.

D.3 Stereo Calibration of the image space

The cameras were centralized and focused on the unloaded and lateral wall surface approximately 1,800 mm above floor to avoid distortion effects resulting of the misalignment between the middle of the wall and the lens position. Camera System, 1 and 2 used an appropriate aperture number to allow a specific amount of light to go through each camera and to prevent the blurring or brightening of the resulting image. Care was taken to ensure that the aperture was not been changed between the time of calibration and the wall specimen test.

A 56 mm calibration grid was used to capture an average of 30 calibration images per system. This grid was temporally placed on the surface to cover the 100% of the area of the wall on both sides. Smooth rotations of the grid about the X, Y, and Z axes helped to the system to identify the grid.

Stereo calibration was conducted simultaneously for both camera systems. The stereo system calibration tool from the Vic 3D software was then adjusted to run with a distortion order of "2" since 1.4/8 mm and 1.4/17 mm lenses were using during the test. Images during this process received a final average error score of 0.03. The average error between the position where a target point was found in the specimen image, and the assumed position where the mathematical calibration model from the Vic 3D software places the point (Correlated Solutions 2010). This procedure was identified for each camera system once the calibration images were acquired.

D.4 Post Processing of the Specimen Images

Snapshots were collected through Vic-Snap acquisition software during the test and ranged from 68 to 264 pictures per wall test. The number of images depended on the test duration time. For instance, a UB wall had more images than an UR wall since the latter reached the ultimate load at an early stage. Subset sizes of 51 x 51 and 29 x 29 pixels were chosen using an Aoi tool (i.e. set of tools for drawing and editing) for the correlation analysis of the unloaded wall surface and the lateral surface, respectively. A larger subset was chosen for the analysis of the unloaded wall surface to allow the Vic 3D software acquires a larger number of speckle and to obtain a strain map within the most of the wall surface without affecting the accuracy of the results. The Aoi tool permitted the selectection and editing of areas of interest on the wall surface for being analyzed. The principal strain contours were displayed in 2D and the data for analysis was extracted using the Inspector tool. This tool provided a variety of data as a result of the analysis such as: displacements in different directions, measurement strains, and the extension between two points. This information was used for crack detection and crack mapping for the walls at different displacement stages.

(a)   (b)

(c)

Figure D.1. Pattern for applying the speckle pattern on the wall specimen: (a) painting the unloaded face of a wall, (b) application of the speckle pattern template to a lateral wall face, and (c) applying the black paint for obtaining the speckle pattern.

Appendix E: Digital Imaging Correlation System Results

This appendix presents the strain contours measured by the two-dimensional imaging correlation system (DICS) based upon the images acquired during wall testing. The DICS analysis presented in this appendix considered wall pictures during the elastic range of the tests as the cracking load was approached in order to avoid discontinuities on the wall face that ocurr following cracking.

During this experimental program, camera systems 1 and 2 acquired images of the unloaded face and the lateral face walls, respectively. Figures in this appendix show the strain maps as displayed for the UR, UB and PGR wall specimens. Figures E.1 to E.6 show the strain contours for the UR wall specimens. Similarly, Figures E.7 to E.14 present the images for the UB wall specimens. Finally, Figures E.15 to E.20 show the strain contour measurements for the PGR wall specimens.
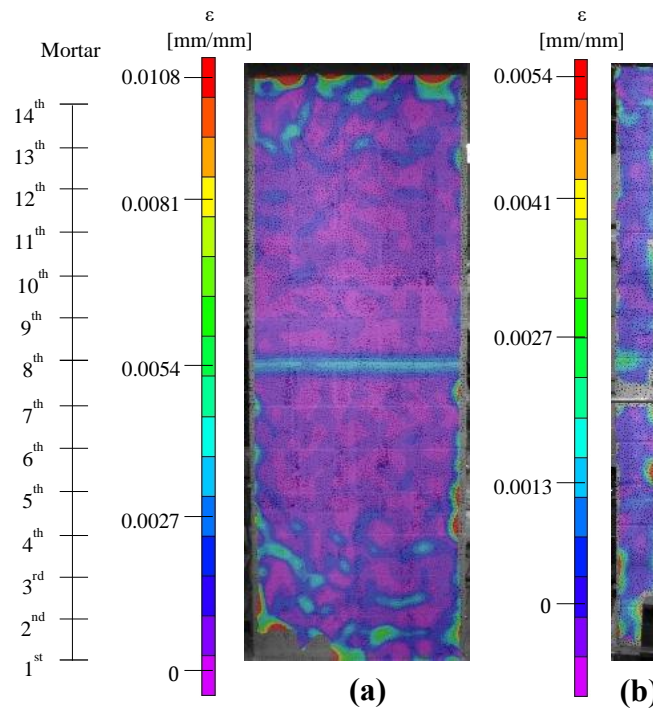
Figure E.1: Strain contours as measured using the DICS for UR-1: (a) unloaded wall face, and
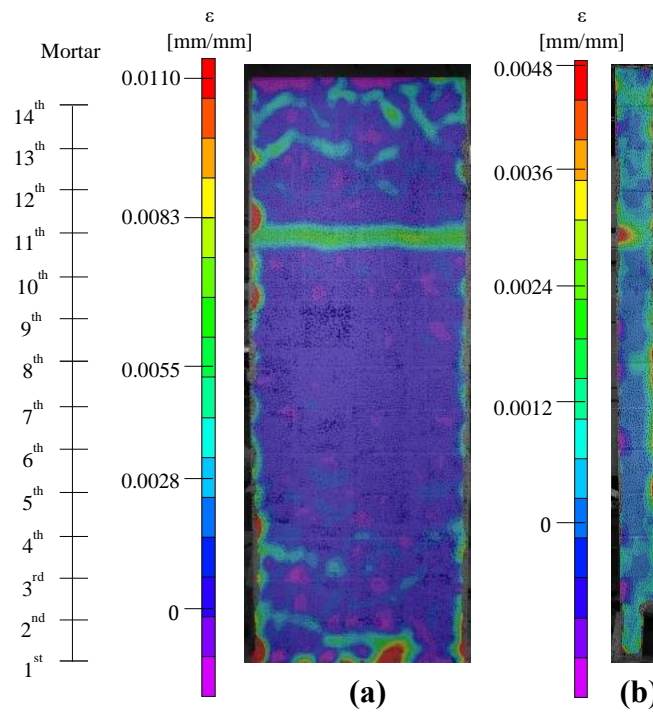
(b) lateral wall face.

Figure E.2: Strain contours as measured using the DICS for UR-2: (a) unloaded wall face, and
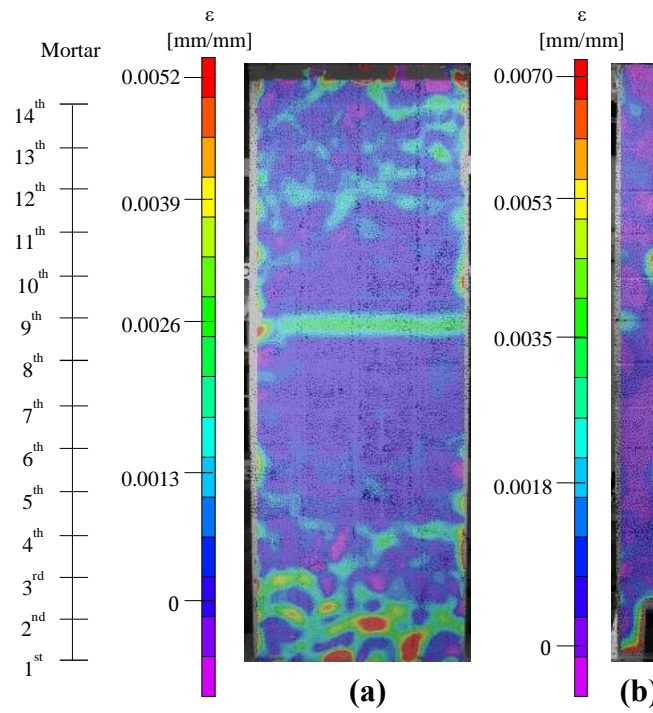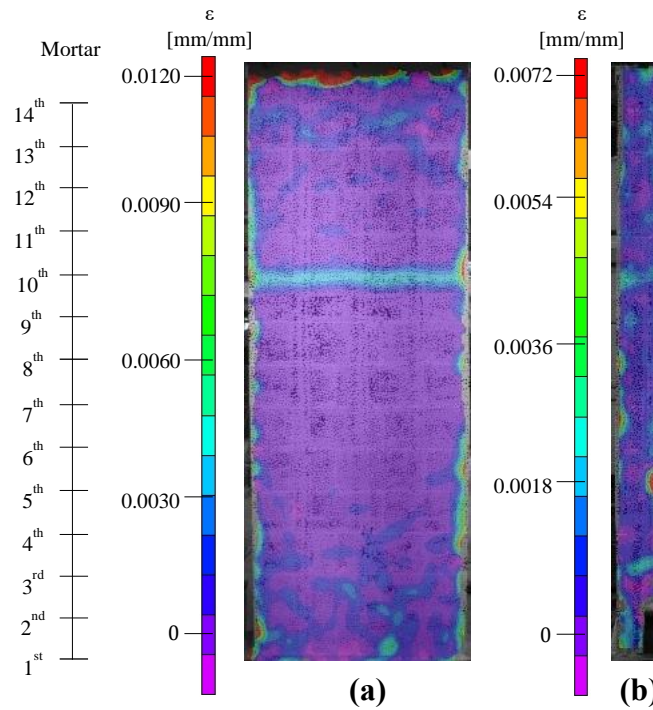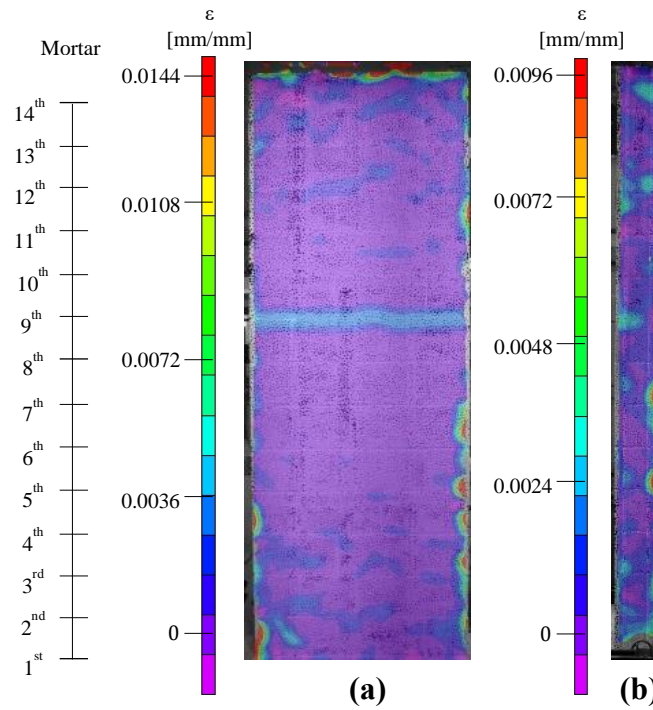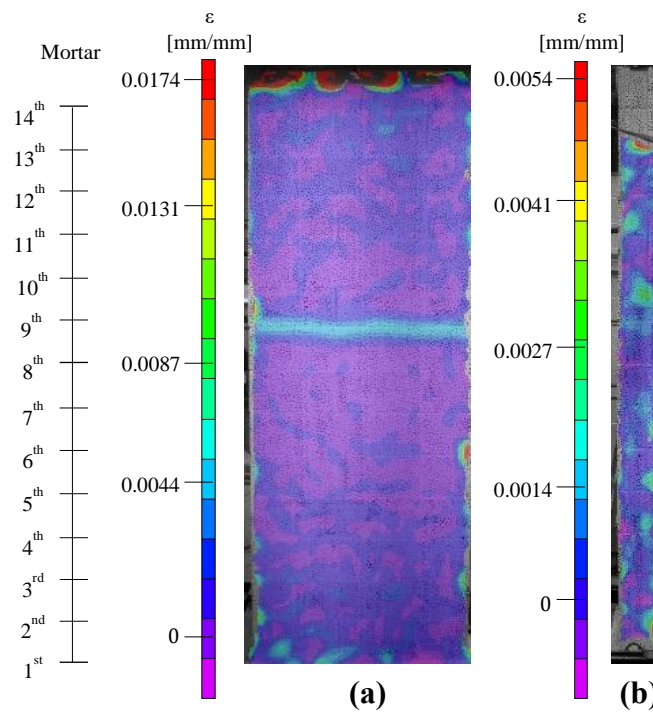
(b) lateral wall face.

Figure E.3: Strain contours as measured using the DICS for UR-3: (a) unloaded wall face, and
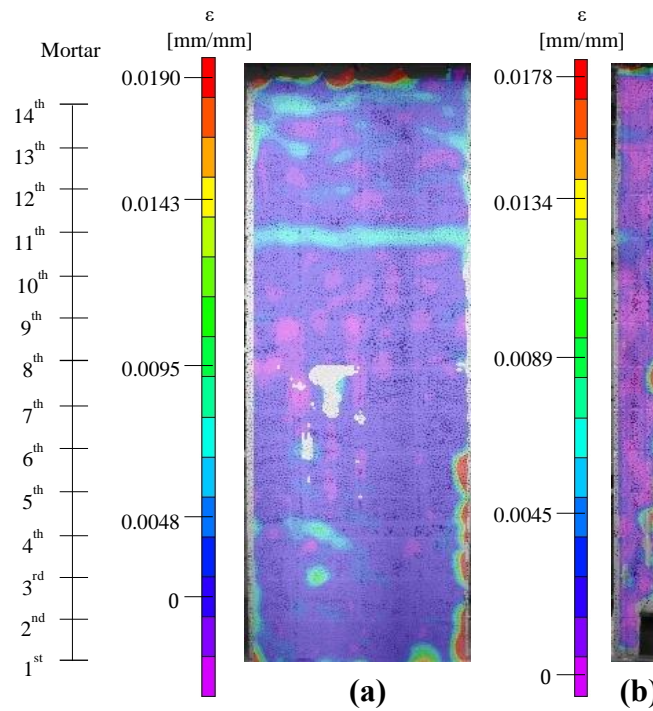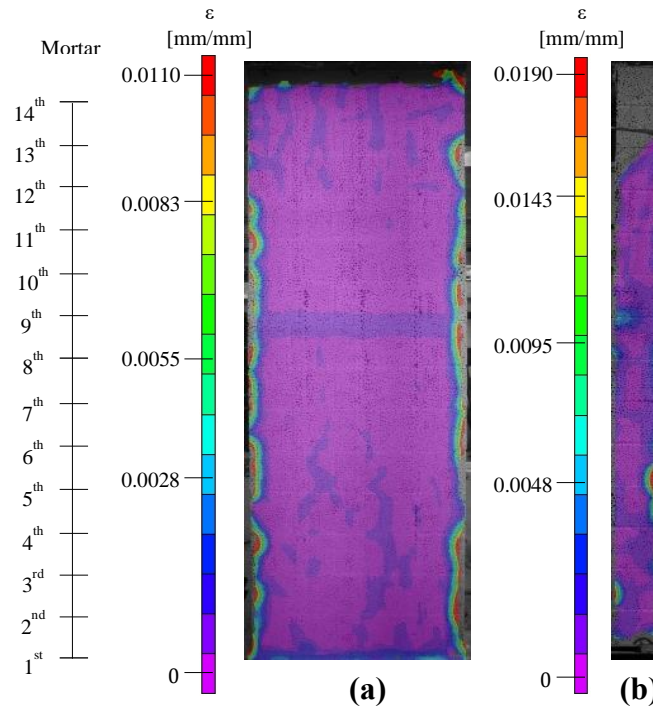
(b) lateral wall face.

Figure E.4: Strain contours as measured using the DICS for UR-4: (a) unloaded wall face, and
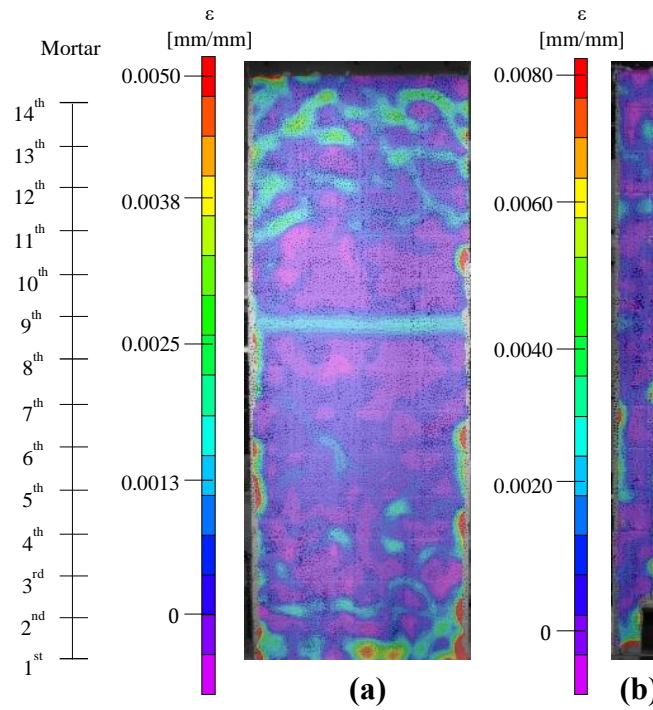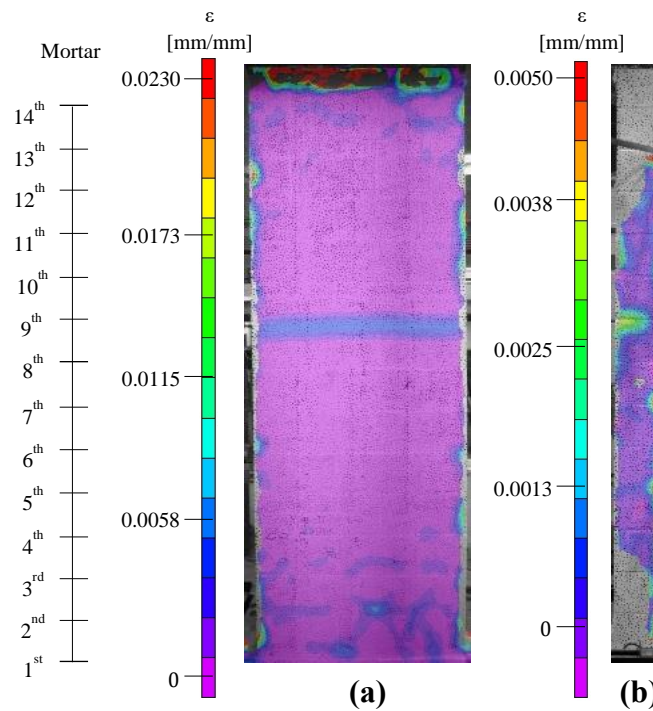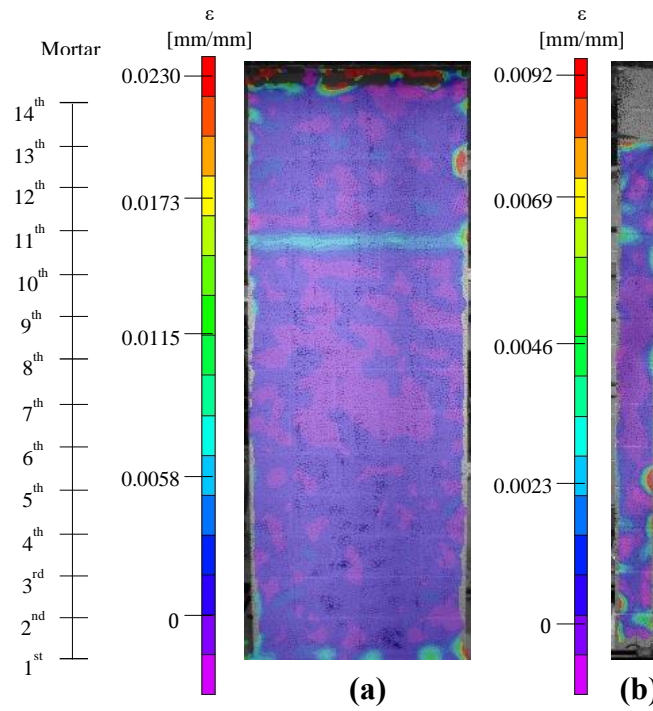
(b) lateral wall face.

Figure E.5: Strain contours as measured using the DICS for UR-5: (a) unloaded wall face, and (b) lateral wall face.

Figure E.6: Strain contours as measured using the DICS for UR-6: (a) unloaded wall face, and (b) lateral wall face.

Figure E.7: Strain contours as measured using the DICS for UB-U2: (a) unloaded wall face, and (b) lateral wall face.

Figure E.8: Strain contours as measured using the DICS for UB-U3: (a) unloaded wall face, and (b) lateral wall face.
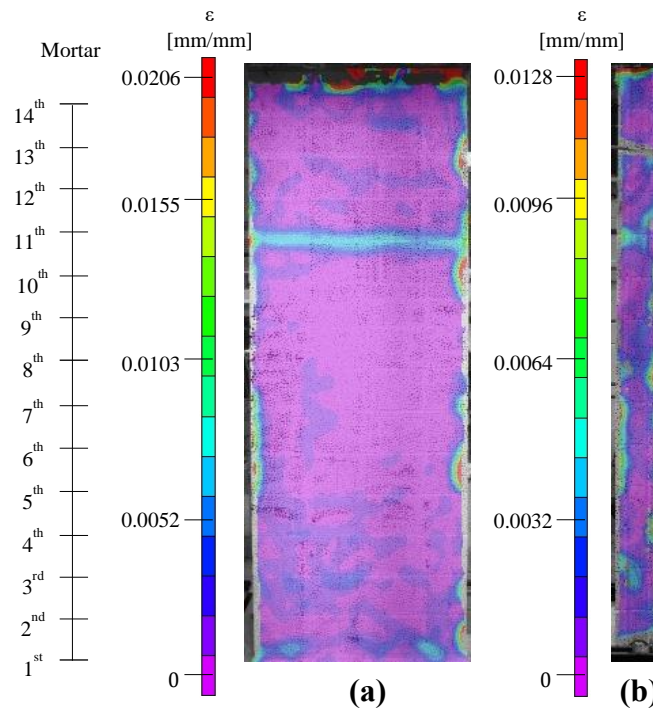
Figure E.9: Strain contours as measured using the DICS for UB-G1: (a) unloaded wall face, and (b) lateral wall face.
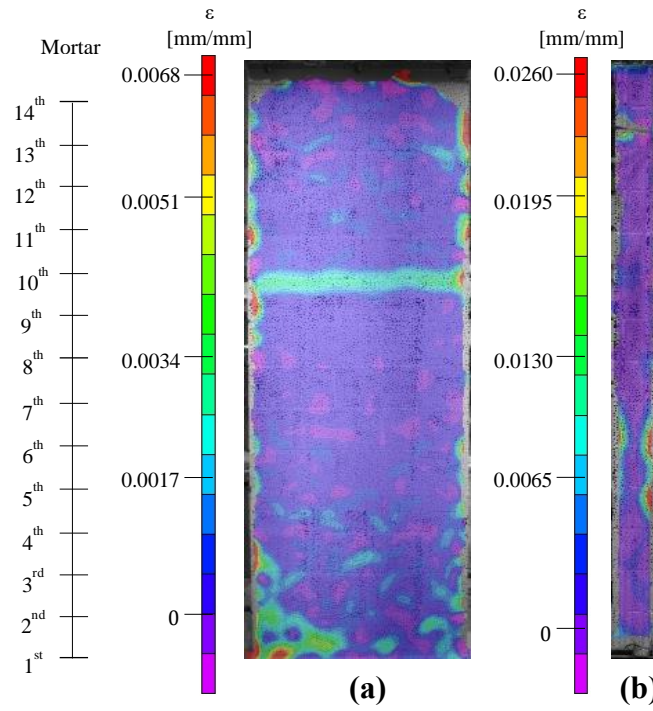

Figure E.10: Strain contours as measured using the DICS for UB-G2: (a) unloaded wall face, and (b) lateral wall face.

Figure E.11: Strain contours as measured using the DICS for UB-G3: (a) unloaded wall face, and (b) lateral wall face.
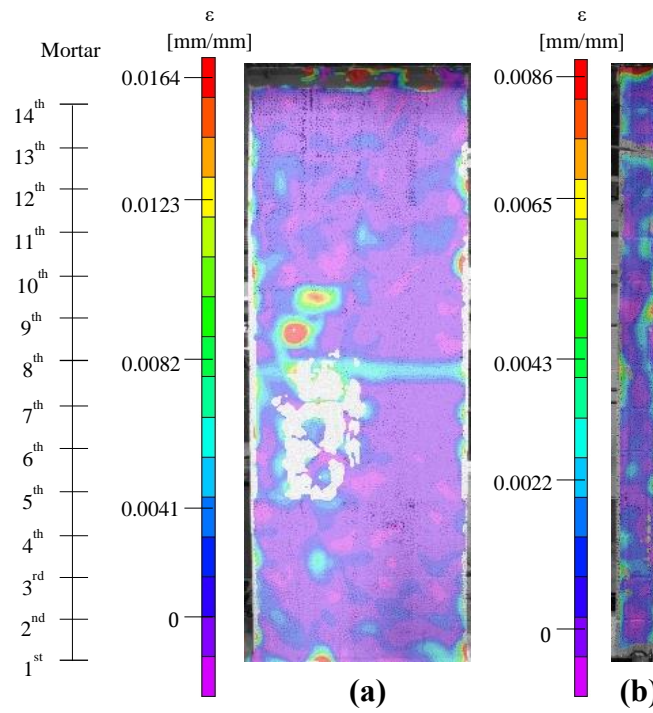

Figure E.12: Strain contours as measured using the DICS for UB-G4: (a) unloaded wall face, and (b) lateral wall face.

117

Figure E.13: Strain contours as measured using the DICS for UB-G5: (a) unloaded wall face, and (b) lateral wall face.

Figure E.14: Strain contours as measured using the DICS for UB-G6: (a) unloaded wall face, and (b) lateral wall face.
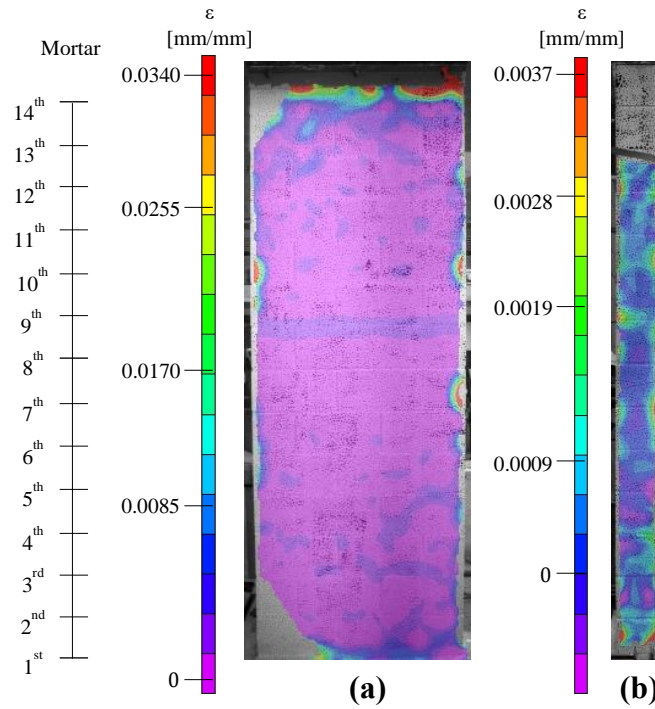
Figure E.15: Strain contours as measured using the DICS for PGR-1: (a) unloaded wall face, and (b) lateral wall face.

Figure E.16: Strain contours as measured using the DICS for PGR-2: (a) unloaded wall face, and (b) lateral wall face.

Figure E.17: Strain contours as measured using the DICS for PGR-3: (a) unloaded wall face, and (b) lateral wall face.
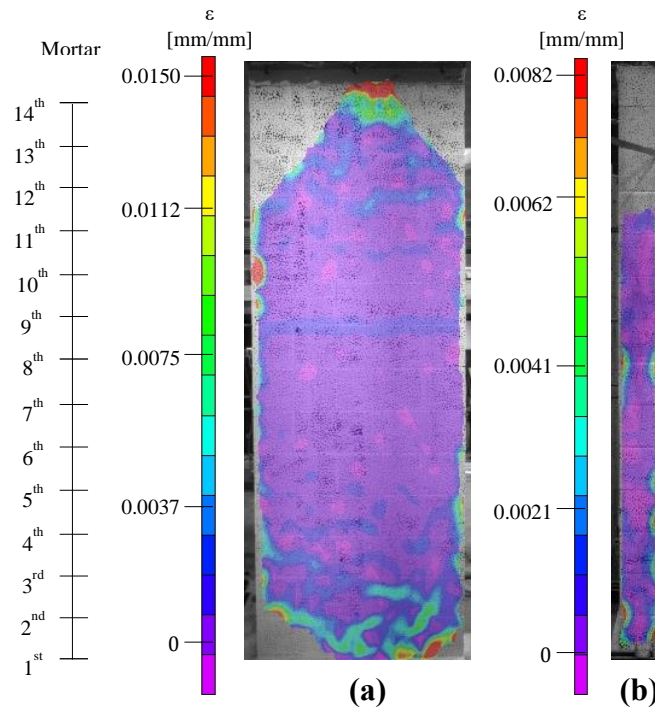

Figure E.18: Strain contours as measured using the DICS for PGR-4: (a) unloaded wall face, and (b) lateral wall face.
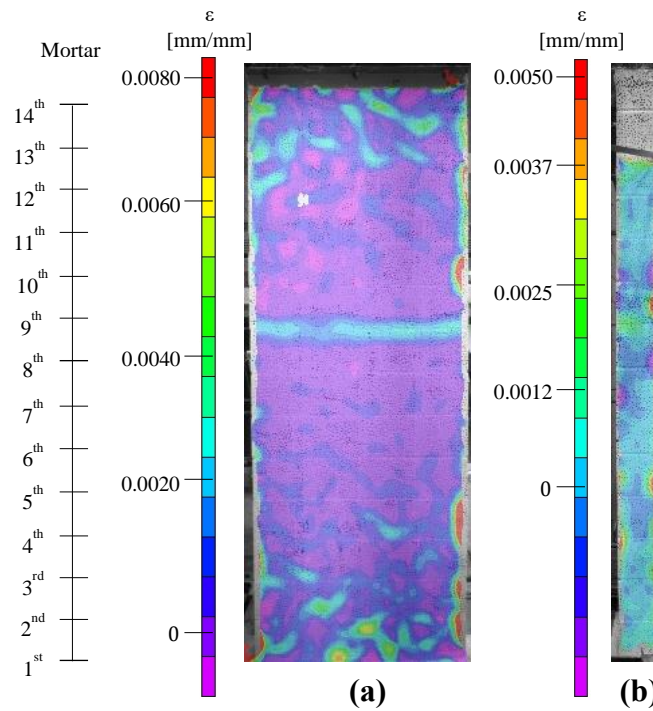
120

Figure E.19: Strain contours as measured using the DICS for PGR-5: (a) unloaded wall face, and (b) lateral wall face.

Figure E.20: Strain contours as measured using the DICS for PGR-6: (a) unloaded wall face, and (b) lateral wall face.
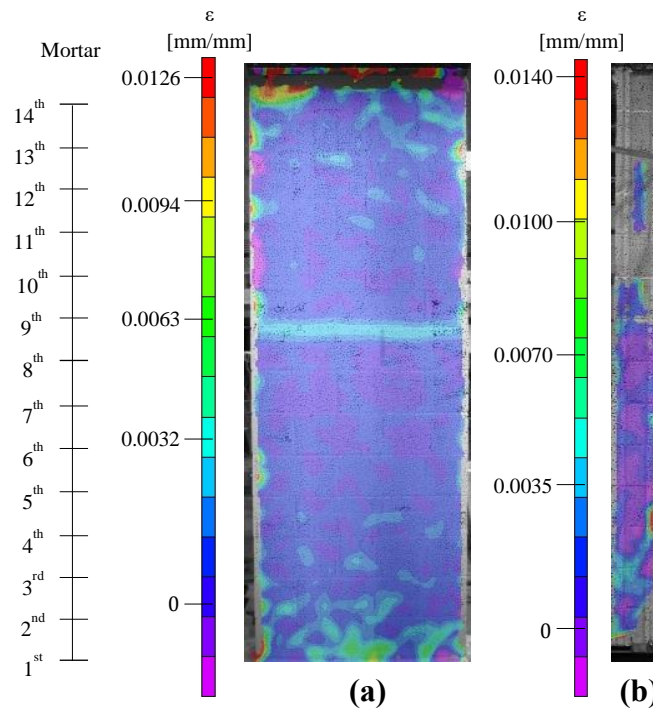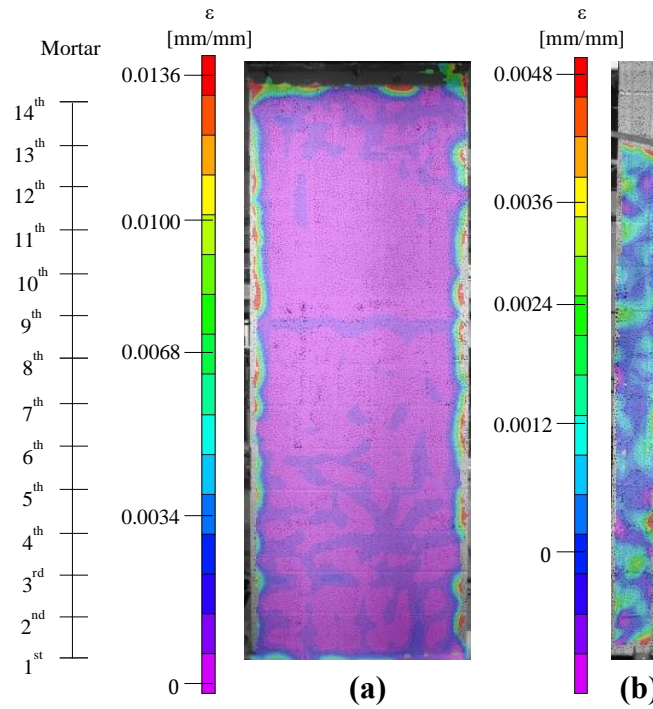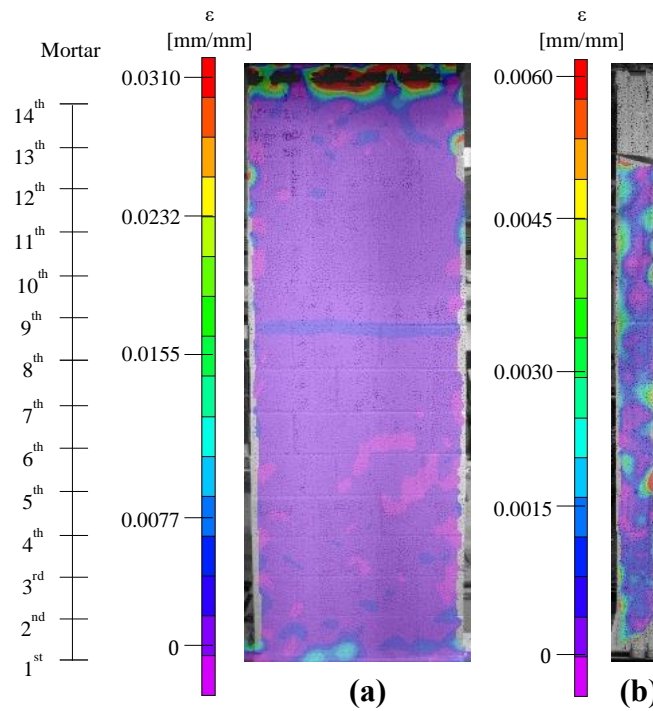
Appendix F: Assumptions Used in the Analytical Model to Determine the Load-Deflection Response of Walls with Unbonded Reinforcement

Three models based on different assumptions were considered, as shown in Table F.1, in order to determine the load-deflection curve for UB-U and UB-G walls. The first model involved the elastoplastic-hardening behaviour of the 6.4 mm reinforcement as indicated by the actual stress versus strain response established from tests conducted in the Structures Laboratory, and the crack locations associated with the experimental tests. The second model was based on the assumption that the main crack was located at mid-height of the wall for all specimens. The final model was based on the assumption of elastic-perfectly plastic behaviour of the reinforcement and a crack formation at mid-height of the wall. The crack location defined the size of the two post-cracking segments, while the behaviour of the reinforcement inserted in the wall specimen could be compared to the strain measurements provided by the eight strain gauges attached along the each reinforcement.

The first model assumed a stress versus strain curve for steel based on the actual tensile test and exhibited an elastic and a plastic region. In addition, this model considered the actual crack location for each wall specimen observed during testing.

The second version of the model was based on the assumption that the stress versus strain curve for steel had two regions, as described above, but that the plastic region had a constant yield stress value. Strain hardening of the reinforcement was not taken into account. This model was based on the assumption that the crack formed at mid-height of the wall since that is the location of maximum moment for a wall subjected to uniform distributed loaded. As a result, the maximum deflection is expected at this wall location, making it an obvious location for crack formation.

The third version of the model was based on the assumption that the stress versus strain response of the reinforcement was that resulting of the actual tests of tensile specimen. The stress versus strain curve characteristics for this model were taken to be similar to those previously described for the first model. In addition, this model assumed that the cracks established three hinges located in a similar fashion to that described for the second model.

Figure F.1(a) shows the average engineering stress-strain curve for the 6.4 mm reinforcement bar as determined from the tensile tests of five bar samples, as explained in Appendix C in Section C.4, and used as input for the first and third analytical models. Three points were used to construct the average curve: the proportional limit, the maximum tensile stress, and the coordinates at the specimen failure. In contrast, Figure F.1(b) presents the elasto-perfectly plastic curve obtained assuming an average Young's modulus of 205 GPa and an average yielding stress of 563 MPa. This stress-strain curve was implemented for the second analytical model.

A series of load-deflection curves from the first, second, and third models were plotted and compared with the experimental results obtained from tests of the eight walls with unbonded reinforcement in order to assess the accuracy of the analytical model. The assessment was based on similarities between the load-deflection curves, and an analysis of the displacement corresponding to analysis of their maximum applied load measured during testing. Figure F.2 shows typical measured load-deflection curves for selected specimens compared to the results derived from the three analytical models. It was determined that the results from analytical Model Nos.2 and 3 showed more consistent agreement with experimental than those resulting from the first analytical model. Figures F.3 to F.10 show a series of load-deflection curves determined using the results from the Model No.1 and 3, respectively.

The load-deflection curves plotted in Figures F.3 to F.6 according to the Model No.1 showed that, in most cases, the calculated curve tends to overestimate the measured curve when the crack is not formed at mid-height of the wall. This might be due to this model over-estimating the force per reinforcing bar once the crack has been formed as a result of the out-of-plane loading. For instance, curves for wall specimens UB-U2, UB-3, UB-G3, UB-G4 and UB-G5 at an approximated deflection of 15 mm showed the calculated load is larger than the experimental values. It is difficult to determine the reasons why the curve for wall specimen UB-G1 under-estimated the calculated load since the experimentally obtained curve did not show a similar pattern behaviour to the other curves. Additionally, wall specimens UB-G2 and UB-G6 showed a consistent result quite similar to the experimental curves.

Figures F.7 to F.10 present a series of curves plotted using Model No.3. Most curves showed a similar post-cracking slope that follow a similar pattern to those obtained from for the experimental testing. The force per reinforcing bar is not over-estimated in the same way as it was for the Model No.1. For instance, wall specimens UB-U2, UB-U3, UB-G4, and UB-G5 showed a curve slope than became higher that the experimental curve. For the wall specimen UB-G6, the calculated curve and the experimental curve showed an increase in the deflection without a corresponding increase in load resistance since the reinforcement started yielding.

Table F.2 presents a comparison of the maximum applied load acquired during tests of walls with unbonded reinforcement and calculated analytically at the same value of mid-height deflection. Most of the analytical values obtained using the Model No.1 over-estimated the maximum applied load for all walls specimens, varying from -28.2% for UB-G1 to +127% for UB-G4. However, the percentage errors associated to UB-G1 and UB-G2 were smaller than the values resulting from the Models No.2 and 3. Similarly, Model No.2 output exhibited percentage errors ranging from -38.1% for UB-G1 to +14.5% for UB-G5. The calculated applied load at the ultimate condition had the highest accuracy for specimens UB-U2, UB-U3, UB-G4, and UB-G5 in comparison to the results from Models No.1 and 3. Finally, Model No.3 resulted in percentage errors ranging from -33.8% for UB-G1 to +16.2% for UB-G4. This model provided a maximum applied load for UB-G3 and UB-G6 with higher accuracy than observed with results obtained from the other models. In summary, Models No.1 and 3 provided two calculated load values each that were close to the values experimentally obtained while Model No.2 resulted in four such instances. As a result, Model No.2 was selected for use, and its assumed wall geometry and free body diagram were shown in Figure 4.8 as well as its results presented in Figures 4.9 and 4.10 in Chapter 4.

Table F.1: Assumptions used for the analytical model of UB walls

Model No.	As-Tested Stress versus Strain Response	Elasto-Perfectly Plastic Behaviour	Crack at Mid-Height	Actual Crack Location[a]
1	X			X
2		X	X	
3	X		X	

[a] Crack location associated with each wall specimen during the out-of-plane loading test.

Table F.2: Comparison of the analytical models and experimental results for wall with unbonded reinforcement

Specimen ID	P_{max}						
	Test [kN]	Model 1 [kN]	Error [%]	Model 2 [kN]	Error [%]	Model 3 [kN]	Error [%]
UB-U1[a]	4.35	n/a	n/a	n/a	n/a	n/a	n/a
UB-U2	6.89	8.56	+24.3	7.24	+5.08[b]	7.70	+11.8
UB-U3	6.80	8.16	+20.1	6.85	+0.735[b]	7.33	+7.84
UB-G1	8.51	6.11	-28.2[b]	5.27	-38.1	5.63	-33.8
UB-G2	7.49	7.70	+2.80[b]	6.48	-13.5	6.96	-7.10
UB-G3	7.27	14.3	+96.8	6.63	-8.80	7.1	-2.02[b]
UB-G4	6.91	15.7	+127	7.62	+10.3[b]	8.03	+16.2
UB-G5	7.54	12.0	+58.7	8.63	+14.5[b]	8.71	+15.5
UB-G6	9.45	9.23	-2.33	9.75	+3.17	9.23	-2.33[b]

[a] Specimen identified as an outlier.
[b] Minimum absolute value taking from the analysis of the percentage errors associated with each wall.
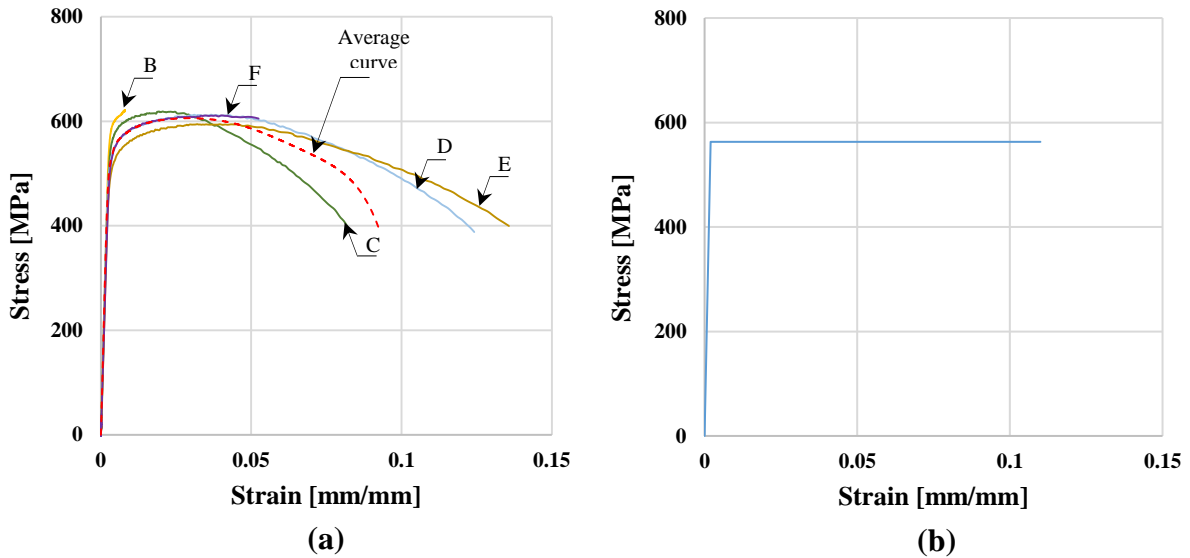
Figure (a) excludes sample A since UTM Machine stopped during the test

Figure F.1: Stress-strain curve for tensile test of the reinforcement: (a) elastoplastic-hardening assumption for Model No.1 and 2, and (b) elasto-perfectly plastic assumption for Model No.3.
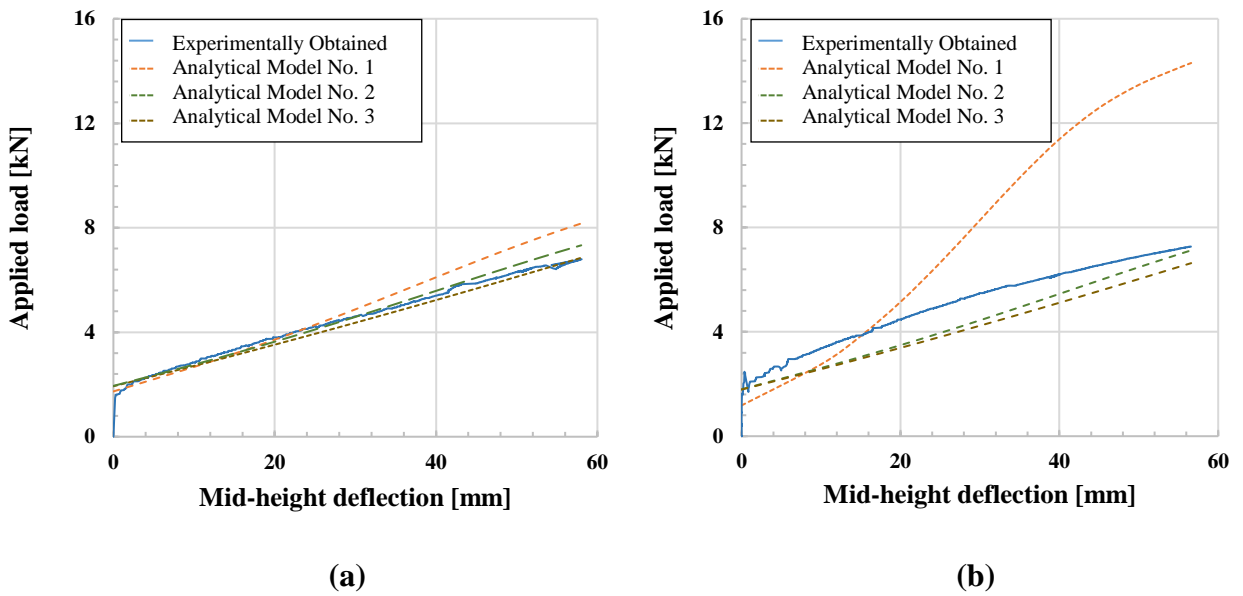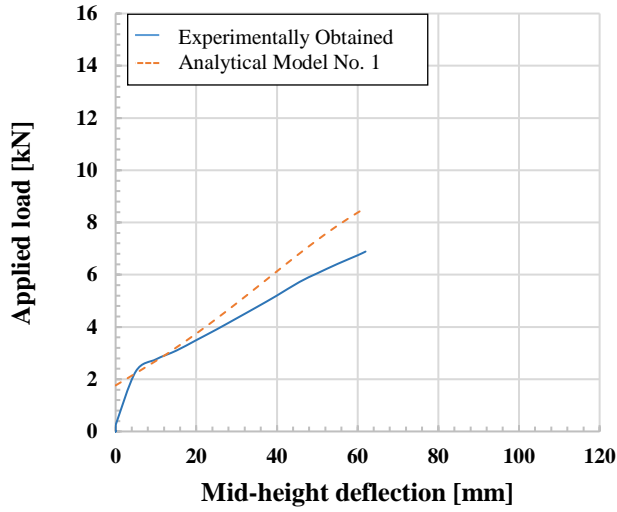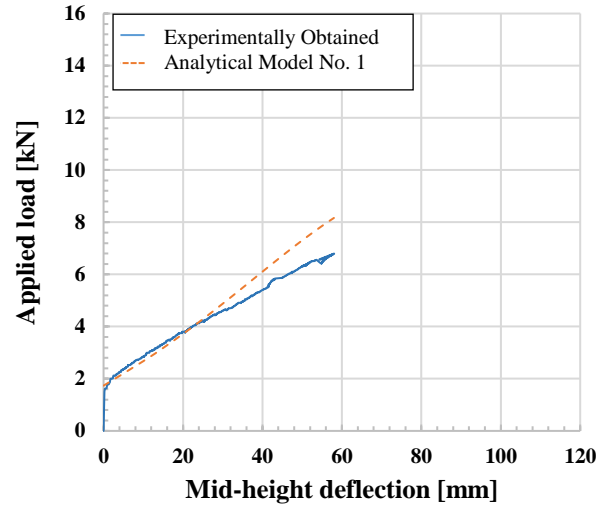

(a)   **(b)**

Figure F.2: Experimental versus analytically derived load-deflection curves: (a) wall specimen UB-U3, and (b) wall specimen UB-G3.

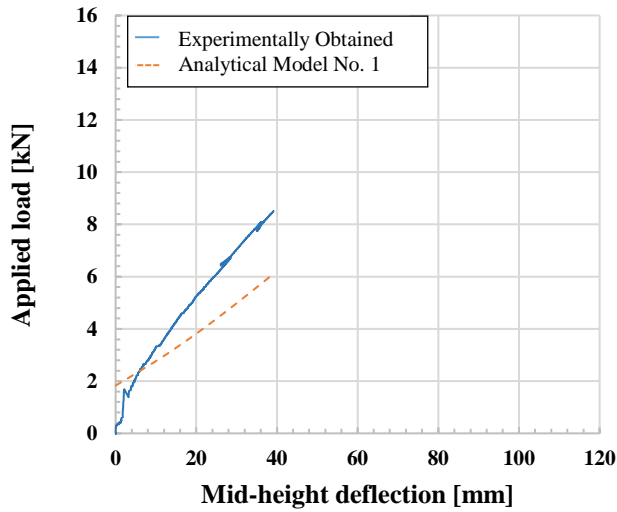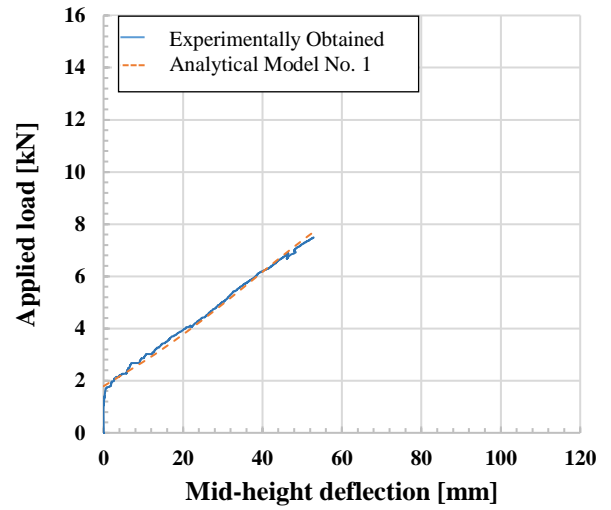**(a)**   **(b)**

Figure F.3: Comparison between analytical model No.1 and experimental results: (a) UB-U2, and (b) UB-U3.

(a)   **(b)**

Figure F.4: Comparison between analytical model No.1 and experimental results: (a) UB-G1, and (b) UB-G2.

127

(a)　　　　　　　　　　　　　　　　**(b)**

Figure F.5: Comparison between analytical model No.1 and experimental results: (a) UB-G3, and (b) UB-G4.

(a)　　　　　　　　　　　　　　　　**(b)**

Figure F.6: Comparison between analytical model No.1 and experimental results: (a) UB-G5, and (b) UB-G6.

(a)　　　　　　　　　　　　　　　　　　**(b)**

Figure F.7: Comparison between analytical model No.3 and experimental results: (a) UB-U2, and (b) UB-U3.
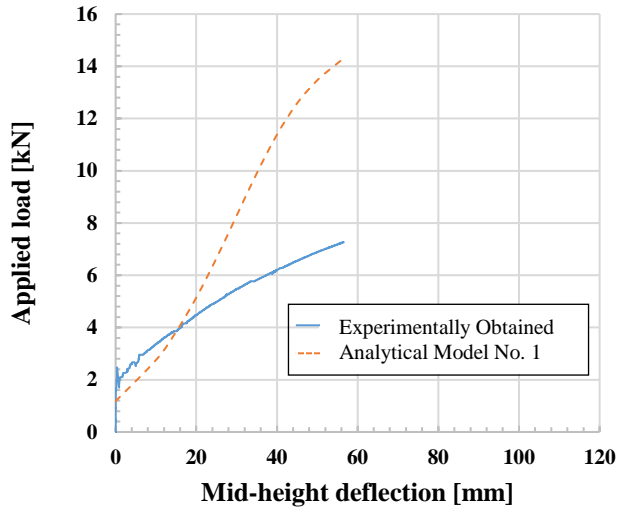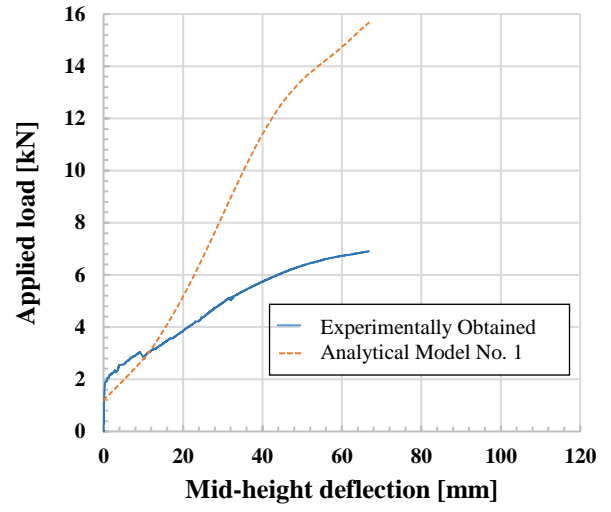

(a)　　　　　　　　　　　　　　　　　　**(b)**

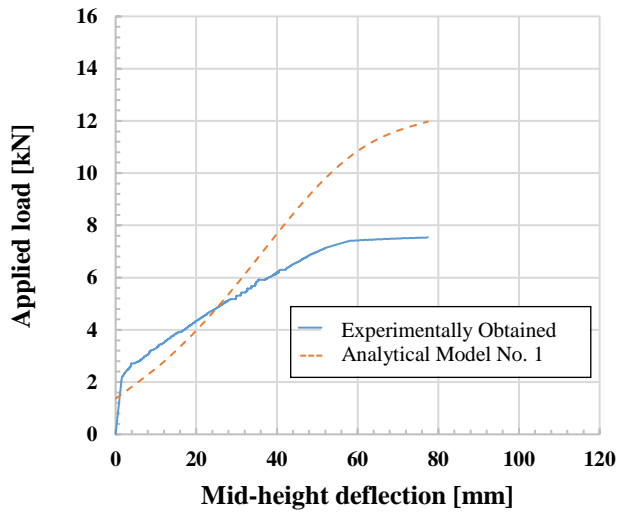**Figure F.8:** Comparison between analytical model No.3 and experimental results: (a) UB-G1, and (b) UB-G2.

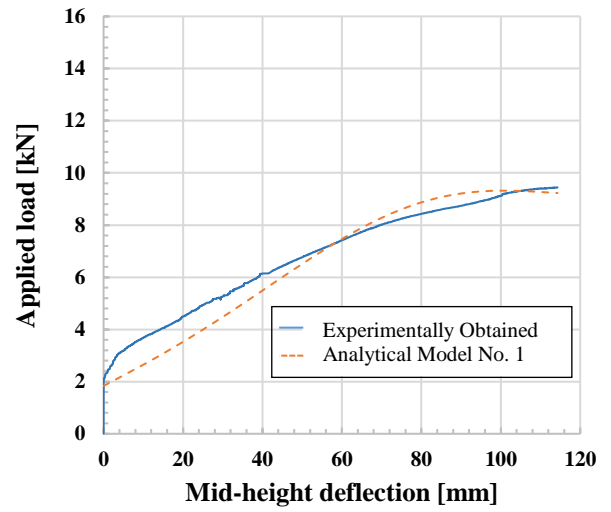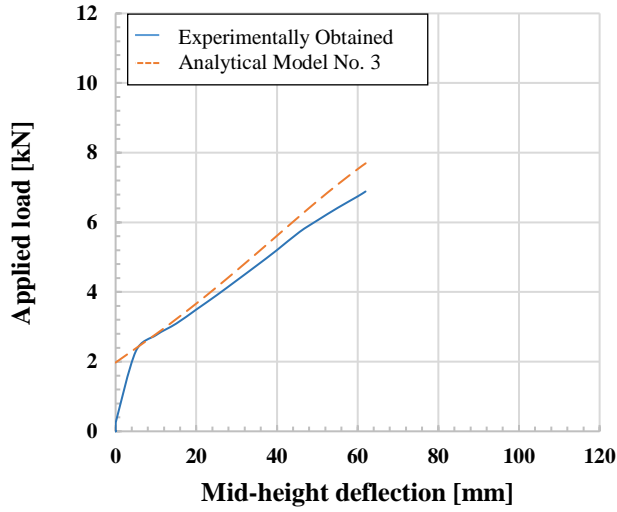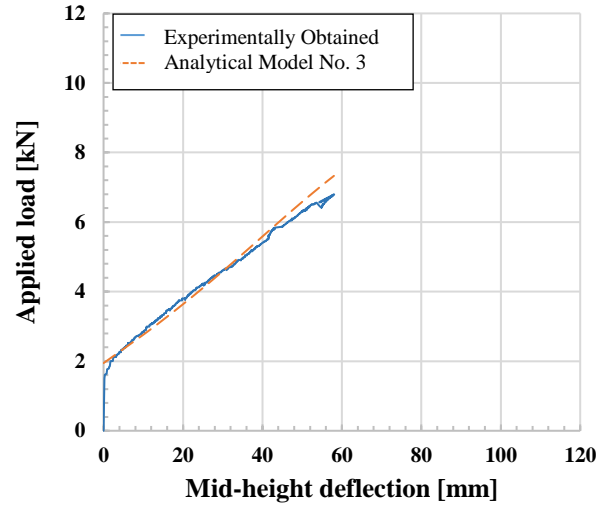**Figure F.9:** Comparison between analytical model No.3 and experimental results: (a) UB-G3, and (b) UB-G4.

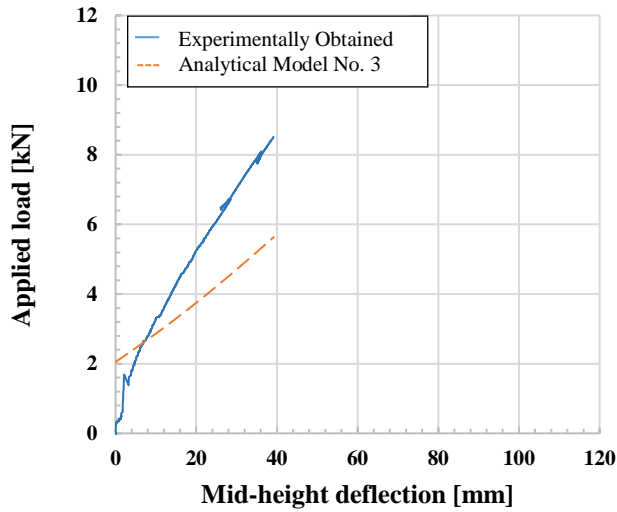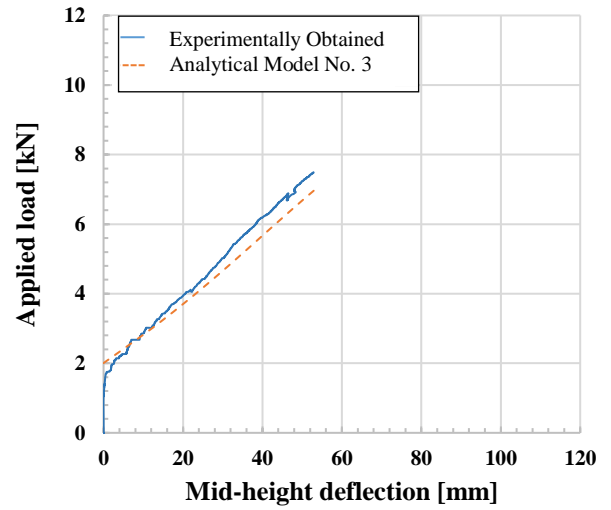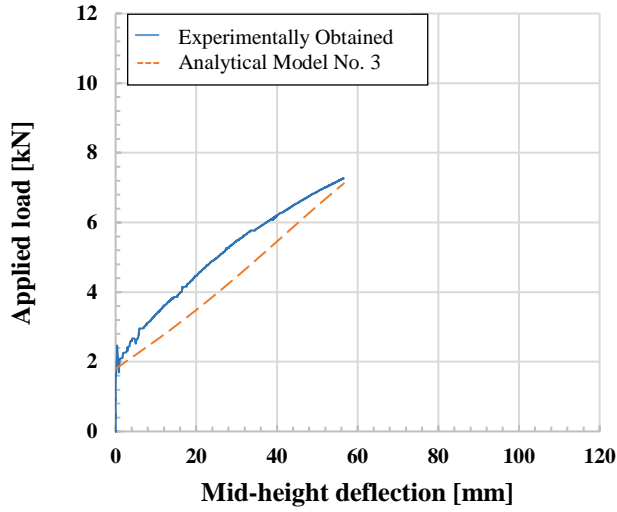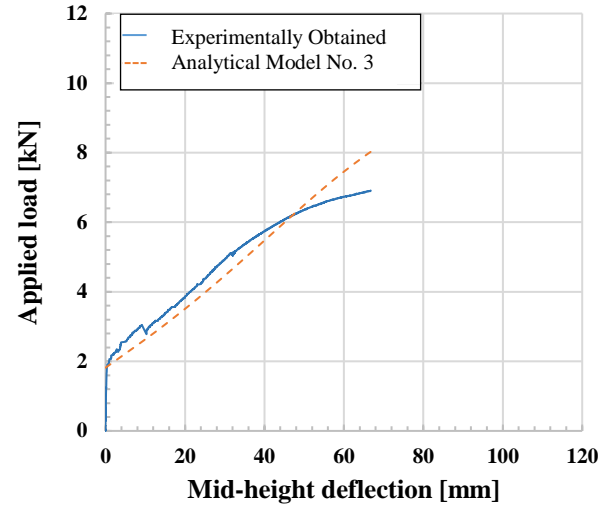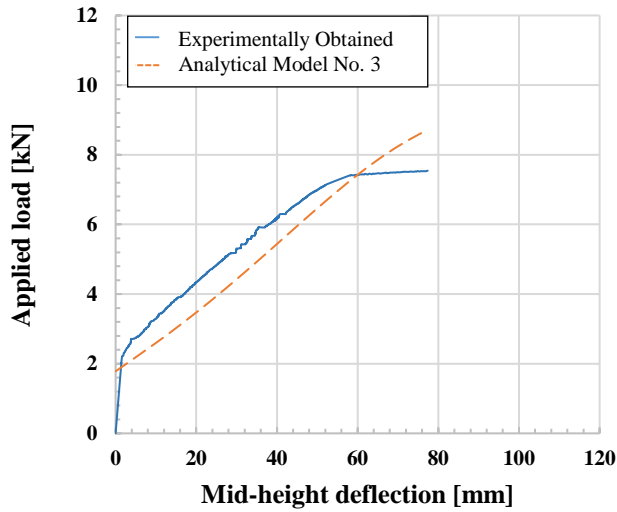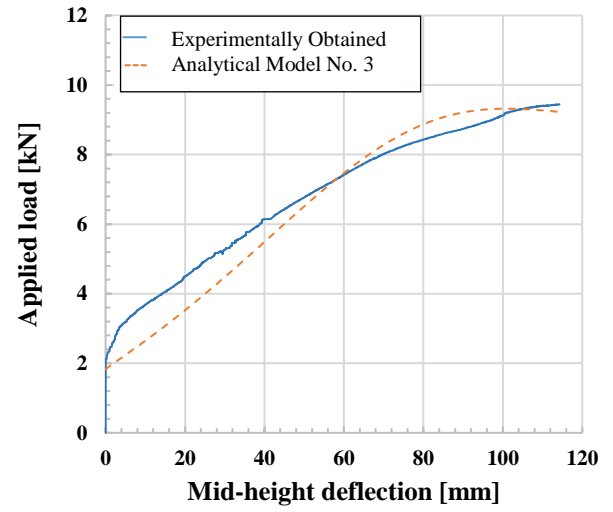**Figure F.10:** Comparison between analytical model No.3 and experimental results: (a) UB-G5, and (b) UB-G6.

Appendix G: Copyright Permissions for Figure 2.1

Request permission/copyright material

Sparling, Bruce

Today, 12:46 PM

Dear Henry,

You have my permission to reproduce the three figures noted in your message below in your MSc thesis.

All the best,

Bruce Sparling, Ph.D., P.Eng., FCSCE
Professor Structures / Materials Group
Dept. of Civil, Geological & Environmental Engineering
College of Engineering, University of Saskatchewan
Rm. 2A01, Engineering Building, 57 Campus Dr.
Saskatoon, SK S7N 5A9
Tel: (306) **966-5366**
Email: bruce.sparling@usask.ca

Confidentiality Warning
This email, including any attachments, is confidential and is intended only for the addressee. If you are not the intended recipient, you are notified that any distribution or copying of this email is strictly prohibited. If you have received this email in error, please notify us immediately by return email and delete all copies of the message. Thank you.
Please think "Green" before printing this email

Miranda Orellana, Henry

Today, 11:04 AM

Sparling, Bruce

Dear Dr. Sparling,

I would like to request your permission to use copyright material of the Thesis titled " Realistic Wind Loads on Unreinforced Masonry walls" originally published in University of Saskatchewan website (HARVEST).
I want to include in my MSc thesis the following figures:
 - Figure 3.15: Realistic pin support specimen showing the bottom connection
- Figure 3.16: Ideal pin showing the bottom knife-edge connection
- Figure 3.17: Realistic pin showing the top connection
The complete thesis will be posted in the University of Saskatchewan research archive.
I appreciate your consideration of my permission request.

Sincerely,

Henry Miranda Orellana

Appendix H: Copyright Permissions for Figure 2.5

EARTHQUAKE ENGINEERING RESEARCH INSTITUTE
499 14th Street, Suite 220
Oakland, California 94612-1934 USA
Phone (510) 451-0905 Fax (510) 451-5411 E-mail: eeri@eeri.org

EERI Permission Clearance Form

Date: 01/25/2019

To: **Henry Paul Miranda Orellana**
        Department of Civil, Geological and Environmental Engineering
        College of Engineering
        University of Saskatchewan
        Saskatoon, SK, CA, SK S7N 5A9

Permission is granted to Henry Paul Miranda Orelleana, to use the following items in the thesis titled, *"OUT-OF-PLANE BEHAVIOUR OF CONCRETE BLOCK WALLS WITH UNBONDED REINFORCEMEN*T", by Miranda Orellana, H

> **Figure 5.** Idealized model for transverse arching action from the: *"Out-of-plane strength of unreinforced masonry infill panels"* by Abrams, D. P., Angel, R., and Uzarski, J. (1996), *Earthquake Spectra,* Volume 12, Issue 4, (825-844), Earthquake Engineering Research Institute.

Author must include the full citation of the source document and credit the Earthquake Engineering Research Institute with permission to reproduce.

Permission is granted on a one-time basis for print and electronic use by:

Heidi Tremayne
Executive Director
Federal ID no. 94-6082215

Appendix I: Copyright Permissions for Figure 2.7 and 2.8

Thank you for your order with RightsLink / American Society of Civil Engineers

no-reply@copyright.com

Fri 1/18/2019 2:26 PM
To: Miranda Orellana, Henry <hpm916@mail.usask.ca>;

Header
Thank you for your order!
Dear Mr. Henry Miranda Orellana,

Thank you for placing your order through Copyright Clearance Center's RightsLink$^{®}$ service.

Order Summary

Licensee:	University of Saskatchewan
Order Date:	Jan 18, 2019
Order Number:	4512080257669
Title:	Journal of Structural Engineering
Type of Use:	Thesis/Dissertation
Order Total:	0.00 USD

(Original Order Number: 501456575)

View or print complete details of your order and the publisher's terms and conditions.

Sincerely,

Copyright Clearance Center

Tel: +1-855-239-3415 / +1-978-646-2777
customercare@copyright.com
https://myaccount.copyright.com

Jan 18, 2019

This is a License Agreement between University of Saskatchewan -- Henry Miranda

Orellana ("You") and American Society of Civil Engineers ("American Society of Civil Engineers") provided by Copyright Clearance Center ("CCC"). The license consists of your order details, the terms and conditions provided by American Society of Civil Engineers, and the payment terms and conditions.

All payments must be made in full to CCC. For payment instructions, please see information listed at the bottom of this form.

License Number	4512080257669
License date	Jan 15, 2019
Licensed content publisher	American Society of Civil Engineers
Licensed content title	Journal of Structural Engineering
Licensed content date	Jan 1, 1983
Type of Use	Thesis/Dissertation
Requestor type	Academic institution
Format	Electronic
Portion	image/photo
Number of images/photos requested	2
The requesting person/organization is:	HENRY PAUL MIRANDA ORELLANA

134

Title or numeric reference of Out-of-plane strength of confined masonry walls, Figure 8 and the portion(s)   Figure 11. This figures will be redrawn on the thesis manuscript. Also, symbology will be modified.

Title of the article or chapter n/a the portion
is from

Editor of portion(s)   American Society of Civil Engineers

Author of portion(s)   Varela et al.

Volume of serial or 138(11) monograph.

Page range of the portion   1337-1338

Publication date of portion   2012

Rights for   Main product

Duration of use   Life of current edition

Creation of copies for the   no disabled

With minor editing privileges yes

For distribution to   Canada

In the following language(s) Original language of publication
With incidental promotional use   no

The lifetime unit quantity of new   Up to 499
product

Title   Proof of Concept Investigation of Unbonded Reinforcement in Concrete Block Masonry

Institution name   University of saskatchewan

Expected presentation date   Oct 2018

Billing Type   Invoice

Billing Address   University of Saskatchewan 205 Taylor
                                       St W

                                       Saskatoon, SK S7M0C4
                                       Canada
                                       Attn: Henry P Miranda Orellana

Total (may include CCC user 0.00 USD fee)

Terms and Conditions

TERMS AND CONDITIONS
The following terms are individual to this publisher:

None

Other Terms and Conditions:
A full credit line must be added to the material being reprinted. For reuse in non-ASCE publications, add the words "With permission from ASCE" to your source citation. For Intranet posting, add the following

additional notice: "This material may be downloaded for personal use only. Any other use requires prior permission of the American Society of Civil

Engineers. This material may be found at [URL/link of abstract in the ASCE Library or Civil Engineering Database]." Each license is unique, covering only the terms and conditions specified in it. Even if you have obtained a license for certain ASCE copyrighted content, you will need to obtain another license if you plan to reuse that content outside the terms of the existing license. For example: If you already have a license to reuse a figure in a journal, you still need a new license to use the same figure in a magazine. You need a separate license for each edition.

<div align="center">STANDARD TERMS AND CONDITIONS</div>

1. Description of Service; Defined Terms. This Republication License enables the User toobtain licenses for republication of one or more copyrighted works as described in detail on the relevant Order Confirmation (the "Work(s)"). Copyright Clearance Center, Inc. ("CCC") grants licenses through the Service on behalf of the rightsholder identified on the Order Confirmation (the "Rightsholder"). "Republication", as used herein, generally means the inclusion of a Work, in whole or in part, in a new work or works, also as described on the Order Confirmation. "User", as used herein, means the person or entity making such republication.

2. The terms set forth in the relevant Order Confirmation, and any terms set by theRightsholder with respect to a particular Work, govern the terms of use of Works in connection with the Service. By using the Service, the person transacting for a republication license on behalf of the User represents and warrants that he/she/it (a) has been duly authorized by the User to accept, and hereby does accept, all such terms and conditions on behalf of User, and (b) shall inform User of all such terms and conditions. In the event such person is a "freelancer" or other third party independent of User and CCC, such party shall be deemed jointly a "User" for purposes of these terms and conditions. In any event, User shall be deemed to have accepted and agreed to all such terms and conditions if User republishes the Work in any fashion.

3. Scope of License; Limitations and Obligations.

    3.1 All Works and all rights therein, including copyright rights, remain the sole andexclusive property of the Rightsholder. The license created by the exchange of an Order Confirmation (and/or any invoice) and payment by User of the full amount set forth on that document includes only those rights expressly set forth in the Order Confirmation and in these terms and conditions, and conveys no other rights in the Work(s) to User. All rights not expressly granted are hereby reserved.

    3.2 General Payment Terms: You may pay by credit card or through an account with uspayable at the end of the month. If you and we agree that you may establish a standing account with CCC, then the following terms apply: Remit Payment to: Copyright Clearance Center, 29118 Network Place, Chicago, IL 60673-1291. Payments Due: Invoices are payable upon their delivery to you (or upon our notice to you that they are available to you for downloading). After 30 days, outstanding amounts will be subject to a service charge of 1-1/2% per month or, if less, the maximum rate allowed by applicable law. Unless otherwise specifically set forth in the Order Confirmation or in a separate written agreement signed by CCC, invoices are due and payable on "net 30" terms. While User may exercise the rights licensed immediately upon issuance of the Order Confirmation, the license is automatically revoked and is null and void, as if it had never been issued, if complete payment for the license is not

<div align="center">136</div>

received on a timely basis either from User directly or through a payment agent, such as a credit card company.

3.3 Unless otherwise provided in the Order Confirmation, any grant of rights to User (i) is"one-time" (including the editions and product family specified in the license), (ii) is nonexclusive and non-transferable and (iii) is subject to any and all limitations and restrictions (such as, but not limited to, limitations on duration of use or circulation) included in the Order Confirmation or invoice and/or in these terms and conditions. Upon completion of the licensed use, User shall either secure a new permission for further use of the Work(s) or immediately cease any new use of the Work(s) and shall render inaccessible (such as by deleting or by removing or severing links or other locators) any further copies of the Work (except for copies printed on paper in accordance with this license and still in User's stock at the end of such period).

3.4 In the event that the material for which a republication license is sought includes thirdparty materials (such as photographs, illustrations, graphs, inserts and similar materials) which are identified in such material as having been used by permission, User is responsible for identifying, and seeking separate licenses (under this Service or otherwise) for, any of such third party materials; without a separate license, such third party materials may not be used.

3.5 Use of proper copyright notice for a Work is required as a condition of any licensegranted under the Service. Unless otherwise provided in the Order Confirmation, a proper copyright notice will read substantially as follows: "Republished with permission of [Rightsholder's name], from [Work's title, author, volume, edition number and year of copyright]; permission conveyed through Copyright Clearance Center, Inc. " Such notice must be provided in a reasonably legible font size and must be placed either immediately adjacent to the Work as used (for example, as part of a by-line or footnote but not as a separate electronic link) or in the place where substantially all other credits or notices for the new work containing the republished Work are located. Failure to include the required notice results in loss to the Rightsholder and CCC, and the User shall be liable to pay liquidated damages for each such failure equal to twice the use fee specified in the Order Confirmation, in addition to the use fee itself and any other fees and charges specified.

3.6 User may only make alterations to the Work if and as expressly set forth in the OrderConfirmation. No Work may be used in any way that is defamatory, violates the rights of third parties (including such third parties' rights of copyright, privacy, publicity, or other tangible or intangible property), or is otherwise illegal, sexually explicit or obscene. In addition, User may not conjoin a Work with any other material that may result in damage to the reputation of the Rightsholder. User agrees to inform CCC if it becomes aware of any infringement of any rights in a Work and to cooperate with any reasonable request of CCC or the Rightsholder in connection therewith.

4. Indemnity. User hereby indemnifies and agrees to defend the Rightsholder and CCC, andtheir respective employees and directors, against all claims, liability, damages, costs and expenses, including legal fees and expenses, arising out of any use of a Work beyond the scope of the rights granted herein, or any use of a Work which has been altered in any unauthorized way by User, including claims of defamation or infringement of rights of copyright, publicity, privacy or other tangible or intangible property.

5. Limitation of Liability. UNDER NO CIRCUMSTANCES WILL CCC OR THE

RIGHTSHOLDER BE LIABLE FOR ANY DIRECT, INDIRECT, CONSEQUENTIAL OR

INCIDENTAL DAMAGES (INCLUDING WITHOUT LIMITATION DAMAGES FOR

LOSS OF BUSINESS PROFITS OR INFORMATION, OR FOR BUSINESS

INTERRUPTION) ARISING OUT OF THE USE OR INABILITY TO USE A WORK,

EVEN IF ONE OF THEM HAS BEEN ADVISED OF THE POSSIBILITY OF SUCH

DAMAGES. In any event, the total liability of the Rightsholder and CCC (including their respective employees and directors) shall not exceed the total amount actually paid by User for this license. User assumes full liability for the actions and omissions of its principals, employees, agents, affiliates, successors and assigns.

6. Limited Warranties. THE WORK(S) AND RIGHT(S) ARE PROVIDED "AS IS". CCCHAS THE RIGHT TO GRANT TO USER THE RIGHTS GRANTED IN THE ORDER
CONFIRMATION DOCUMENT. CCC AND THE RIGHTSHOLDER DISCLAIM ALL

OTHER WARRANTIES RELATING TO THE WORK(S) AND RIGHT(S), EITHER

EXPRESS OR IMPLIED, INCLUDING WITHOUT LIMITATION IMPLIED

WARRANTIES OF MERCHANTABILITY OR FITNESS FOR A PARTICULAR

PURPOSE. ADDITIONAL RIGHTS MAY BE REQUIRED TO USE ILLUSTRATIONS,

GRAPHS, PHOTOGRAPHS, ABSTRACTS, INSERTS OR OTHER PORTIONS OF THE

WORK (AS OPPOSED TO THE ENTIRE WORK) IN A MANNER CONTEMPLATED BY USER; USER UNDERSTANDS AND AGREES THAT NEITHER CCC NOR THE RIGHTSHOLDER MAY HAVE SUCH ADDITIONAL RIGHTS TO GRANT.

7. Effect of Breach. Any failure by User to pay any amount when due, or any use by User ofa Work beyond the scope of the license set forth in the Order Confirmation and/or these terms and conditions, shall be a material breach of the license created by the Order Confirmation and these terms and conditions. Any breach not cured within 30 days of written notice thereof shall result in immediate termination of such license without further notice. Any unauthorized (but licensable) use of a Work that is terminated immediately upon notice thereof may be liquidated by payment of the Rightsholder's ordinary license price therefor; any unauthorized (and unlicensable) use that is not terminated immediately for any reason (including, for example, because materials containing the Work cannot reasonably be recalled) will be subject to all remedies available at law or in equity, but in no event to a payment of less than three times the Rightsholder's ordinary license price for the most closely analogous licensable use plus Rightsholder's and/or CCC's costs and expenses incurred in collecting such payment.
8. Miscellaneous.

8.1 User acknowledges that CCC may, from time to time, make changes or additions to the Service or to these terms and conditions, and CCC reserves the right to send notice to the User by electronic mail or otherwise for the purposes of notifying User of such changes or additions; provided that any such changes or additions shall not apply to permissions already secured and paid for.

8.2 Use of User-related information collected through the Service is governed by CCC'sprivacy policy, available online here: http://www.copyright.com/content/cc3/en/tools/footer/privacypolicy.html.

8.3 The licensing transaction described in the Order Confirmation is personal to User.Therefore, User may not assign or transfer to any other person (whether a natural person or an organization of any kind) the license created by the Order Confirmation and these terms and conditions or any rights granted hereunder; provided, however, that User may assign such license in its entirety on written notice to CCC in the event of a transfer of all or substantially all of User's rights in the new material which includes the Work(s) licensed under this Service.

8.4 No amendment or waiver of any terms is binding unless set forth in writing and signedby the parties. The Rightsholder and CCC hereby object to any terms contained in any writing prepared by the User or its principals, employees, agents or affiliates and purporting to govern or otherwise relate to the licensing transaction described in the Order

Confirmation, which terms are in any way inconsistent with any terms set forth in the Order Confirmation and/or in these terms and conditions or CCC's standard operating procedures, whether such writing is prepared prior to, simultaneously with or subsequent to the Order Confirmation, and whether such writing appears on a copy of the Order Confirmation or in a separate instrument.

8.5 The licensing transaction described in the Order Confirmation document shall begoverned by and construed under the law of the State of New York, USA, without regard to the principles thereof of conflicts of law. Any case, controversy, suit, action, or proceeding arising out of, in connection with, or related to such licensing transaction shall be brought, at CCC's sole discretion, in any federal or state court located in the County of New York, State of New York, USA, or in any federal or state court whose geographical jurisdiction covers the location of the Rightsholder set forth in the Order Confirmation. The parties expressly submit to the personal jurisdiction and venue of each such federal or state court.If you have any comments or questions about the Service or Copyright Clearance Center, please contact us at 978-750-8400 or send an e-mail to info@copyright.com. v 1.1

Questions? customercare@copyright.com or +1-855-239-3415 (toll free in the US) or +1-978-646-2777.

Appendix J: Copyright Permissions for Figure 2.9

RE: Request permission/copyright material

Bennett Banting <Bbanting@canadamasonrycentre.com>
Mon 1/14/2019 1:08 PM

T.Miranda Orellana, Henry<hpm916@mail.usask.ca>;

Hello Henry, you are free to use any symposium material, including figures etc. for your thesis, all that is required is that you cite the publication.

Thanks

Sincerely,

BENNETT R. BANTING, PH.D., P.ENG.
DIRECTOR OF TECHNICAL SERVICES, ENGINEERED MASONRY
CANADA MASONRY DESIGN CENTRE
http://www.canadamasonrydesigncentre.com/
360 Superior Blvd.
Mississauga, ON   L5T 2N7
Tel: (888) 338-3336   Tor: (905) 564-0666
Fax: (905) 564-5744

Appendix K: Copyright Permissions for Chapter 3

Mahmoud Lardjane <Mahmoud.Lardjane@csce.ca>

Fri 8/3/2018, 1:13 PM
Miranda Orellana, Henry;
info@csce.ca;
henrypaul2004@yahoo.com.mx
Inbox

Hello Henry,

We happily grant you our approval to reuse the content of your paper. Please simply indicate that it was presented at the CSCE 2016 Annual Conference.

I wish you success with your thesis.

Regards,
Mahmoud

Mahmoud Lardjane
Membership Information and Programs Director
Directeur des programmes et informations adhésion
300, rue St-Sacrement, bur. 521, Montréal, QC H2Y 1X4
514-933-2634 # 4   514-933-3504   www.csce.ca

Canadian Society for Civil Engineering | CSCE CGC | Société canadienne de génie civil

   Join us in Laval, QC for
our 2019 Annual Conference & AGM June 12-15, 2019.
   Joignez-vous à nous à notre congrès annuel 2019 à Laval, QC, du 12 au 15 juin 2019.

Appendix L: Copyright Permissions for Chapter 4

License Number	4405490548807
License date	Aug 02, 2018
Licensed content publisher	Canadian Science Publishing
Licensed content title	Canadian journal of civil engineering : Revue canadienne de génie civil
Licensed content date	Jan 1, 1974
Type of Use	Thesis/Dissertation
Requestor type	Author of requested content
Format	Print, Electronic
Portion	chapter/article
The requesting person/organization is:	Henry Paul Miranda Orellana
Title or numeric reference of the portion(s)	N/A
Title of the article or chapter the portion is from	Proof of Concept Investigation of Unbonded Reinforcement in Concrete Block Masonry (Abstract, Introduction, Experimental Investigation, Experimental Results, Analytical Results, Summary and Conclusions, References, Tables and Figures)
Editor of portion(s)	Henry Paul Miranda Orellana
Author of portion(s)	Henry Paul Miranda Orellana
Volume of serial or monograph.	N/A
Page range of the portion	
Publication date of portion	N/A
Rights for	Main product
Duration of use	Life of current edition
Creation of copies for the disabled	no

Terms and Conditions

TERMS AND CONDITIONS

The following terms are individual to this publisher:

None

Other Terms and Conditions:

Please cite original source.

STANDARD TERMS AND CONDITIONS

1. Description of Service; Defined Terms. This Republication License enables the User toobtain licenses for republication of one or more copyrighted works as described in detail on the relevant Order Confirmation (the "Work(s)"). Copyright Clearance Center, Inc. ("CCC") grants licenses through the Service on behalf of the rightsholder identified on the Order Confirmation (the "Rightsholder"). "Republication", as used herein, generally means the inclusion of a Work, in whole or in part, in a new work or works, also as described on the Order Confirmation. "User", as used herein, means the person or entity making such republication.

2. The terms set forth in the relevant Order Confirmation, and any terms set by theRightsholder with respect to a particular Work, govern the terms of use of Works in connection with the Service. By using the Service, the person transacting for a republication license on behalf of the User represents and warrants that he/she/it (a) has been duly authorized by the User to accept, and hereby does accept, all such terms and conditions on behalf of User, and (b) shall inform User of all such terms

and conditions. In the event such person is a "freelancer" or other third party independent of User and CCC, such party shall be deemed jointly a "User" for purposes of these terms and conditions. In any event, User shall be deemed to have accepted and agreed to all such terms and conditions if User republishes the Work in any fashion.

3. Scope of License; Limitations and Obligations.

    3.1 All Works and all rights therein, including copyright rights, remain the sole andexclusive property of the Rightsholder. The license created by the exchange of an Order Confirmation (and/or any invoice) and payment by User of the full amount set forth on that document includes only those rights expressly set forth in the Order Confirmation and in these terms and conditions, and conveys no other rights in the Work(s) to User. All rights not expressly granted are hereby reserved.

    3.2 General Payment Terms: You may pay by credit card or through an account with uspayable at the end of the month. If you and we agree that you may establish a standing account with CCC, then the following terms apply: Remit Payment to: Copyright Clearance Center, 29118 Network Place, Chicago, IL 60673-1291. Payments Due: Invoices are payable upon their delivery to you (or upon our notice to you that they are available to you for downloading). After 30 days, outstanding amounts will be subject to a service charge of 1-1/2% per month or, if less, the maximum rate allowed by applicable law. Unless otherwise specifically set forth in the Order Confirmation or in a separate written agreement signed by CCC, invoices are due and payable on "net 30" terms. While User may exercise the rights licensed immediately upon issuance of the Order Confirmation, the license is automatically revoked and is null and void, as if it had never been issued, if complete payment for the license is not received on a timely basis either from User directly or through a payment agent, such as a credit card company.

    3.3 Unless otherwise provided in the Order Confirmation, any grant of rights to User (i) is"one-time" (including the editions and product family specified in the license), (ii) is nonexclusive and non-transferable and (iii) is subject to any and all limitations and restrictions (such as, but not limited to, limitations on duration of use or circulation) included in the Order Confirmation or invoice and/or in these terms and conditions. Upon completion of the licensed use, User shall either secure a new permission for further use of the Work(s) or immediately cease any new use of the Work(s) and shall render inaccessible (such as by deleting or by removing or severing links or other locators) any further copies of the Work (except for copies printed on paper in accordance with this license and still in User's stock at the end of such period).

    3.4 In the event that the material for which a republication license is sought includes thirdparty materials (such as photographs, illustrations, graphs, inserts and similar materials) which are identified in such material as having been used by permission, User is responsible for identifying, and seeking separate licenses (under this Service or otherwise) for, any of such third party materials; without a separate license, such third party materials may not be used.

    3.5 Use of proper copyright notice for a Work is required as a condition of any licensegranted under the Service. Unless otherwise provided in the Order Confirmation, a proper copyright notice will read substantially as follows: "Republished with permission of [Rightsholder's name], from [Work's title, author, volume, edition number and year of copyright];

permission conveyed through Copyright Clearance Center, Inc. " Such notice must be provided in a reasonably legible font size and must be placed either immediately adjacent to the Work as used (for example, as part of a by-line or footnote but not as a separate electronic link) or in the place where substantially all other credits or notices for the new work containing the republished Work are located. Failure to include the required notice results in loss to the Rightsholder and CCC, and the User shall be liable to pay liquidated damages for each such failure equal to twice the use fee specified in the Order Confirmation, in addition to the use fee itself and any other fees and charges specified.

3.6 User may only make alterations to the Work if and as expressly set forth in the Order Confirmation. No Work may be used in any way that is defamatory, violates the rights of third parties (including such third parties' rights of copyright, privacy, publicity, or other tangible or intangible property), or is otherwise illegal, sexually explicit or obscene. In addition, User may not conjoin a Work with any other material that may result in damage to the reputation of the Rightsholder. User agrees to inform CCC if it becomes aware of any infringement of any rights in a Work and to cooperate with any reasonable request of CCC or the Rightsholder in connection therewith.

4. Indemnity. User hereby indemnifies and agrees to defend the Rightsholder and CCC, andtheir respective employees and directors, against all claims, liability, damages, costs and expenses, including legal fees and expenses, arising out of any use of a Work beyond the scope of the rights granted herein, or any use of a Work which has been altered in any unauthorized way by User, including claims of defamation or infringement of rights of copyright, publicity, privacy or other tangible or intangible property.

5. Limitation of Liability. UNDER NO CIRCUMSTANCES WILL CCC OR THE RIGHTSHOLDER BE LIABLE FOR ANY DIRECT, INDIRECT, CONSEQUENTIAL OR INCIDENTAL DAMAGES (INCLUDING WITHOUT LIMITATION DAMAGES FOR LOSS OF BUSINESS PROFITS OR INFORMATION, OR FOR BUSINESS INTERRUPTION) ARISING OUT OF THE USE OR INABILITY TO USE A WORK, EVEN IF ONE OF THEM HAS BEEN ADVISED OF THE POSSIBILITY OF SUCH DAMAGES. In any event, the total liability of the Rightsholder and CCC (including their respective employees and directors) shall not exceed the total amount actually paid by User for this license. User assumes full liability for the actions and omissions of its principals, employees, agents, affiliates, successors and assigns.

6. Limited Warranties. THE WORK(S) AND RIGHT(S) ARE PROVIDED "AS IS". CCCHAS THE RIGHT TO GRANT TO USER THE RIGHTS GRANTED IN THE ORDER CONFIRMATION DOCUMENT. CCC AND THE RIGHTSHOLDER DISCLAIM ALL OTHER WARRANTIES RELATING TO THE WORK(S) AND RIGHT(S), EITHER EXPRESS OR IMPLIED, INCLUDING WITHOUT LIMITATION IMPLIED WARRANTIES OF MERCHANTABILITY OR FITNESS FOR A PARTICULAR PURPOSE. ADDITIONAL RIGHTS MAY BE REQUIRED TO USE ILLUSTRATIONS, GRAPHS, PHOTOGRAPHS, ABSTRACTS, INSERTS OR OTHER PORTIONS OF THE WORK (AS OPPOSED TO THE ENTIRE WORK) IN A MANNER CONTEMPLATED BY USER; USER UNDERSTANDS AND AGREES THAT NEITHER CCC NOR THE RIGHTSHOLDER MAY HAVE SUCH ADDITIONAL RIGHTS TO GRANT.

7. Effect of Breach. Any failure by User to pay any amount when due, or any use by User ofa Work beyond the scope of the license set forth in the Order Confirmation and/or these terms and conditions, shall be a material breach of the license created by the Order Confirmation and these terms and conditions. Any breach not cured within 30 days of written notice thereof shall result in immediate termination of such license without further notice. Any unauthorized (but licensable) use

of a Work that is terminated immediately upon notice thereof may be liquidated by payment of the Rightsholder's ordinary license price therefor; any unauthorized (and unlicensable) use that is not terminated immediately for any reason (including, for example, because materials containing the Work cannot reasonably be recalled) will be subject to all remedies available at law or in equity, but in no event to a payment of less than three times the Rightsholder's ordinary license price for the most closely analogous licensable use plus Rightsholder's and/or CCC's costs and expenses incurred in collecting such payment.

8. Miscellaneous.

8.1 User acknowledges that CCC may, from time to time, make changes or additions to the Service or to these terms and conditions, and CCC reserves the right to send notice to the User by electronic mail or otherwise for the purposes of notifying User of such changes or additions; provided that any such changes or additions shall not apply to permissions already secured and paid for.

8.2 Use of User-related information collected through the Service is governed by CCC'sprivacy policy, available online here: http://www.copyright.com/content/cc3/en/tools/footer/privacypolicy.html.

8.3 The licensing transaction described in the Order Confirmation is personal to User.Therefore, User may not assign or transfer to any other person (whether a natural person or an organization of any kind) the license created by the Order Confirmation and these terms and conditions or any rights granted hereunder; provided, however, that User may assign such license in its entirety on written notice to CCC in the event of a transfer of all or substantially all of User's rights in the new material which includes the Work(s) licensed under this Service.

8.4 No amendment or waiver of any terms is binding unless set forth in writing and signedby the parties. The Rightsholder and CCC hereby object to any terms contained in any writing prepared by the User or its principals, employees, agents or affiliates and purporting to govern or otherwise relate to the licensing transaction described in the Order Confirmation, which terms are in any way inconsistent with any terms set forth in the Order Confirmation and/or in these terms and conditions or CCC's standard operating procedures, whether such writing is prepared prior to, simultaneously with or subsequent to the Order Confirmation, and whether such writing appears on a copy of the Order Confirmation or in a separate instrument.

8.5 The licensing transaction described in the Order Confirmation document shall begoverned by and construed under the law of the State of New York, USA, without regard to the principles thereof of conflicts of law. Any case, controversy, suit, action, or proceeding arising out of, in connection with, or related to such licensing transaction shall be brought, at CCC's sole discretion, in any federal or state court located in the County of New York, State of New York, USA, or in any federal or state court whose geographical jurisdiction covers the location of the Rightsholder set forth in the Order Confirmation. The parties expressly submit to the personal jurisdiction and venue of each such federal or state court.If you have any comments or questions about the Service or Copyright Clearance Center, please contact us at 978-750-8400 or send an e-mail to info@copyright.com. v 1.1

Questions? customercare@copyright.com or +1-855-239-3415 (toll free in the US) or +1-978-646-2777.